8-2022

Integrin-Mediated Mechanotransduction Controls Activation Of Yap And Invasive Growth Of Breast Cancer

Xiaobo Wang

INTEGRIN-MEDIATED MECHANOTRANSDUCTION CONTROLS ACTIVATION OF YAP AND INVASIVE GROWTH OF BREAST CANCER

by

Xiaobo Wang, Master of Science

APPROVED:

_____
Filippo Giancotti, M.D., Ph.D.
Advisory Professor

_____
Pierre McCrea, Ph.D.
On-Site Advisory Professor

_____
Nicholas Navin, Ph.D.

_____
Andrea Viale, M.D.

_____
Giannicola Genovese, M.D., Ph.D.

_____
Florian Muller, Ph.D.

APPROVED:

_____
Dean, The University of Texas
MD Anderson Cancer Center UTHealth Graduate School of Biomedical Sciences

INTEGRIN-MEDIATED MECHANOTRANSDUCTION CONTROLS ACTIVATION OF YAP AND INVASIVE GROWTH OF BREAST CANCER

A

Dissertation

Presented to the Faculty of

The University of Texas

MD Anderson Cancer Center UTHealth

Graduate School of Biomedical Sciences

in Partial Fulfillment

of the Requirements

for the Degree of

DOCTOR OF PHILOSOPHY

by

Xiaobo Wang, Master of Science
Houston, Texas

August 2022

Dedication

To my dearest father Yu Wang. Thank you for your wholehearted love and support.

Acknowledgements

Before setting out on the Ph.D. journey, I had never imagined it would be so adventurous. The unprecedented tropical storm, the pandemic, and the polarized society have been breeding uncertainty, which makes it not easy to navigate life far away from home. Despite the challenges, I have met a lot of mentors and friends who help me grow personally and professionally. When the six-year long graduate training comes to an end, I am deeply grateful for their support and faith in me.

First and foremost, I would like to show my sincere gratitude to my advisor, Dr. Filippo Giancotti, for his invaluable advice and continuous support in the course my Ph.D. studies. His comprehensive knowledge and experience have inspired me at every stage of the research project. I will always appreciate the good memories from our scientific discussions from which I gained knowledge and professional expertise, as well as the holiday gatherings where I saw how gentle and considerate he is. I am also very thankful for the opportunity to study in two distinguished institutions and to explore two distinct cities. Furthermore, I have learnt the importance of resilience and perseverance.

I would like to offer my special thanks to my on-site advisor, Dr. Pierre McCrea, and my mentor during the rotation, Dr. Florian Muller. As an experienced and prestigious mentor, Dr. McCrea always assures that I am on the right track in and outside of the lab. In addition to scientific input, he provides guidance on how to be a better person. I feel very lucky to have him as my on-site advisor to keep my close bond with the graduate school when I am working off campus. During my rotation with

Dr. Muller, I was amazed by his immense knowledge and endless passion for science. This will always encourage me to think more broadly and deeply. I appreciate his mentorship and help when I was still at the very early phase of the graduate studies. I would like to extend my thanks to other members of my advisory committee, Dr. Andrea Viale, Dr. Nicholas Navin, and Dr. Giannicola Genovese, for their precious scientific guidance and support for my academic endeavors at GSBS. I would also like to thank Dr. Daniel Frigo for serving in my candidacy examination committee and defense committee and providing insightful feedback, and Dr. Jian Hu for the very helpful discussions about Cancer Biology Program and the personal growth. I would also like to thank the administrative team of GSBS, including but not limited to Dr. Bill Mattox, Brenda, Raquel, Natalie, Bunny, Pat, Elisabet, and Joy, and our program coordinator, Amy, for their relentless efforts to establish a congenial environment and to improve the training experience for all GSBS students.

I would like to thank all the members of Giancotti Lab, Yan Wang, Shimin, Hsiang-Hsi, Sara, Nancy, Yan Jiang, Junfeng, Josu, Jiankang, Dhiraj, Alekya, Harsha, Seong-Yeon, Lauren, Melda, and Fei, for the supportive and collaborative lab environment. I also appreciate the friendship that I have made. I would like to express my thanks to my friends, I-Lin, Jing, Sunada, Hieu, and Feng, for going through ups and downs together with me.

Finally, many thanks as always to my family. I am extremely grateful for the unconditional and caring support from my family. The heartwarming encouragement is always received although it has been more than four years since we met last time.

To my father, I am indebted for everything you have sacrificed for me to study abroad and pursue my dream. To my grandma, thank you for taking care of me during difficult times and always being my cheerleader.

INTEGRIN-MEDIATED MECHANOTRANSDUCTION CONTROLS ACTIVATION OF YAP AND INVASIVE GROWTH OF BREAST CANCER

Xiaobo Wang, M.S.

Advisory Professor: Filippo Giancotti, M.D., Ph.D.

On-Site Advisory Professor: Pierre McCrea, Ph.D.

Tumor extracellular matrix (ECM) stiffness is correlated with the aggressiveness of breast cancer. Integrin-mediated adhesion and signaling are crucial for mammary tumorigenesis and tumor progression, in which focal adhesion kinase (FAK) - Src family kinases (SFKs) serves as a hub to relay the mechanical cues from the ECM. We have investigated the mechanisms through which integrin signaling controls mammary tumorigenesis and found that integrin-mediated mechanotransduction controls invasive growth of breast cancer cells in stiff matrices through activation of FAK and YAP. Mechanistic studies revealed that integrin signaling induces - via activation SFKs - tyrosine phosphorylation and inactivation of LATS1 and MOB1. The ensuing activation of YAP is necessary for invasive growth of HER2+ breast cancer cells. Engagement of HER2/HER3 with neuregulin impinges on SFKs to amplify activation of YAP in HER2+ breast cancer cells, suggesting that integrin-mediated mechanotransduction functions as a rheostat to regulate HER2 oncogenic signaling. Finally, administration of Dasatinib combined with Lapatinib significantly increases the efficacy of HER2 inhibition in the MMTV-Neu mouse model of HER2+ breast cancer. These findings reveal a major mechanism through which the Hippo tumor suppressive pathway is disabled in breast cancer and suggest that targeting HER2 and SFKs simultaneously may be a rational strategy in selected cases of breast cancer.

Table of Contents

List of Figures

List of Tables

Chapter 1. Introduction

1.1 Breast Cancer and Fibrosis

Breast cancer has surpassed lung cancer to become the leading cause of cancer incidence worldwide (*1*). Among female cancer patients in the United States, breast cancer is estimated to account for 31% of cancer cases and for 15% of cancer deaths in 2022 (*2*). The major classification scheme of breast cancer is based on molecular profiling analysis and referred as following subtypes - luminal hormone receptor (HR) positive (luminal A and luminal B) [estrogen receptor (ER)+ and/or progesterone receptor (PR)+], human epidermal growth factor receptor 2 (HER2) positive (HER2+), and basal-like triple negative (ER-, PR-, HER2+) (*3, 4*). The molecular classification is of great importance in risk stratification and treatment planning. Compared to luminal A and luminal B subtypes, HER2 positive and triple negative subtypes have more aggressive biological behavior and poorer clinical outcomes (*5, 6*) (**Figure 1**).

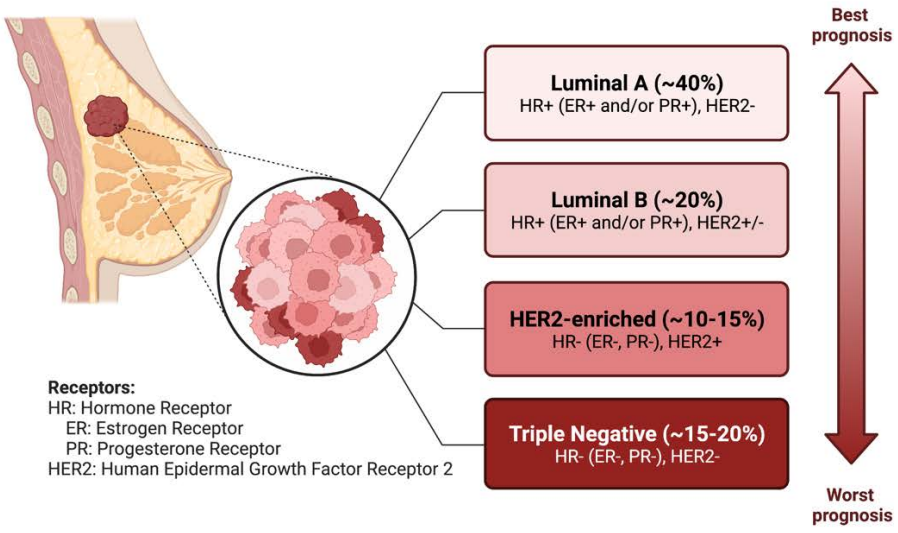

Figure 1. Molecular Subtypes of Breast Cancer.

Breast cancer is classified as Luminal A, Luminal B, HER2+, and Triple Negative subtypes based on the status of HRs (ER and PR) and HER2.

Although HER2-targeted therapy is a milestone that has improved patient outcomes in HER2 positive breast cancer, the durable drug response is still challenging to obtain due to the drug resistance (*7*). Triple negative breast cancer remains the most refractory subtype for clinical treatment (*6*). Therefore, revealing the mechanisms underlying tumor progression and metastasis, discovering novel therapeutic vulnerabilities, identifying new biomarkers for therapy guidance, and developing rational combination therapy remain urgent and important.

Tumor stromal stiffness correlates with the aggressiveness of breast cancer. The stroma of more aggressive HER2 positive and triple negative subtypes are stiffer than less aggressive luminal A and luminal B subtypes, and the invasive front regions in HER2 positive and triple negative subtypes are the stiffest (*8*). In mouse breast cancer models, mammary tumors from MMTV-Her2/neu, Myc, and Ras transgenic mice and MMTV-PyMT mice are significantly stiffer than phenotypically normal mammary tissues (*9, 10*). In human breast cancer, the cancer transformation and progression are accompanied by a significant increase in stromal stiffening (*8*).

The stromal fibrosis to stiffen the tumor is mainly caused by ECM deposition, remodeling, and crosslinking (*11*) (**Figure 2**). Both tumor cells and stromal cells, including but not limited to cancer-associated fibroblasts (CAFs) (*12*) and tumor-associated macrophages (TAMs) (*13*), are responsible for tumor stiffening. ECM

deposition is characterized by the accumulation of matrix components, such as collagen and fibronectin. Stromal cells residing in the tumor microenvironment are important sources of ECM components. In colorectal cancer, palladin and Collagen VI are upregulated in CAFs to mediate matrix stiffening (*14*). In the obesity-related breast tumorigenesis, mammary adipose stromal cells (ASCs) from obese mice contain more CAFs and deposited stiffer and denser ECMs with more fibronectin compared to those isolated from lean and healthy mice (*15*). The stiffness-promoting matrix proteins can also be secreted by tumor cells. In lung adenocarcinoma, loss of the tumor suppressor RASSF1A can result in the upregulation of collagen prolyl hydroxylase P4HA2, which leads to the increased collagen deposition and matrix stiffness (*16*). ECM remodeling is affected by the contraction of surrounding cells. Contractile CAFs from MMTV-PyMT breast cancer mouse model induces actomyosin-mediated contraction and cytoskeletal remodeling that promote ECM remodeling and stiffening (*17*). ECM crosslinking among fibrillar collagens leads to the densification and linearization of the matrix, which enhances ECM rigidity. ECM crosslinking is regulated by a series of catalytic reactions, in which Lysyl hydroxylase (LH) and Lysyl oxidase (LOX) family proteins are among the crucial regulatory enzymes. LOX-mediated collagen crosslinking is required for MMTV-Neu-induced fibrosis and breast malignancy (*18*). Consistently, the aggressiveness of lung (*19*), pancreas (*20*), and colon (*21*) cancers are associated with the deposition, remodeling, and crosslinking of ECM in the tumor tissues.

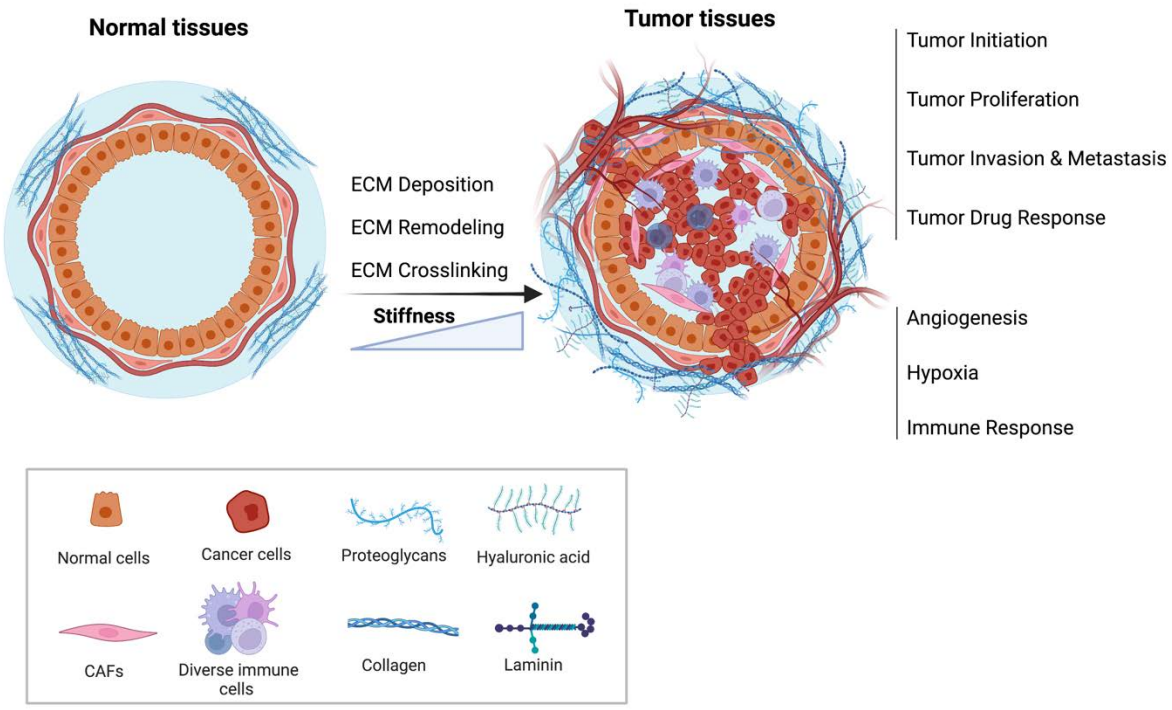

Figure 2. Extracellular (ECM) Stiffening During Tumor Initiation and Progression.

Schematic illustration of ECM stiffening during the transformation and development of tumors. ECM stiffening is caused by ECM deposition, remodeling, and crosslinking; and regulates multiple steps of tumor development through direct effects on tumor cells and indirect effects on the tumor microenvironment.

1.2 ECM Stiffness in Cancer Progression

Tumor stiffening has been shown to regulate tumor initiation, proliferation, migration, and drug resistance, and also to modulate angiogenesis, hypoxia, and immune response in the tumor microenvironment (**Figure 2**).

1.2.1 Tumor Initiation

Tumor initiation occurs when the normal cells transform to cancer cells with abnormal proliferation. Mammary epithelial cells can normally differentiate to form duct-like tubules on soft matrices. However, when seeded on stiff matrices, the cells show deficiency in tubulogenesis and undergo morphological changes (*22*). Similarly, Matthew J.Paszek et al. reported that when mammary epithelial cells are plated on a rigid matrix, the cytoskeleton tension is elevated, followed by tissue polarity perturbation and architecture disruption, cell growth increase, and normal lumen formation defects, which resemble tumor initiation (*10*). Consistent with these studies, when the mammary epithelial cells are seeded on methacrylated hyaluronic acid hydrogels with higher stiffness, they begin to lose epithelial features and gain mesenchymal characteristics in a time- and stiffness degree- dependent manner (*23*). The tumor initiation triggered by matrix rigidity is further validated in mouse models. In PyMt/wt and PyMt/Col1a1^{tmJae} breast cancer mouse models, PyMt/Col1a1^{tmJae} mice have higher collagen density, which increases the tumor incidence, suggesting that matrix stiffening, as a result of collagen densification, is critical for breast tumor formation (*24*). Tissue stiffness drives the epidermal hyperplasia and tumorigenesis through mechanosensing signals in response to actomyosin-mediated cellular tension (*25*). Therefore, matrix stiffness triggers malignant transformation of epithelial cells and tumor initiation.

1.2.2 Tumor proliferation

During cancer growth, increased ECM stiffness promotes the proliferative capacity of cancer cells in breast cancer (*18, 26*), colorectal cancer (*27*), non-small cell lung cancer (*28, 29*), pancreatic cancer (*30*), and hepatocellular carcinoma (*31*).

In addition to ECM stiffness per se, cancer proliferation is also stimulated via indirect effects. Upon stimuli from stiff matrix, mesenchymal stem cells (MSCs) differentiate into CAFs and secrete prosaposin, which promotes the survival and proliferation of mammary tumor cells (*32*). CAFs and cancer cells also can establish a metabolic crosstalk. In response to a stiffer environment, CAF-derived aspartate can sustain cancer cell growth (*33*). Moreover, matrix stiffness can induce autophagy in stromal cells, such as CAFs and stellate cells, which will help form a tumor supportive niche, in which the growth of neighboring cancer cells is enhanced (*34*). Thus, ECM rigidity promotes tumor proliferation via both direct and indirect effects.

1.2.3 Tumor invasion and metastasis

ECM stiffness confers an invasive phenotype to tumor cells, which invade through the basement membrane (BM), allowing metastatic dissemination to begin (*18, 26*). In the metastatic cascade, the invasion is followed by intravasation, transit of tumor cells in circulatory vessels, extravasation, colonization and outgrowth in target organs (*35*). Matrix stiffness regulates metastasis at different stages. Rigid matrix promotes epithelial-to-mesenchymal transition (EMT), cell invasion, and metastasis in human MCF10A and mouse Eph4Ras mammary epithelial cells (*36, 37*). Mechanical signals from the stiff matrix stabilize microtubules to guide breast cancer metastasis (*38*). These studies show the transitory and immediate effects of the rigid matrix on breast cancer invasion and metastasis, whether tumor cells can maintain the stiffness-induced phenotypes in distant organs after the metastatic dissemination is poorly understood. Adam W. Watson et al. showed that in bone metastasis of breast cancer, the stiffness-induced characteristics are preserved in distant metastatic sites even in

soft microenvironment like bone marrow (*39*). The invasion and/or metastasis promoting roles of the matrix stiffness are also found in other types of cancers, such as hepatocellular carcinoma (*40, 41*), ovarian cancer (*42*), osteosarcoma (*43*), and lung cancer (*16, 19, 28*). Similar to indirect effects of ECM stiffness on the proliferation, tumor invasion and metastasis can also be indirectly regulated by CAFs in the fibrotic microenvironment. In the rigid stroma, aspartate derived from CAFs can promote cancer cell invasion and metastasis (*33*). However, matrix stiffening may exert inhibitory effects on metastasis. Prosaposin secreted by CAFs enhances proliferation but inhibits metastasis in breast cancer models (*32*). In summary, matrix rigidity promotes tumor invasion and metastasis, but in some studies, ECM stiffness negatively regulates metastasis, which may result from tensional constraints imposed on tumor cells or modulation of other components in the tumor microenvironment.

1.2.4 Cancer drug resistance

Drug resistance is an important reason for poor patient outcomes in aggressive cancers. ECM stiffness is a double-edged sword in regulating drug response. On one hand, matrix rigidity promotes drug resistance. The dense and stiff matrix may compromise the penetration and bioavailability of the drugs. Tumor stiffness evaluated by breast elastography is found to be a predictive biomarker for poorer response to adjuvant chemotherapy in breast cancer. The high stiffness is significantly corelated with lower clinical complete response (*44*). In HER2 positive breast cancer, ECM rigidity drives resistance to HER2 inhibitor Lapatinib (*45*). In triple negative breast cancer, chemotherapy induces Collagen IV upregulation in the ECM, which in turn leads to drug resistance and promotes cell invasion (*46*). Cirrhotic stiffness induces

resistance to Sorafenib in hepatocellular carcinoma (*47*). Ying Shen et al. reported that liver metastases of colorectal cancers are stiffer than primary tumors because of the accumulation of metastasis-associated fibroblasts. The stiffness induces resistance to bevacizumab; and inhibiting the fibroblast contraction and ECM deposition improve responses of metastatic tumors to bevacizumab (*48*). On the other hand, drug resistance develops in softer microenvironment. In triple negative breast cancer, chemotherapy-resistant residual tumors reside in a softer microenvironment (*49*). Jörg Schrader et al. found that seeding on stiffer matrices sensitize the hepatocellular carcinoma cells to cisplatin (*31*). These studies demonstrate the drug response on different stiffness levels of the ECM is context specific.

1.2.5 Angiogenesis

The intra-tumoral blood vessels are responsible for the delivery of oxygen and nutrients to sustain tumor growth. Vascular endothelial growth factor (VEGF) is a crucial regulator of angiogenesis. Matrix stiffness upregulates the VEGF expression in hepatocellular carcinoma cells (*50*), A549 lung cancer cells and human umbilical vein endothelial cells (HUVECs) (*51*). In the liver metastases of colorectal cancer, the increased stiffness induces angiogenesis. The inhibition of fibroblast contractile tensions improves the responses to VEGF inhibitor (*48*). These studies indicate the ECM rigidity can induce angiogenesis.

1.2.6 Hypoxia

As the solid tumor grows, the increasing mass can impose tensile forces on surrounding cells and lead to deformation of the surrounding tissues, which in turn

compresses the intra-tumoral blood and lymphatic vessels. The structural deformation of the vessels and the reduced blood flow caused by the compression of intra-tumoral blood vessels lead to hypoxia (*52*). Hypoxia-inducible factor 1-alpha (HIF1α) expression is correlated positively with tumor stiffness and reversely with responses to neoadjuvant chemotherapy and overall survival in breast cancer patients (*53*). Interestingly, the chronic hypoxia has been reported to decrease stiffness by inactivate CAFs. The chronic hypoxia can stabilize HIF1α, leading to the decreased expression of alpha-smooth muscle actin (αSMA) and periostin and reduced activity of myosin II, which result in loss of contractile forces in CAFs and matrix softening (*54*). Taken together, ECM stiffness can foster a hypoxic microenvironment due to the blood vessel structural deformation and reduced blood flow. Meanwhile, the crosstalk between hypoxia and matrix stiffness exists and allows the rigidity to be regulated by hypoxia.

1.2.7 Immune modulation

Both innate and adaptive immune responses of tumors are regulated by ECM stiffness. Matrix rigidity induces the formation of neutrophil extracellular traps and secretion of pro-inflammatory cytokines (*55*). In a breast cancer study, BAPN, a lysyl oxidase inhibitor, reduces the matrix stiffness of tumors and decreases infiltration of tumor-promoting M2-like macrophages in MMTV-PyMT mouse model. Higher matrix rigidity upregulates Colony Stimulating Factor 1 (CSF-1) expression in breast cancer cells and induces macrophage recruitment (*56*). Both Programmed Cell Death Protein 1 (PD-1) and its ligand Programmed Cell Death Ligand 1 (PD-L1) are immune checkpoint proteins, which can attenuate tumor immunity. PD-1/PD-L1 axis have been

successfully targeted in cancer patients to improve the outcomes. Matrix stiffness enhances PD-L1 expression in breast cancer cells (*57*) and lung cancer cells (*58*), which can be a mechanism of the immune evasion. In addition, ECM stiffness impinges on immune responses through the mechanical constraints or molecules secreted from CAFs in the tumor microenvironment. CAFs mediate tumor-enhancing inflammation in squamous skin carcinoma, pancreatic tumor, and mammary tumor mouse models (*59*). In hepatocellular carcinoma, CAF-derived prostaglandin E2 (PGE2) and indoleamine 2,3-dioxygenase (IDO) suppress NK activation (*60*). In metastatic urothelial cancers, the penetration of $CD8^+$ T cells into the tumor parenchyma is compromised. Instead, they are trapped in the collagen-rich peritumoral regions. The effects are mediated by transforming growth factor β (TGFβ) signaling in CAFs (*61*). In breast cancer, CAF-derived Chitinase 3-like 1 (Chi3L1) enhances macrophage recruitment and reprogramming to an M2-like phenotype, and decreases tumor infiltration by $CD8^+$ and $CD4^+$ T cells (*62*). In triple negative breast cancer, CAFs recruit and retain $CD4^+$ $CD25^+$ T cells by secreting CXCL12. CAFs also increase the survival of T lymphocytes and promote their differentiation into tumor suppressive $FoxP3^+$ regulatory T cells (Tregs) through B7H3, CD73, and DPP4 (*63*). In summary, ECM stiffness exerts immune suppressive effects via physical prevention of the effective immune cell infiltration, inhibition of immune cell activation, induction of pro-tumor inflammation and cytokine secretion, recruitment and reprogramming of tumor suppressive immune cells, and upregulation of immune inhibitory molecules.

To sum up, ECM stiffens during the tumorigenesis and tumor development. The stiff matrix regulates multiple cellular behaviors at different stages of tumor

pathogenesis. In the next section, I will address the question: How do the mechanical signals from the surrounding ECM control the cell fate and functions?

1.3 Integrin-Mediated Mechanosensing and Mechanotransduction

Cells sense mechanical stimuli arising from ECM and translate the mechanical cues into biochemical signals. The process is collectively termed as mechanotransduction. The mechanical cues are perceived by cells through different molecules at the cell membrane, including integrins, growth factor receptors, stretch-activated ion channels, and G protein coupled-receptors (*64*) (**Figure 3**). Integrin-based adhesion sites serve as the main hub at the cell-matrix interface for sensing the mechanical signals from the extracellular milieu. Integrins connect the ECM with intracellular actin cytoskeleton as mediators to integrate extracellular and intracellular compartments. The integrins consist of a family of 24 heterodimeric receptors (α and β subunits), which mediate adhesion to ECM components. Upon ligand binding, integrins recruit and associate with the cytoskeletal protein talin and other cytoskeletal linker proteins, leading to the integrin clustering. Integrin adhesion to the ECM promotes the formation of focal adhesions, which recruit adhesion plaque proteins to reorganize the cytoskeletal structure and trigger the activation of the signaling cascades, focal adhesion kinase (FAK) and Src family kinases (SFKs), and ensuing pro-mitogenic and pro-survival signaling pathways, including Ras-ERK, PI3K/AKT, and YAP/TAZ pathways (*65*).

Accumulating evidence suggests that the microenvironment rigidity can promote tumor progression through enhancing integrin clustering and focal adhesion assembly, and activation of growth factor signaling pathways (*65, 66*). The integrin signaling and growth factor signaling receptor tyrosine kinases (RTKs), including HER2, epidermal growth factor receptor (EGFR), fibroblast growth factor (FGFR), and platelet-derived growth factors (PDGFR), cooperate to regulate downstream pro-mitogenic and pro-survival signaling pathways. The reciprocal interplay between the integrin signaling and RTKs is evidenced in SFK-induced phosphorylation of the P loop of RTKs and RTK-induced phosphorylation of FAK or integrin β subunits (*67*).

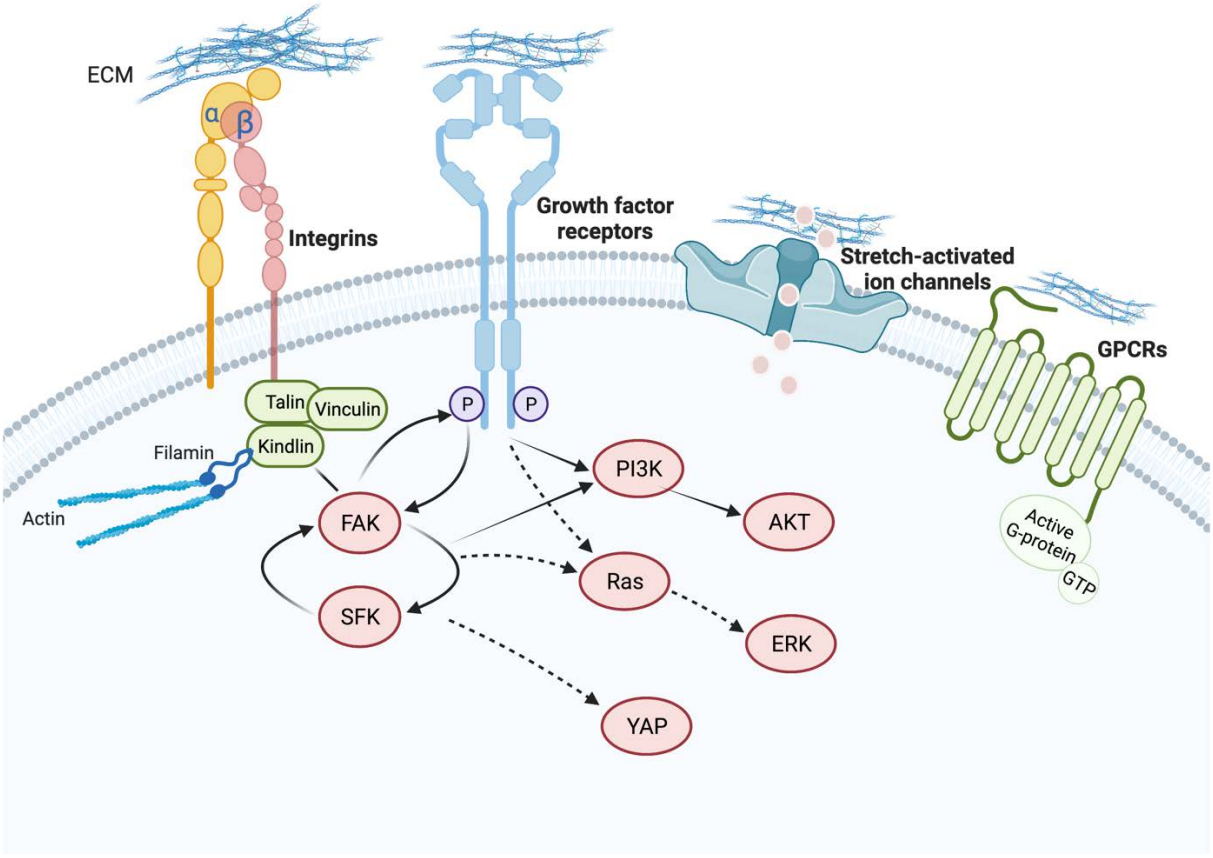

Figure 3. Mechanosensors of ECM Stiffness.

The mechanosensors at the cell-matrix interface include integrins, growth factor receptors, stretch-activated ion channels, and G protein-coupled receptors (GPCRs). Upon binding to the ligands in the ECM, integrins recruit and associate with the cytoskeletal protein talin and kindlin, leading to the integrin clustering followed by activation of focal adhesion kinase (FAK) and Src family kinases (SFKs). The integrin complexes sense the matrix stiffness and reinforce their adhesion to ECM in a vinculin-dependent manner. Integrins can cooperate with growth factor receptors to induce downstream pro-mitogenic/pro-survival signaling pathways, including Ras-ERK, PI3K/AKT, and YAP signaling pathways.

In breast cancer, integrin-mediated adhesion and signaling via FAK and SFKs are important for mammary tumorigenesis, tumor development, and treatment response. FAK sustains Ras- and PI3K-dependent mammary tumor initiation by promoting Src-mediated phosphorylation of $p130^{Cas}$ (*68*). Integrin $\beta5$ promotes the tumorigenic potential of breast cancer cells through the FAK-Src and MEK-ERK signaling pathways (*69*). In addition, in triple negative breast cancer, chemotherapy induces Collagen IV upregulation in the ECM, which in turn promotes cell invasion by activating FAK and Src downstream of integrin $\alpha1$ and $\alpha2$ (*46*). Moreover, hypoxia upregulates LOX, which is a key enzyme for ECM crosslinking, leading to chemotherapy resistance through the integrin $\alpha5$/fibronectin-FAK/Src axis in triple negative breast cancer (*70*). The joint regulation by integrin signaling and RTKs have been demonstrated in different breast cancer models. Mouse genetic studies have demonstrated that integrin $\beta4$ coopts with ErbB2 to disrupt epithelial adhesion and polarity, and to enhance proliferation and invasion during mammary tumorigenesis

(*71*). EGFR/Src-signaling induces the tyrosine phosphorylation of integrin β4, which, in turn, recruits FAK to integrin β4 and activates FAK signaling (*72*). During metastasis of breast cancer, EZH2 transcriptionally upregulates integrin β1, which activates FAK. The activated FAK activates TGFβ signaling by phosphorylating TGFβ receptor and promotes the bone metastasis (*73*). As for the drug treatment, the simultaneous inhibition of integrin/FAK and EGFR signaling exerts synergistic effects on suppressing the progression and metastasis of triple negative breast cancer (*74*). In HER2 positive breast cancer, inhibition of the laminin-binding integrins α6β4 and α3β1 or associated tetraspanin protein CD151 sensitizes cancer cells to Trastuzumab and Lapatinib (*75*).

Integrin signaling senses mechanical cues from the stiff ECM and relays the signals to the downstream effectors, which determine the cellular functions.

1.4 YAP/TAZ in Mechanotransduction

The Hippo signaling pathway effectors Yorkie-homologues YES-associated protein (YAP) and transcriptional coactivator with PDZ-binding motif (TAZ, also known as WWTR1) are the most well-studied transcriptional co-activators that respond to the mechanical cues from ECM stiffness and mediate cellular responses (*76-78*). Before elaborating on the YAP/TAZ activation triggered by matrix stiffness, I will briefly summarize the Hippo signaling in general.

1.4.1 Hippo signaling overview

The Hippo signaling pathway, initially elucidated in Drosophila melanogaster, is a highly conserved signal transduction pathway that plays important roles in organ size control and tumor suppression (*79-81*). When the Hippo pathway is activated, MST and LATS are successively phosphorylated with the support of SAV1 and MOB1. MST-dependent LATS phosphorylation (LATS1: S909 and T1079; LATS2: T1041) increases the kinase activity of LATS (*82, 83*). Subsequently, MOB1 binds to LATS, relieves LATS autoinhibition, and induces activating autophosphorylation (LATS1: S674 and S1049; LATS2: S835) (*84*). Then, the activated LATS phosphorylates transcriptional co-activators YAP and TAZ, which prevent them from entering the nucleus and activating downstream gene expression (*85-88*) (**Figure 4**). YAP/TAZ regulate the contact inhibition of proliferation, which is a hallmark of normal cell growth, and its deregulation can lead to tumorigenesis. In sparsely populated cells, activated YAP/TAZ are in the nucleus and drive proliferation. When the cells are densely populated, YAP/TAZ are inactivated and localize in the cytoplasm to orchestrate contact inhibition of proliferation (*89*). YAP signaling is also crucial for the tumorigenesis and tumor development. In transgenic mouse models, loss of YAP suppresses oncogene-induced tumor growth (*90*).

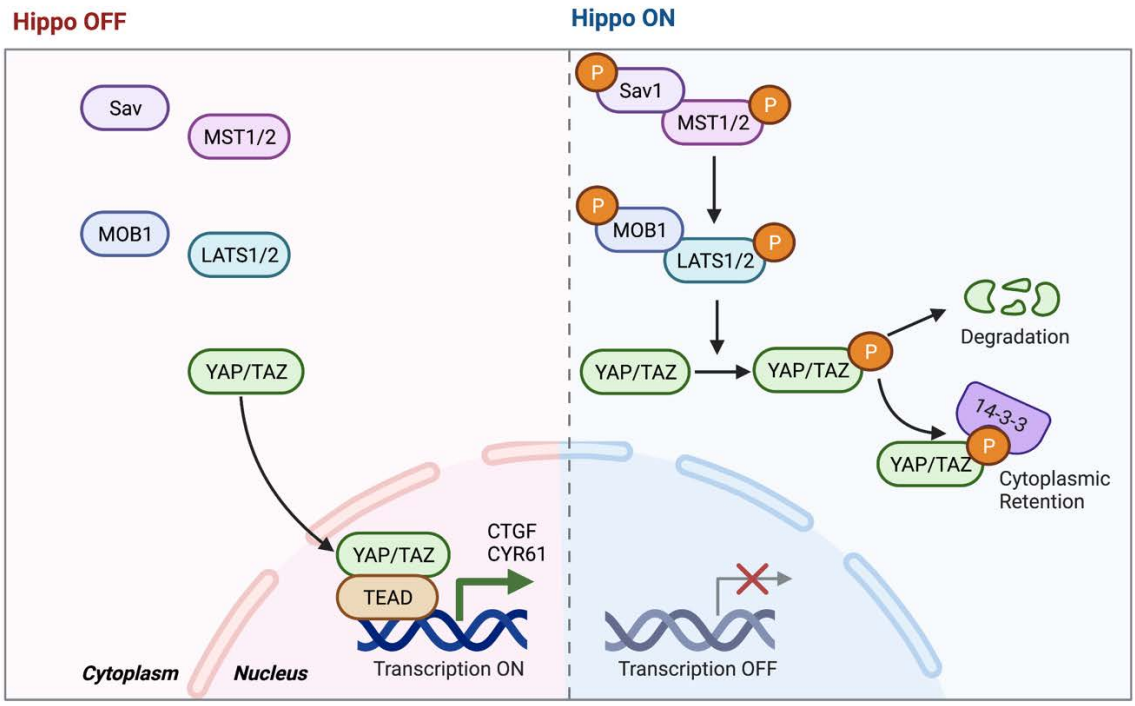

Figure 4. Core Components of Hippo Signaling Pathway.

When the tumor-suppressive Hippo signaling pathway is off, YAP/TAZ enter the nucleus, where they bind to TEAD and induce gene transcription. When Hippo pathway is on, YAP/TAZ are phosphorylated, which leads to degradation or cytoplasmic retention (*91*).

In the mechanotransduction to relay the mechanical cues, YAP/TAZ activation is found in both cancer cells and stromal cells.

1.4.2 YAP/TAZ activation by ECM stiffness in tumor cells

ECM stiffness is associated with tumor aggressiveness, and YAP activity is higher in stiffer bladder and breast cancers as opposed to that in the less rigid counterparts (*8, 92*). Matrix rigidity activates YAP/TAZ in different cancers, including

breast cancer (*23, 45, 77, 93*), lung cancer (*29, 94*), pancreatic cancer (*30, 95*), hepatocellular carcinoma (*96, 97*), prostate cancer (*94*), osteosarcoma (*98*), melanoma (*99*), and colorectal cancer (*100*). When MCF10A cells are shifted from stiff to soft matrix, YAP and TAZ translocate from the nucleus to the cytoplasm and become inactivated (*77*). The activation of YAP/TAZ by the stiff matrix can enhance tumor proliferation, migration and invasion, and drug resistance (*29, 30, 45, 47, 78, 93, 97, 100, 101*).

The molecular mechanisms underlying how ECM stiffness activates YAP/TAZ is poorly understood. One of the key mechanisms of YAP/TAZ activation in response to mechanical cues is through Rho GTPase (Rho kinase, ROCK) that regulates the formation of actin bundles, stress fibers and contractile actomyosin structures via phosphorylating myosin light chain (MLC). Rho activity and cytoskeletal tension induced by stiff matrix are required for YAP/TAZ activation, but the detailed biochemical mechanisms have not been well characterized (*78*). Ras-related GTPase RAP2 is another key intracellular molecule for YAP/TAZ activation that mediates signals from ECM stiffness. The low matrix stiffness activates RAP2, which binds to and stimulates MAP4K4s and ARHGAP29, thus activating LATS1/2 to inhibit YAP/TAZ (*77*). In addition, JNKs and MAPKs by a fstiffer matrix activates YAP in hepatocellular carcinoma cells (*97*). Furthermore, the cell structural deformation also regulates YAP/TAZ activation. The cytoskeletal contraction by a stiff matrix imposes forces to the nucleus, which flattens the nucleus, reduces mechanical restrictions, stretches nuclear pores, and enhances nuclear import of YAP (*102*). Another mechanism of YAP/TAZ activation by matrix rigidity occurs via post-translational

regulation. The stiff matrix upregulates the expression of C-X-C motif chemokine receptor 4 (CXCR4), which induces downregulation of ubiquitin domain-containing protein 1 (UBTD1) and ensuing reduced YAP ubiquitylation and degradation, and finally enhances YAP activity in cancer cells (*94, 103*).

1.4.3 YAP/TAZ activation by ECM stiffness in tumor stromal cells

Matrix stiffness activates YAP in stromal cells, which in turn orchestrates differentiation of CAFs and multiple pro-tumor functions of the stroma. YAP is required for the differentiation of mesenchymal stem cells (MSCs) (*32*) and conversion of vascular pericytes into CAFs (*104*). In MMTV-PyMT model, ROCK-mediated actomyosin contractility and Src function are crucial for YAP activation induced by matrix stiffness. YAP activation and ECM stiffening forms a feed-forward self-reinforcing loop that maintains CAF phenotypes and promotes cancer cell invasion and angiogenesis (*17*). Dickkopf-3 (DKK3) expression in the tumor stroma is associated with aggressive breast, ovarian, and colorectal cancers. DKK3 modulates the pro-tumor behaviors of CAFs by activating YAP/TAZ (*105*). YAP activation in CAFs is also triggered by increasing SNAIL1 protein on a stiff matrix (*106*). In addition, YAP/TAZ activation is required for the amino acid crosstalk between CAFs and cancer cells, in which CAFs provide aspartate for the sustaining of cancer cell growth and cancer cells supply glutamate to balance the redox state of CAFs to promote ECM remodeling (*33*). Hence, matrix stiffness-induced YAP/TAZ activation in stromal cells promotes tumor progression.

YAP/TAZ are activated in response to matrix stiffening in different cancer cells and stromal cells. Although studies have shown several upstream regulators of

YAP/TAZ and demonstrated the requirement of cytoskeletal contractile tension and ROCK in YAP/TAZ activation, the detailed biochemical mechanisms await further exploration.

Chapter 2. Materials and Methods

2.1 Cell lines

MDA-MB-231, SK-BR-3, BT-474 were obtained from ATCC. MDA-MB-231 cells were cultured in Dulbecco's Modified Eagle's Medium and Ham's F-12 Nutrient Mixture (DMEM-F12, Gibco) supplemented with Fetal Bovine Serum (FBS, 10%; Gibco) and Penicillin/Streptomycin (100 IU/ml, Corning). SK-BR-3 and BT-474 cells were cultured in RPMI 1640 medium (Gibco) supplemented with FBS (10%) and Penicillin/Streptomycin (100 IU/ml). 293FT packaging cells were from Invitrogen and cultured according to manufacturer's instructions. 293T cells and B77 cells were cultured in DMEM (Gibco) supplemented with FBS (10%) and Penicillin/Streptomycin (100 IU/ml). The mouse MMTV-Neu cell line was established in our lab as previously described (*71*). Briefly, MMTV-Neu cells were isolated from MMTV-Neu (YD) mice and dissociated by incubation with dispase (2.5 mg/ml) and collagenase type I (Invitrogen) for 2-4 hours and were then plated on Collagen I (20 μg/ml) in DMEM supplemented with FBS (10%) and Penicillin/Streptomycin (100 IU/ml). However, after three to four passages, these isolated cells lost expression of Neu (YD), presumably because of inactivation of the MMTV LTR promoter. To overcome this limitation, the cells were transduced with pWZL-Neu8142, which encodes oncogenic rat ErbB2. The transduced cell line was cultured in DMEM supplemented with FBS (10%) and Penicillin/Streptomycin (100 IU/ml). All cell lines were grown at 37 °C, 5% CO_2, and 95% humidity.

2.2 Compounds

The inhibitors purchased from Selleckchem were pre-prepared as a 10 mM stock solution in DMSO and used in *in vitro* cell assays. The inhibitors from MedChemExpress (MCE) were prepared in accordance with the manufacturer's guidelines and used in *in vivo* mouse experiments. Different solvents were used in the bulk compound solution preparation (**Table 1**). The drug concentration was adjusted in alignment with the dosage in mouse treatment. For Dasatinib, Defactinib, and Lapatinib, the following solvents were added to the drug individually and in order: 5% DMSO + 40% PEG 300 + 5% Tween 80 + 50% Saline. The final concentration of Dasatinib was 5 mg/ml or 12.5 mg/ml, Defactinib 25 mg/ml, and Lapatinib 12.5 mg/ml. For PF-562271 (PF271), the following solvents were added to the drug individually and in order: 10% DMSO + 40% PEG 300 + 5% Tween 80 + 45% Saline. The final concentration was 12.5 mg/ml.

Table 1. List of inhibitors

Inhibitor	Target	Source	Catalog #
Dasatinib (*In vitro* assays)	Src	Selleckchem	S1021
Dasatinib (*In vivo* studies)	Src	MCE	HY-10181
Saracatinib	Src	Selleckchem	S1006
PF-562271 (PF271, *In vitro* assays)	FAK	Selleckchem	S2890
PF-562271 (PF271, *In vivo* studies)	FAK	MCE	HY-10459
TAE226	FAK	Selleckchem	S2820
Defactinib	FAK	MCE	HY-12289
Lapatinib	HER2	MCE	HY-50898

2.3 Mice

For all the animal studies in the present study, the study protocols were approved by the Institutional Animal Care and Use Committee (IACUC) of UT MD Anderson Cancer Center (MDACC). Mice were housed in the pathogen-free animal facility at MDACC. Female BALB/c nude mice, female FVB/NJ mice, and female nude mice (aged 6-8 weeks) were obtained from The Jackson Laboratory. The MMTV-Neu (YD) transgenic model was established in our lab as previously described (*71*). Different tumor cell injection routes were applied to generate mammary primary and lung metastatic tumors. For the primary tumor growth experiments, cells were re-suspended in 100 μl of PBS with Matrigel in 1:1 ratio and injected into the fat pad of mammary gland number 3. The volume of the tumors was calculated as V = L x W x W/2, where L and W stand for tumor length and width, respectively. The experimental lung metastasis assays were performed as previously described (*96, 107*). Cells were re-suspended in 100 μl of PBS and injected into the tail vein with a 26G tuberculin syringe. Metastatic burden was detected through non-invasive bioluminescence imaging of experimental animals using an IVIS Spectrum. To investigate the effects of drug treatment *in vivo*, compounds were delivered once a day (qd) through oral gavage, and mice in the control group were treated with vehicle. The dosage varied among different drugs – Dasatinib: 20-50 mg/kg; PF271: 50 mg/kg; Lapatinib: 50 mg/kg; Defactinib: 100 mg/kg. Bioluminescence signals were measured once or twice per week using IVIS and quantitatively analyzed with the ROI tool in Living Image software (Xenogen) to verify successful injection into lungs right after the tail vein

injection and to monitor metastatic outgrowth after genetic perturbation or pharmaceutical inhibition.

2.4 Inducible knockdown of gene expression

Inducible shRNAs constructs were generated Gene Editing & Screening Core (GES Core), Memorial Sloan Kettering Cancer Center. shRNAs were designed using the SplashRNA algorithm (*108*). A previously described optimized lentiviral miR-E expression backbone system was used for Dox inducible LT3RENIR (Neomycin, dsRed), LT3REPIR (Puromycin, dsRed), and LT3GEPIR (Puromycin, Green) expression (*109*). The shRNA antisense guide sequences used in this project are listed below (**Table 2**).

Table 2. List of inducible shRNAs

shRNA	Vector	antisense guide sequence
Yap-1	LT3REPIR	TATTGGTTGTCATTGTTCTCAA
Yap-2	LT3REPIR	GTTAACAAAGGAATCTGTCTGC
Taz-1	LT3RENIR	TATCTGCCACAGAAATGCAGGC
Taz-2	LT3RENIR	ATTCATTGCGAGATTCGGCTGG
Ptk2-1	LT3GEPIR	CCCTGTGTACAGATTTGACAA
Ptk2-2	LT3GEPIR	ATGAGGTCATTTTTGCAAGTA

2.5 CRISPR/Cas9-mediated gene knockout

LentiCRISPRv2 vectors were used for the gene knockout (*110, 111*). Guide RNA (gRNA) oligos were designed on the CHOPCHOP website (http://chopchop.cbu.uib.no/) (*112*). The target site sequence was flanked on the 3'

end by an NGG PAM sequence. NGG PAM sequence was not included in the designed oligos (**Table 3**). Each pair of oligos were phosphorylated and annealed, followed by the ligation by Quick Ligase (NEB) to BsmBI-digested and purified LentiCRISPRv2 (antibiotic markers: Puromycin or Blasticidin) backbone vectors.

Table 3. List of gRNAs for gene knockout

Target	Oligo Design	Sequence
mLats1-1	Target	**TGAAAGCCCCAACTCACAGG**
	Oligo 1	CACCG**TGAAAGCCCCAACTCACAGG**
	Oligo 2	AAAC**CCTGTGAGTTGGGGCTTTCA**C
mLats1-2	Target	**CCTGCGCAGTCATCCCCAAG**
	Oligo 1	CACCG**CCTGCGCAGTCATCCCCAAG**
	Oligo 2	AAAC**CTTGGGGATGACTGCGCAGG**C
mLats2-1	Target	**CGGCAATATTTAGACTTTCT**
	Oligo 1	CACCG**CGGCAATATTTAGACTTTCT**
	Oligo 2	AAAC**AGAAAGTCTAAATATTGCCG**C
mLats2-2	Target	**CCCCGAAGTTTGGACCTTAT**
	Oligo 1	CACCG**CCCCGAAGTTTGGACCTTAT**
	Oligo 2	AAAC**ATAAGGTCCAAACTTCGGGG**C
hLATS1	Target	**GGTGGATTTCTGACTTGTCG**
	Oligo 1	CACCG**GGTGGATTTCTGACTTGTCG**
	Oligo 2	AAAC**CGACAAGTCAGAAATCCACC**C
hLATS2	Target	**TGTGTCTAACTGTCGGTGTG**
	Oligo 1	CACCG**TGTGTCTAACTGTCGGTGTG**
	Oligo 2	AAAC**CACACCGACAGTTAGACACA**C
mMob1a-1	Target	**AGCTGCCCAGTCATGTCGGC**
	Oligo 1	CACCG**AGCTGCCCAGTCATGTCGGC**
	Oligo 2	AAAC**GCCGACATGACTGGGCAGCT**C

mMob1a-2	Target	**CTCTCGGAAGTGGCAATCTG**
	Oligo 1	CACCG**CTCTCGGAAGTGGCAATCTG**
	Oligo 2	AAAC**CAGATTGCCACTTCCGAGAG**C
mMob1b	Target	**CAAGAAGCTCATGTCGGCCG**
	Oligo 1	CACCG**CAAGAAGCTCATGTCGGCCG**
	Oligo 2	AAAC**CGGCCGACATGAGCTTCTTG**C
hMOB1A-1	Target	**TTCCATATAACATGTTGATC**
	Oligo 1	CACCG**TTCCATATAACATGTTGATC**
	Oligo 2	AAAC**GATCAACATGTTATATGGAA**C
hMOB1A-2	Target	**AGTTGTCCAGTGATGTCAGC**
	Oligo 1	CACCG**AGTTGTCCAGTGATGTCAGC**
	Oligo 2	AAAC**GCTGACATCACTGGACAACT**C
hMOB1b	Target	**TCATACTGGTGAGAACCCTC**
	Oligo 1	CACCG**TCATACTGGTGAGAACCCTC**
	Oligo 2	AAAC**GAGGGTTCTCACCAGTATGA**C
mCtrl	Target	**GCGAGGTATTCGGCTCCGCG**
	Oligo 1	CACCG**GCGAGGTATTCGGCTCCGCG**
	Oligo 2	AAAC**CGCGGAGCCGAATACCTCGC**C
hCtrl	Target	**ACGGAGGCTAAGCGTCGCAA**
	Oligo 1	CACCG**ACGGAGGCTAAGCGTCGCAA**
	Oligo 2	AAAC**TTGCGACGCTTAGCCTCCGT**C

2.6 Mutagenesis

The site-directed mutagenesis on LATS1 and MOB1 plasmids was introduced using QuikChange II XL Site-Directed Mutagenesis Kit (Agilent Technologies) according to the manufacturer's guidelines.

2.7 Cell culture with polyacrylamide-based hydrogels

Glass coverslips were methacrylated in methacrylation buffer (20 ml of 100% Ethanol; 600 μl of 1:10 Acetic acid; 100 μl of Methacrylate) for 3 minutes. Slides were treated with DCDMS (Sigma) for 1 minute and excess DCDMS was removed with a KimWipe. 2D culture on hydrogels of high (40.40 ± 2.39 kPa) and low (1.00 ± 0.31 kPa) stiffness was prepared as described (*113*). Polyacrylamide gel solution was prepared according to the stiffness and polymerization. Human placenta fibronectin (10 μg/ml) or rat tail collagen I (25–50 μg/ml) were used to coat the sulfo-sanpah-activated hydrogels according to the preferences of the cell lines. Hydrogels were rinsed with PBS 2 times and pre-incubated with culture medium for equilibration. Cells were seeded at the density of 10,000 cells per well for high stiffness, and 20,000 cells per well for low stiffness in a volume of 680 μl per well (*77*).

2.8 MTT cell viability assay

The cell viability was tested using MTT Viability Assay Kit (Thermo Fisher Scientific). Reagents were prepared according to the manufacturer's protocol. PBS was added to MTT [3-(4,5-Dimethylthiazol-2-yl)-2,5-diphenyltetrazolium bromide] to make a 12 mM MTT stock solution. 0.01 M HCL was added to one tube of SDS and mixed by sonication. Cells were plated at 1,000-5,000 cells/well in 96-well plates for 24 hours. After 24 hours, cell medium was removed and replaced with 100 μl of fresh medium and 10 μl of MTT stock solution per well. After the incubation at 37 °C for 2-4 hours, 100 μl of the SDS-HCl solution was added to each well. After another

incubation at 37 °C for 2-4 hours, the samples were mixed by pipetting up and down, and absorbance was measured in a microplate reader at 570 nm.

2.9 Tumor sphere assay

Single cell suspensions (1,000 cells/ml) were plated on ultra-low attachment plates and cultured in serum-free PrEGM (Lonza) supplemented with B27 (1:50; Thermo Fisher Scientific), basic fibroblast growth factor (bFGF, 20 ng/ml) and epidermal growth factor (EGF, 40 ng/ml) for 10 days. Tumor spheres were visualized under phase contrast microscope, photographed, and counted. For serial passage, tumor spheres were collected using 70-mm cell strainers and dissociated with Accutase (STEMCELLTechnologies) at 37 °C for 30 minutes to obtain single cell suspensions.

2.10 Matrigel 3D culture

Dissociated cells were incubated in PrEGM medium (Lonza) supplemented with B27 (1:50), basic fibroblast growth factor (bFGF, 20 ng/ml) and epidermal growth factor (EGF, 40 ng/ml). Matrigel bed was made in 6-well plates by putting 4 separate drops of Matrigel per well (50 μl of Matrigel per drop). Plates were placed in 37 °C CO_2 incubator for 30 minutes to allow the Matrigel to solidify. For each sample, 100 μl of cell suspension was mixed with 100 μl of cold Matrigel and pipetted on top of the Matrigel bed (50 μl each). The plates were then incubated at 37 °C for another 30 min. Warm PrEGM (2.5 ml) was then added to each well. The cells were cultured and

monitored for 10-14 days with 50% of the medium replacement every 3 days. For immunostaining experiments, the cells were cultured in 8-well chamber slide. Cells were fixed with 4% paraformaldehyde for 20 minutes and proceeded to standard immunostaining protocol.

2.11 RNA extraction and quantitative RT-PCR

Total RNA was isolated using the TRIzol (Thermo Fisher Scientific) or RNeasy Mini kit coupled with RNase-free DNase set (Qiagen) according to the manufacturers' protocols. RNA was reversed transcribed using the High-Capacity cDNA Reverse Transcription Kit (Thermo Fisher Scientific). The mRNA expression was evaluated in the Real-Time PCR System Mix (Applied Biosystems), using SYBR Green PCR Master Mix (Applied Biosystems). All quantification were normalized to endogenous GAPDH. The primers used for RT-PCR are listed below (**Table 4**).

Table 4. List of primers for quantitative RT-PCR

Primer	Sequence (Forward)	Sequence (Reverse)
CTGF	CCAATGACAACGCCTCCTG	GAGCTTTCTGGCTGCACCA
CYR61	AGCCTCGCATCCTATACAACC	GAGTGCCGCCTTGTGAAAGAA
ANKRD1	TGAGTATAAACGGACAGCTC	TATCACGGAATTCGATCTGG
EDN1	CCAAGAGAGCCTTGGAGAAT	TGTCTTCAGCCCTGAGTTCTT
GAPDH	ATGGGGAAGGTGAAGGTCG	GGGGTCATTGATGGCAACAAT

2.12 Mass Spectrometry

Phosphorylated LATS was resolved using SDS polyacrylamide gel electrophoresis, followed by staining with Simply Blue and excision of the separated protein bands. *In situ* trypsin digestion of polypeptides in each gel slice was performed as described (*114*). All electrospray ionization experiments were performed using a QSTAR XL hybrid mass spectrometer (AB/MDS Sciex) hyphenated with microscale capillary reversed-phase HPLC [Famos autosampler (LC Packings), Agilent 1100 HPLC pump (Agilent)]. The columns were packed in-house using Magic C18 (5 μm, 200 Å, Michrom BioResources) beads. The buffer compositions are as follows: buffer A: 2.5% acetonitrile, 0.2% formic acid; buffer B: 2.5% H_2O, 0.2% formic acid. For the quantitative experiments, a 5-min gradient was used with mass spectra being acquired every 0.15 sec. Data analysis and quantitation was done using the Analyst software package provided by Applied Biosystems/MDS Sciex.

2.13 Immunoprecipitation

293T cells plated in 6-well plates were transiently transfected with 1 μg of pRK5 plasmid expressing FLAG-HA- tagged LATS1 and 1 μg of the plasmid expressing Src-Y527F by using Lipofectamine 3000 (Invitrogen). After 24 hours, the cells were lysed with RIPA buffer or RIPA buffer without SDS as indicated. To isolate FLAG-HA-LATS1, extracts were pre-cleared with agarose-mouse IgGs and incubated with anti-FLAG M2 Affinity Gel (Sigma) at 4 °C for 2 hours. The immunoprecipitants were washed four times with RIPA buffer or RIPA buffer without SDS as indicated, and bound proteins were dissociated in 20 μL of 1 x SDS sample buffer (25 mM Tris, pH

6.8; 4% SDS; 5% Glycerol; bromophenol blue). Eluted proteins were used for immunoblotting. Other immunoprecipitation experiments were performed following the same protocol.

2.14 Immunoblotting

Cells were lysed with NP-40 or RIPA buffer (Thermo Fisher Scientific) and then diluted in 2x or 4x Laemmli Sample Buffer (BioRad). Proteins from lysed cells or eluted from immunoprecipitation were separated on 4-12% Bis-Tris SDS-PAGE gels (Invitrogen) and transferred to Immobilon-P membranes (Millipore). Membranes were incubated in blocking buffer (5% w/v skim milk or 5% w/v BSA) at room temperature for 1 hour and then with primary antibodies diluted in 5% w/v BSA, 1X TBS, 0.1% Tween 20 at 4°C with gentle shaking, overnight. After three washes with 1x TBST, the membranes were incubated with goat anti-rabbit HRP-conjugated antibody or goat anti-mouse HRP-conjugated antibody at room temperature for 1 hour. After washing for three times with 1x TBST, membranes were subjected to chemiluminescence using ECL (Pierce). The primary antibodies used are listed below (**Table 5**).

2.15 Immunohistochemistry staining

Immunohistochemistry on paraffin-embedded sections was performed using a Discovery XT processor (Ventana Medical Systems). The tissue sections were deparaffinized with EZPrep buffer, and antigen retrieval was performed with CC1 buffer (Ventana Medical Systems). Sections were blocked for 30 minutes with

Background Buster solution (Innovex), followed by avidin-biotin blocking for 8 minutes. Sections were incubated with the primary antibody [anti-YAP; anti-pYap (S127); anti-Ki67; anti-Cleaved Caspase 3] for 5 hours, followed by a 60-minute incubation with biotinylated horse anti-rabbit (Vector Labs, # PK6101) at 1:200 dilution. The detection was performed with DAB detection kit (Ventana Medical Systems) according to the manufacturer's instruction. Slides were counterstained with hematoxylin and cover slipped with Permount (Fisher Scientific). The primary antibodies used for immunohistochemistry staining in this project are listed below (**Table 5**).

2.16 Immunofluorescence staining

For immunofluorescence staining, cells were fixed in 4% formaldehyde/PBS for 10 minutes and then were treated with 0.1% Triton X-100 at room temperature for 15 minutes. After blocking, the cells were stained with the primary antibody (anti-Yap; anti-Yap/Taz) at room temperature for 1 hour, followed by 1 hour incubation with 488/561 conjugated goat anti-rabbit/mouse [Cell signaling Technology (CST), #4412, #4413] at 1:200 dilution. Then samples were covered with ProLong Gold Antifade Reagent with DAPI (CST, #8961) and coverslips. Slides were allowed to cure in the dark at room temperature for 24 hours, then the nail polish was used to seal the coverslips. Fluorescent Images were captured with a Leica SP8 X Confocal Microscope and then were exported from Leica imaging software for further analysis. The primary antibodies used for immunofluorescence in this project are listed below (**Table 5**).

Table 5. List of primary antibodies

Antibody	Application	Source	Catalog #
YAP	IB, IF	Sigma	WH0010413M1
FAK	IB	CST	71433
p-FAK (Y397)	IB	CST	8556
YAP/TAZ	IB, IF	CST	8418
p-YAP (S127)	IB	CST	13008
CTGF	IB	Santa Cruz	Sc-14939
CYR61	IB	Santa Cruz	Sc-13100
RhoGDI	IB	Santa Cruz	sc-360
beta-actin	IB	Santa Cruz	sc-47778
HER2/ErbB2	IB	CST	4290
p-HER2/ErbB2 (Y1221)	IB	CST	2243
Src	IB	CST	2109
p-Src (Y416)	IB	CST	2101
LATS1	IB	CST	3477
p-LATS1 (T1079)	IB	CST	8654
p-Y (4G10)	IB	Sigma	05-321
MST2	IB	CST	3952
p-MOB1 (Y26)	IB	Signalway	12878
FLAG (DYKDDDDK)	IB	CST	14793
HA	IB	CST	3724
HA	IB	CST	5017
HA	IF	Invitrogen	32-6700
YAP	IHC	Invitrogen	PA1-46189
p-YAP (S127)	IHC	Invitrogen	MA5-33207
Ki67	IHC	Abcam	ab16667
Cleaved Caspase 3	IHC	CST	9661

IB: Immunoblotting; IHC: Immunohistochemistry; IF: Immunofluorescence

2.17 RNA-seq Analysis

Total RNA was isolated using the TRIzol (Thermo Fisher Scientific) or RNeasy Mini kit coupled with RNase-free DNase set (Qiagen). Three replicates for each sample were generated and analyzed. Data were sequenced and analyzed by BGI. Libraries were prepared by using the standard methodology from Illumina and run on a HiSeq2500 system. Raw reads were quality-checked and subsequently mapped to the human genome (hg19) using Tophat2 (2.2.4) with default settings (*101*). Differential gene expression was analyzed using the DESeq2 (1.8.1) package in R using default settings (*115*). Gene set enrichment analysis (GSEA) (*116*) was performed on a pre-ranked gene list that was generated based on the gene expression changes between the two groups. The hallmark gene sets, GO gene sets and KEGG pathways from the Molecular Signatures Database (MSigDB v5.1) (*116*) were evaluated by GSEA with 1,000 permutations, and those significantly (FDR < 0.1) enriched pathways and GO gene sets were reported using ggplot2 R package. Heatmap analysis was performed to show the gene expression patterns between groups, using heatmap3 R package with ward2 as distance function. Gene expressions in the heatmap were transformed in logarithm scale and normalized accordingly.

2.18 Quantification and Statistical Analysis

All the statistical details including the statistical tests used, exact number of animals, definition of center, and dispersion and precision measures for the

experiments can be found in the figures, figure legends or in the results. Statistical analyses were performed by using R and GraphPad Prism 8 software, with a minimum of three biologically independent samples for significance. For tumor injection experiments, each mouse was counted as a biologically independent sample. Results are reported as mean ± SD. Comparisons between two groups were performed by using an unpaired two-sided Student's t-test ($P < 0.05$ was considered significant, * $P<0.05$, ** $P<0.01$, ***$P<0.001$). All experiments were reproduced at least three times, unless otherwise indicated.

Chapter 3. Results

3.1 ECM stiffness activates FAK and YAP

YAP functions as an essential effector of mechanotransduction to regulate cell proliferation and differentiation (*76, 78, 93*). GTPase RAP2 has been shown to mediate nuclear-cytoplasmic shuttling of YAP in response to ECM stiffness (*77*), but what upstream signals trigger the event remains unclear. We used different breast cancer cell lines to test the effects of ECM rigidity on YAP localization. The cells were plated on polyacrylamide-based hydrogels with high (40 kPa) and low (1 kPa) stiffness. HER2 positive SK-BR-3 cells and triple negative breast cancer MDA-MB-231 cells showed robust YAP localization changes between stiff and soft matrices. The YAP localization was evaluated with immunofluorescence staining. Under conditions with higher stiffness, YAP tended to localize in the nucleus. However, the soft matrix drove the cytoplasmic translocation of YAP (**Figure 5**). The results demonstrate that YAP is activated in more rigid matrices.

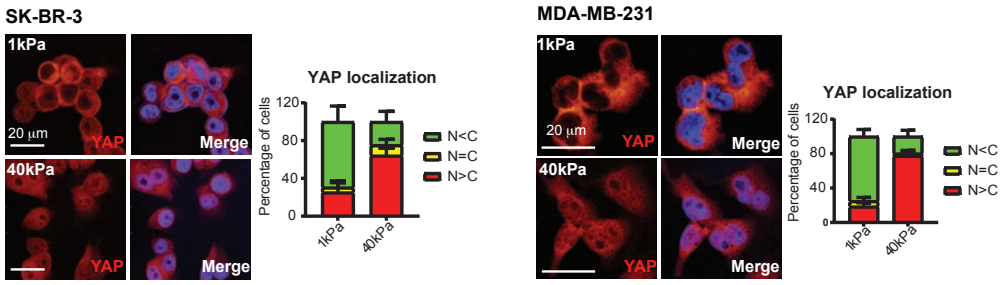

Figure 5. YAP is activated in response to higher stiffness.

Immunofluorescence and quantification of YAP localization in MDA-MB-231 and SK-BR-3 cells subjected to soft matrix (1 kPa) and stiff matrix (40 kPa). Error bars denote Mean + SD;

Scale Bars, 20 μm. (N < C, less YAP in nucleus than in cytoplasm; N = C, similar levels of YAP in cytoplasm and nucleus; N > C, more YAP in nucleus than in cytoplasm.)

Integrin signaling plays important roles in the mechanotransduction in response to ECM stiffness. FAK is a critical component of integrin signaling, which mediates the signals from mechanical signals through the phosphorylation cascade. To understand whether integrin signaling is involved in YAP activation in high stiffness, we used cell adhesion assays and tested FAK activation. Cells were plated on Fibronectin for different time points. Immunoblotting results showed increased FAK activation upon matrix adhesion compared to cells in suspension in MDA-MB-231 and SK-BR-3 cells. Meanwhile, YAP was also activated, which was suggested by reduced p-YAP and upregulation of YAP downstream targets CTGF and CYR61 (**Figure 6A**). To test whether FAK is required for YAP activation on Fibronectin, we knocked down the gene PTK2, which encodes FAK. After FAK knockdown, the p-YAP increased and CTGF decreased when the cells were plated on Fibronectin (**Figure 6B**). Consistently, FAK inhibitors PF271 and Defactinib inhibited the nuclear translocation of YAP under high stiffness (**Figure 6C**). Immunoblotting showed the similar results when the cells seeded on Fibronectin were treated with FAK inhibitors PF271 and TAE226. Both compounds suppressed YAP activation as CTGF decreased (**Figure 6D**). The mRNA levels of YAP targets, CTGF, ANKRD1, EDN1, and CYR61, were downregulated after the treatment (**Figure 6E**). Taken together, these results suggest that matrix adhesion activates YAP in a FAK-dependent manner.

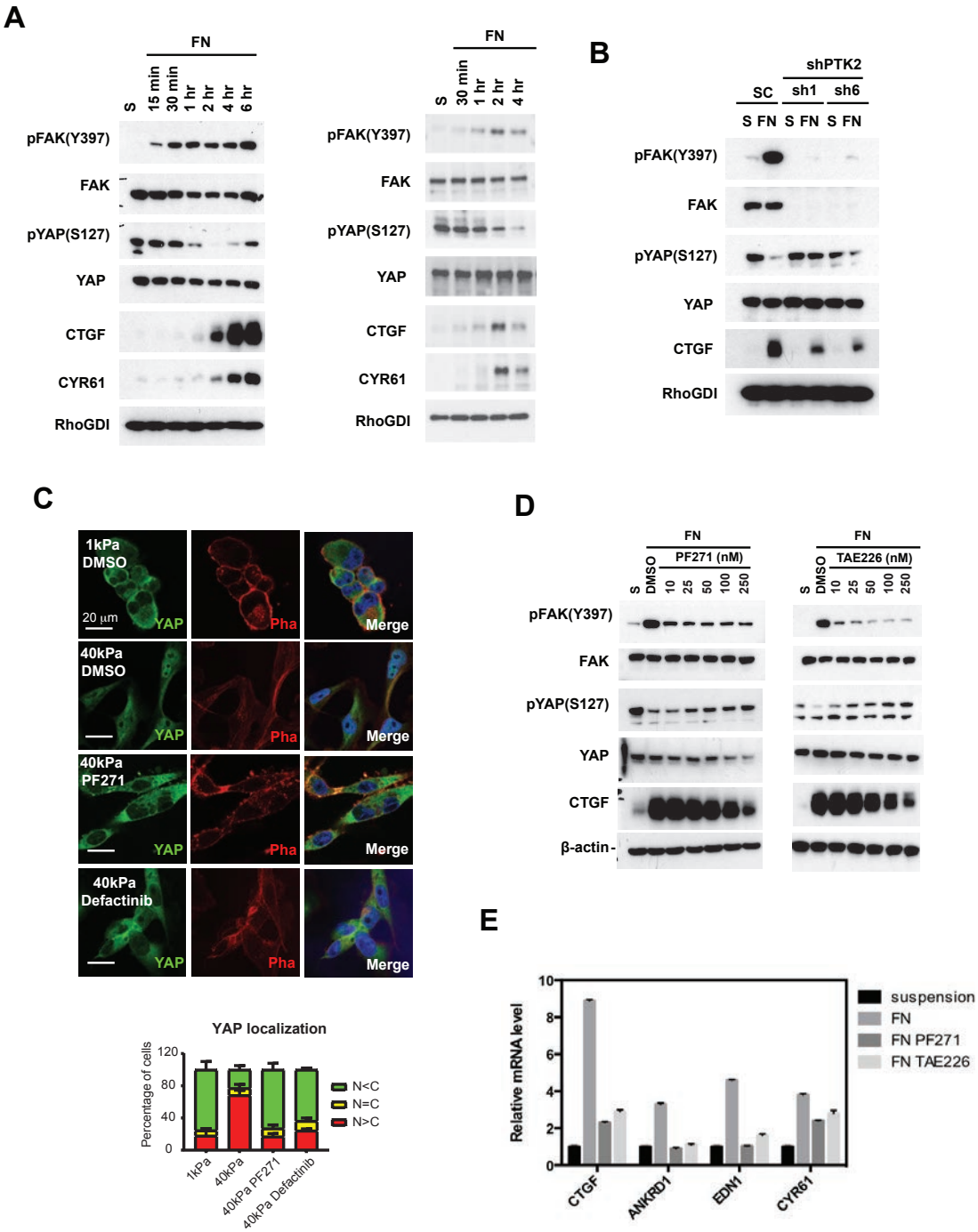

Figure 6. Matrix adhesion activates FAK and YAP.

(A) Immunoblotting with indicated antibodies in MDA-MB-231 cells and SK-BR-3 cells subjected to Fibronectin (FN) at different time points.

(B) Immunoblotting with indicated antibodies in control and shPTK2 MDA-MB-231 cells seeded in suspension (S) or on Fibronectin (FN).

(C) Immunofluorescence imaging and quantification of YAP localization in MDA-MB-231 cells subjected to soft matrix (1 kPa) and stiff matrix (40 kPa). Under stiff conditions, YAP localization was compared across treatment with DMSO and FAK inhibitors PF271 and Defactinib. Error bars denote Mean + SD; Scale Bars, 20 μm.

(D) Immunoblotting of indicated antibodies in MDA-MB-231 cells on Fibronectin with DMSO or different concentrations of FAK inhibitors PF271 and TAE226.

(E) qPCR of CTGF, ANKRD1, EDN1, CYR61 mRNAs in MDA-MB-231 cells seeded in suspension or on Fibronectin with DMSO or FAK inhibitors PF271 and TAE226.

In addition to FAK, we also tested whether another important component in integrin signaling, SFKs, is also required in the YAP activation induced by integrin-mediated mechanotransduction in breast cancer by using the SFK inhibitor, Dasatinob, and compared the effects of Dasatinib with FAK inhibor, PF271. In phos-tag immunoblotting, YAP phosphorylation was induced by both PF271 and Dasatinib (**Figure 7A**). Immunofluorescence staining showed that both Dasatinib and PF271 induced YAP translocation into the cytoplasm, but Dasatinib had more robust effects (**Figure 7B**). Taken together, these results demonstrate that integrin signaling activates YAP via FAK/SFKs.

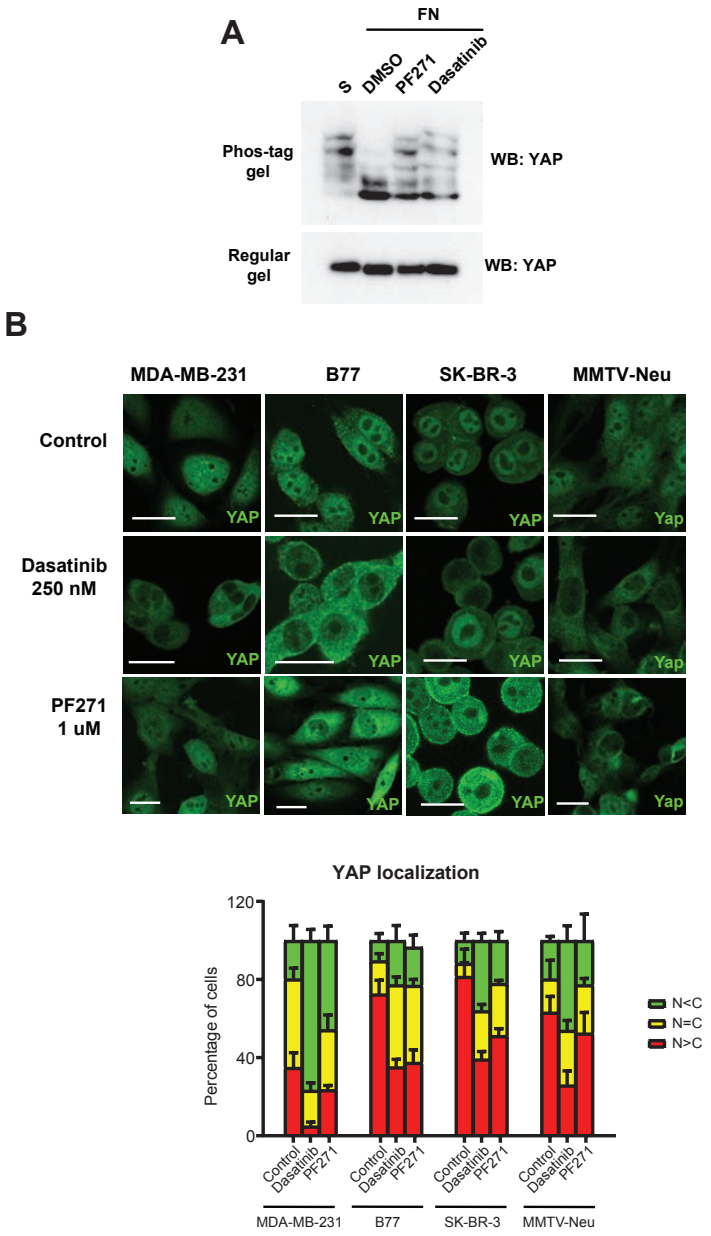

Figure 7. Dasatinib and PF271 inhibits YAP activation.

(A) Immunoblotting of YAP with Phos-tag gel and regular gel in MDA-MB-231 seeded in suspension or on Fibronectin with DMSO, PF271, or Dasatinib.

(B) Immunofluorescence imaging and quantification of YAP localization after treatment with Dasatinib or PF271 in MDA-MB-231, B77, SK-BR-3 and MMTV-Neu cells. Error bars denote Mean + SD. Scale Bars, 20 μm.

3.2 ECM stiffness acts via HER2 to regulate FAK and YAP

To test if ECM stiffness acts through HER2 to regulate YAP, we compared the effects of HER2 on ECM rigidity induced YAP activation in SK-BR-3. We activated HER2 receptor by adding different concentrations of the ligand Neuregulin in soft and stiff matrices. Immunofluorescence staining revealed that in soft matrix, where YAP remains in the cytoplasm, a low dose of Neuregulin was enough to drive YAP from the cytoplasm into the nucleus (**Figure 8A**). Immunoblotting also showed that Neuregulin activated FAK, YAP and YAP downstream effectors, CYR61 and CTGF (**Figure 8B**).

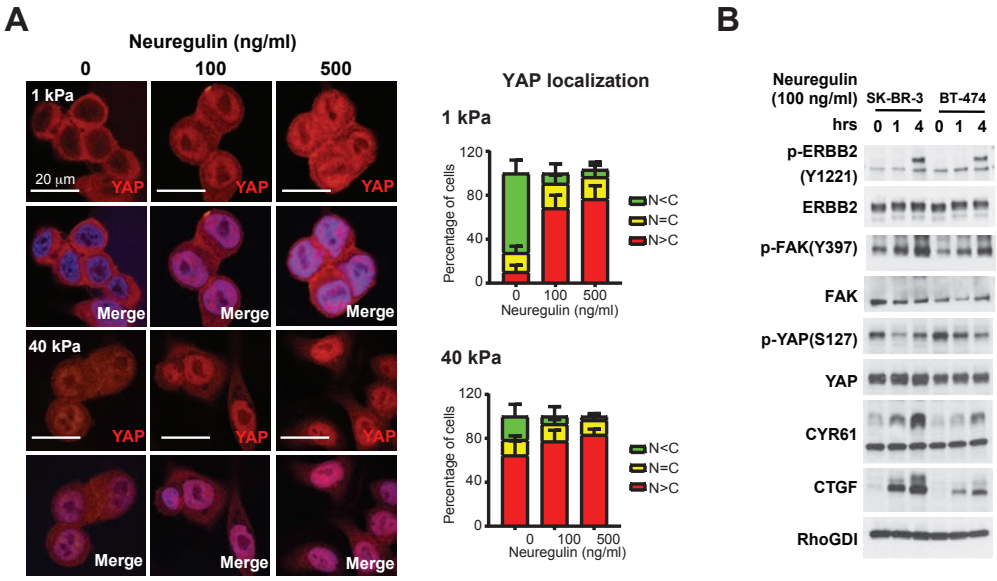

Figure 8. HER2 ligand Neuregulin induces FAK and YAP activation.

(A) Immunofluorescence imaging and quantification of YAP localization in SK-BR-3 cells treated with different concentrations of Neuregulin in soft (1 kPa) and stiff (40 kPa) matrices. Error bars denote Mean + SD; Scale Bars, 20 μm.

(B) Immunoblotting with indicated antibodies in SK-BR-3 cells and BT-474 cells treated with Neuregulin at different time points.

To inactivate HER2, we used the HER2 inhibitor Lapatinib. Lapatinib promoted cytoplasmic translocation of YAP in SK-BR-3 cells seeded on stiff matrix. Same results were also found in MMTV-Neu, a mouse Her2 positive cell line (**Figure 9A**). Consistent with the staining data, immunoblotting showed that Lapatinib dramatically reduced FAK and YAP activity and the expression of downstream targets (**Figure 9B**). These results indicate that ECM stiffness activates FAK and YAP through HER2.

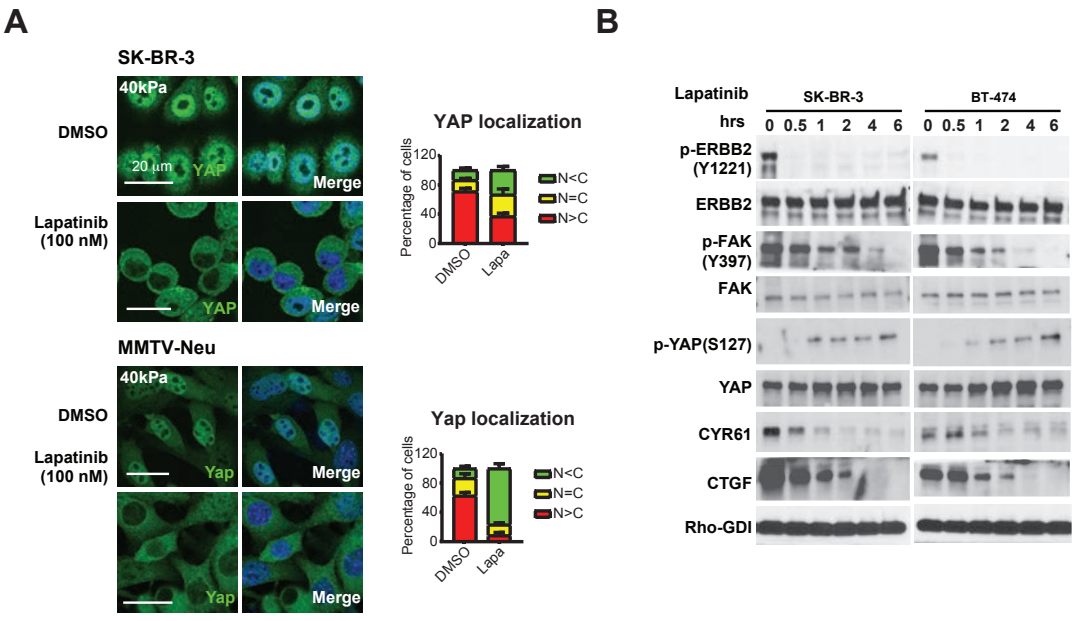

Figure 9. HER2 inhibitor Lapatinib decreases FAK and YAP activation.

(A) Immunofluorescence imaging and quantification of YAP localization in SK-BR-3 cells and MMTV-Neu cells treated with Lapatinib. Error bars denote Mean + SD; Scale Bars, 20 μm.

(B) Immunoblotting with indicated antibodies in SK-BR-3 cells and BT-474 cells treated with Lapatinib at different time points.

To study the connection between HER2 and YAP in breast cancer patients, we examined patient dataset and found that high YAP mRNA level correlated with poor prognosis only in HER2 positive breast cancer but not in other subtypes (**Figures 10-11**). The previous study also demonstrates that ECM stiffness is increased in more aggressive subtypes (triple negative and HER2 positive) of breast cancer compared to less aggressive subtypes (Luminal A and B) (*8*). This further supports the hypothesis that YAP activation via HER2 in response to stiff ECM is crucial for tumor progression. Taking this into consideration, we began to investigate whether we can exploit our findings to develop novel therapies to improve the efficacy of current treatment with HER2 inhibition. To do so, revealing the detailed mechanisms underlying the YAP activation upon high stiffness became urgent.

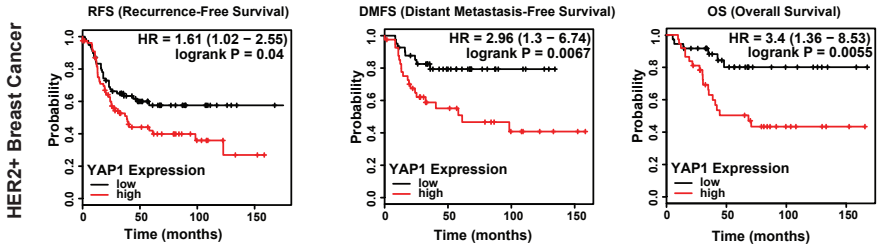

Figure 10. YAP1 expression is correlated with poorer prognosis in HER2 positive breast cancer.

Kaplan-Meier plot showing the expression of YAP1 is correlated with reduced RFS (Recurrence-Free Survival), DMFS (Distant Metastasis-Free Survival), and OS (Overall Survival) in HER2-positive patients.

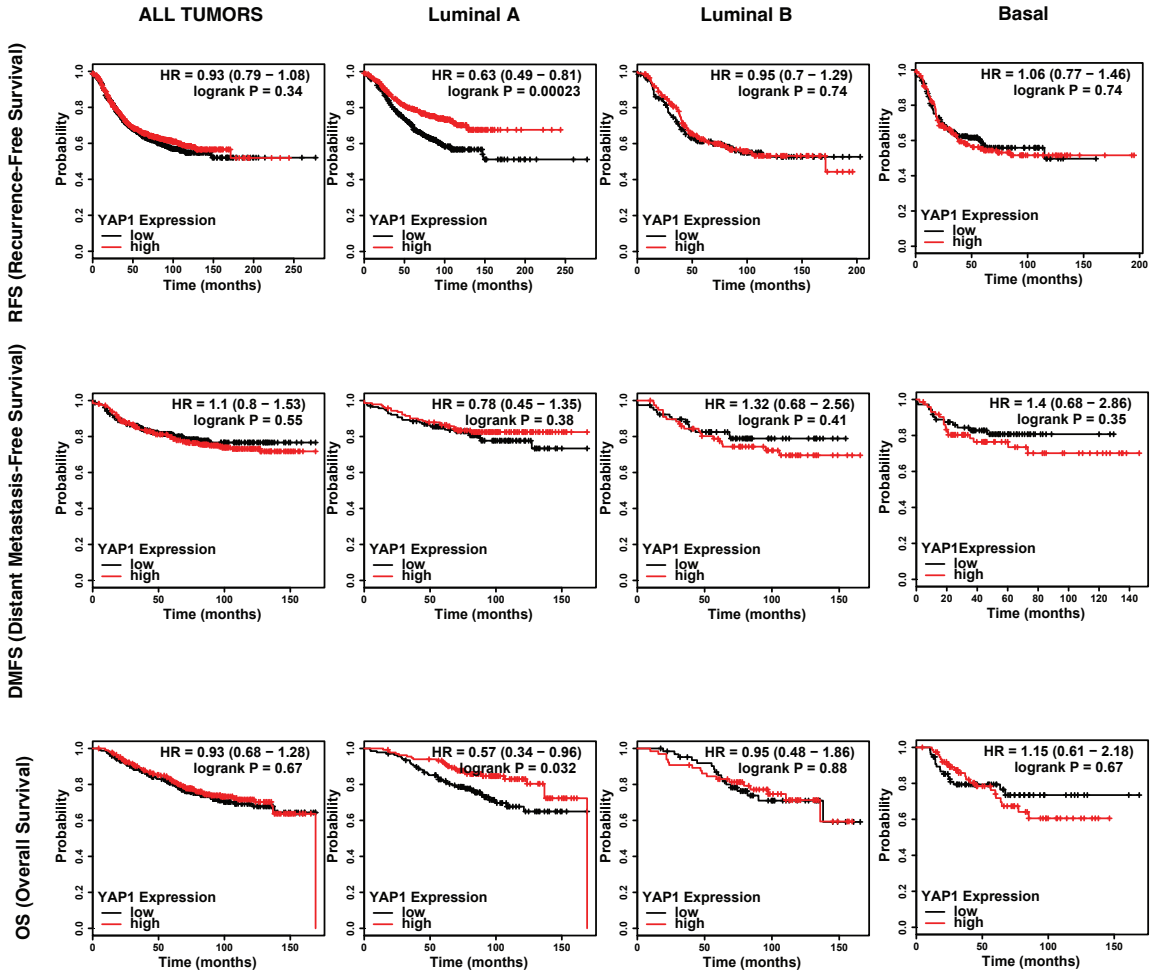

Figure 11. YAP1 expression does not show correlation with prognosis in other subtypes of breast cancer.

Kaplan-Meier plot showing the expression of YAP1 is not correlated with RFS, DMFS, or OS in Luminal A, Luminal B and Basal-like breast cancer patients.

3.3 Active Src induces tyrosine phosphorylation of LATS1

To delineate the mechanisms through which the integrin pathway regulates Hippo pathway, Co-IP experiment was performed to check the interaction between the integrin signaling components and Hippo pathway members. FLAG-FAK was immunoprecipitated and subsequent immunoblotting data showed that FAK and Src, which belong to the integrin pathway, and LATS1, which is included in Hippo pathway, were in the same complex when treated with Fibronectin, whereas disassociated when treated with the FAK inhibitor PF271 (**Figure 12A**). Since both FAK and Src are tyrosine kinases, we speculate that a direct phosphorylation exists. Surprisingly, we found Src, but not FAK, could phosphorylate LATS1 (**Figure 12B**). Moreover, Hippo pathway co-transcription factor YAP was not phosphorylated by neither co-transfected FAK nor Src (**Figure 12C**).

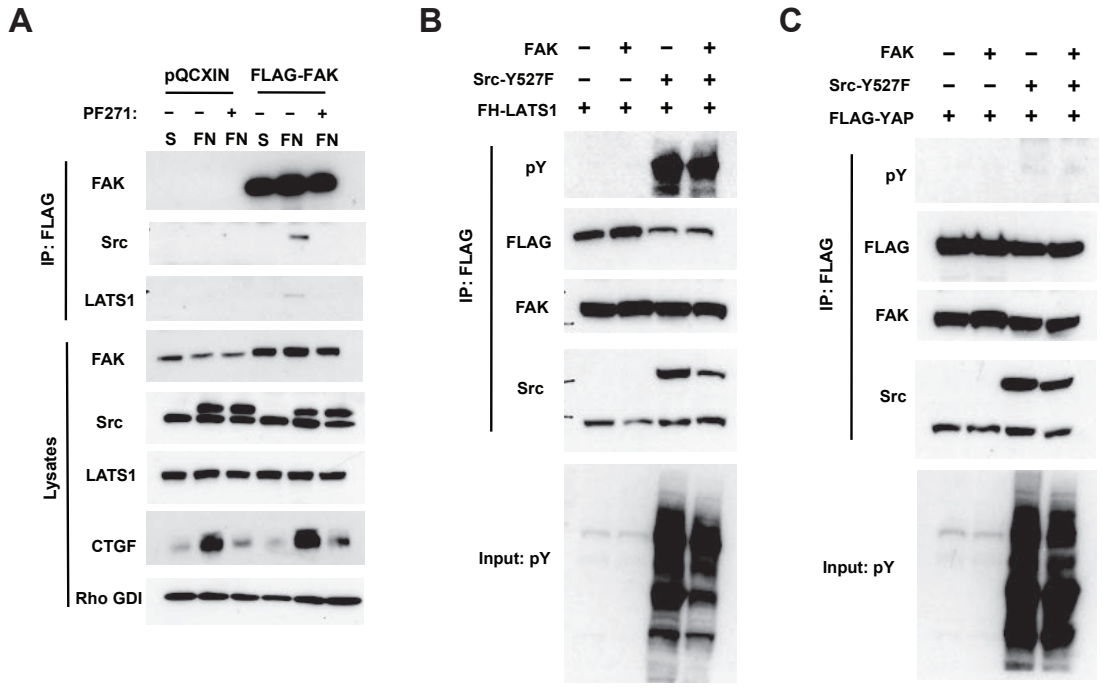

Figure 12. Src, but not FAK, induces tyrosine phosphorylation of LATS1.

(A) 293T cells were seeded in suspension or on Fibronectin with DMSO or PF271, and co-transfected with pQCXIN or pQCXIN-FLAG-FAK and Src-GFP. Immunoprecipitation was performed followed by immunoblotting with indicated antibodies.

(B) 293T cells were transfected with FH-LATS1 with FAK or Src-Y527F. FH-LATS1 was immunoprecipitated and immunoblotted with indicated antibodies.

(C) 293T cells were transfected with FLAG-YAP with FAK or Src-Y527F. FLAG-YAP was immunoprecipitated and immunoblotted with indicated antibodies.

Further analysis indicated that the constitutively active form of Src, Src-Y527F, induced a more robust signal than wild type Src, whereas the kinase dead form, Src-K295R, did not lead to LATS1 tysorine phosphorylation (**Figure 13A**). Consistently, the Src inhibitor Saracatinib, but not FAK inhibitor PF271, could block Src-induced LATS1 phosphorylation (**Figure 13B**). *In vitro* assay using gradient concentrations of purified GST-Src revealed that the phosphorylation on LATS1 by Src was direct (**Figure 13C**). To examine whether the phosphorylation was conserved, SFKs members Yes and Fyn, and LATS1 homolog protein LATS2 were tested. All Src family proteins phosphorylated both LATS1 and LATS2 (**Figure 13D**). These findings confirm that SFKs induces tyrosine phosphorylation of LATS1.

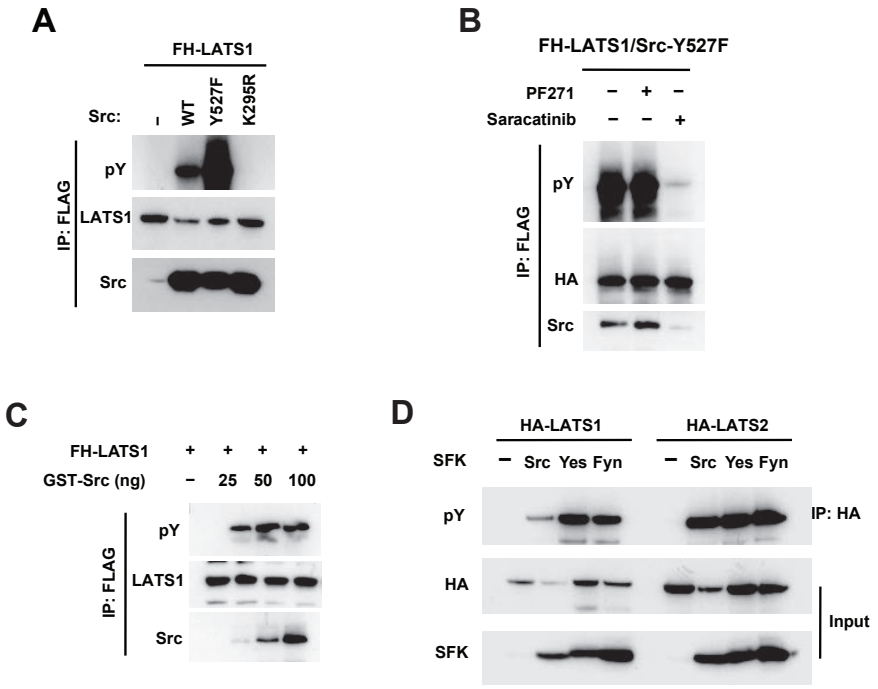

Figure 13. SFKs induces tyrosine phosphorylation of LATS.

(A) FH-LATS1 and Control vector, wild type Src, constitutively active form Src-527F, kinase dead form Src-295R were co-expressed in 293T cells. FH-LATS1 was immunoprecipitated and pY was detected by immunoblotting.

(B) FH-LATS1 and Src-527F were co-expressed in 293T cells. After the treatment with FAK inhibitor PF271 and SRC inhibitor Saracatinib, FH-LATS1 was immunoprecipitated and pY was detected by immunoblotting.

(C) FH-LATS1 was immunoprecipitated from 293T cells after adding different doses of purified GST-Src protein, followed by immunoblotting with indicated antibodies.

(D) HA-LATS1/2 was co-expressed with Src family kinase members, Src, Yes and Fyn, in 293T cells and immunoprecipitated followed by immunoblotting with indicated antibodies.

The core of Hippo signaling was a kinase cascade: Ser/Thr kinase MST1/2 directly phosphorylates LATS1/2, and then LATS1/2 phosphorylates YAP/TAZ, leading to the cytoplasmic retention, and thereby inactivating YAP/TAZ and downstream signaling (14). Immunoblotting results showed that MST1/2, especially MST2 induced YAP phosphorylation and decreased YAP target gene expression, but co-expression of MST2 and active Src decreased YAP phosphorylation level. These results indicate that Src functions downstream of MST2 to inhibit LATS1 kinase activity (**Figure 14**).

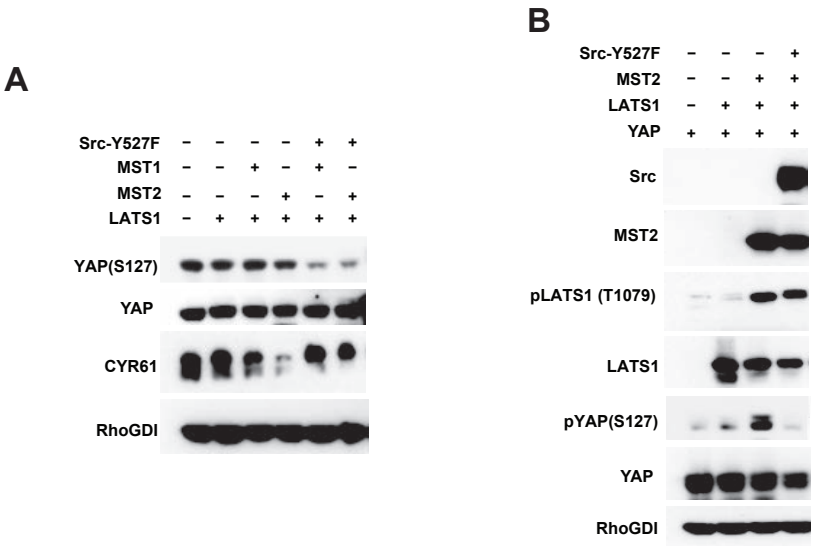

Figure 14. Src functions downstream of MST2 to regulate LATS1 activity.

(A) 293T cells were transfected with indicated plasmids. Cell lysates were subjected to immunoblotting with indicated antibodies.

(B) 293T cells were transfected with MST2, LATS1, YAP, and Src-527F as indicated. Cell lysates were subjected to immunoblotting with indicated antibodies.

3.4 Src-induced LATS1 phosphorylation activates YAP

To test whether LATS1 phosphorylation by Src could change YAP localization, we performed the immunofluorescent staining in 293A cells and found that co-expression of active Src-Y527F, but not kinase dead Src-K295R, dramatically increased YAP nuclear translocation. These results suggest that Src promotes YAP activity in a kinase-dependent manner (**Figure 15**).

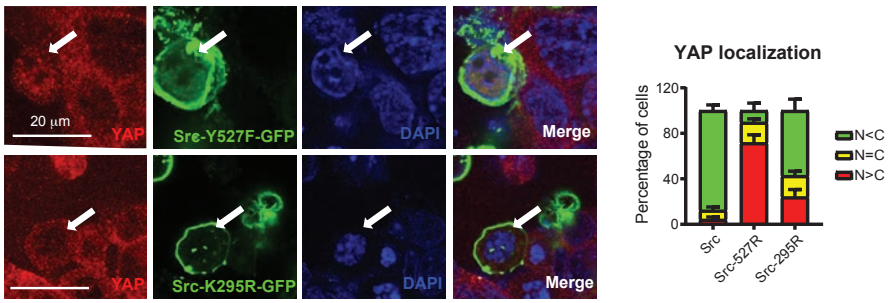

Figure 15. Active Src induces YAP nuclear translocation.

Immunofluorescence imaging and quantification of YAP localization after expressing constitutively active form Src-527R or kinase dead form Src-295R. Error bars denote Mean + SD. Scale Bars, 20 μm.

To further evaluate the roles of Src in breast cancer cells, RNA-seq analysis was performed in MDA-MB-231 and MMTV-Neu cells treated with vehicle or Dasatinib, also with siControl or siSrc. Gene Set Enrichment Analysis (GSEA) indicated YAP conserved signature was enriched in the DMSO treated group compared to Dasatinib treated group. SiCtrl group also showed enriched YAP conserved signature in

comparison with siSrc (**Figure 16**). In B77 cells, compared to the Dasatinib treated group, the control group also showed enriched Yap signature. These results demonstrate that integrin pathway tyrosine kinase Src induces YAP activation.

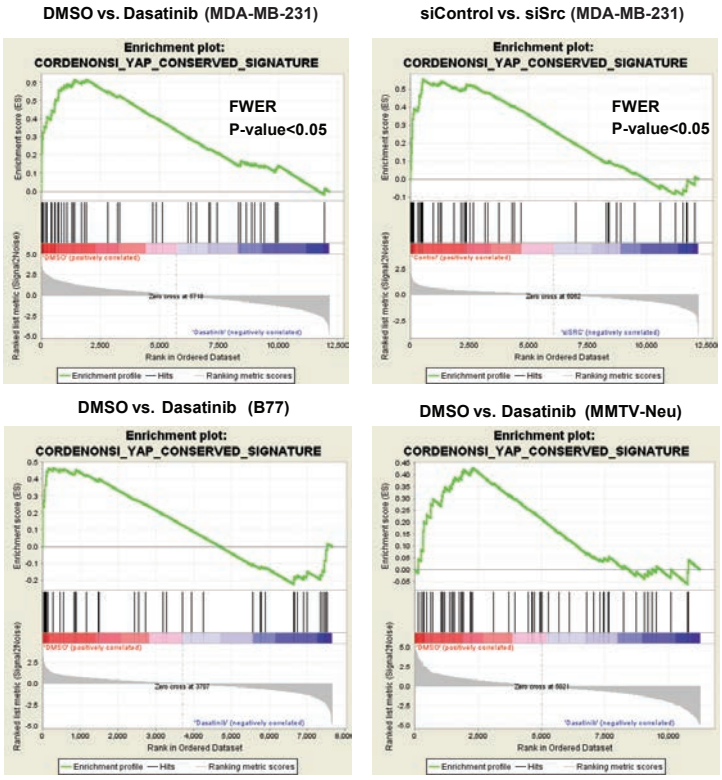

Figure 16. Gene set enrichment analysis of YAP signature after Dasatinib treatment and siSrc.

GSEA of RNA-seq data from MDA-MB-231 cells treated with Dasatinib or genetically silenced with siSrc, and B77 and MMTV-Neu cells treated with Dasatinib.

3.5 Mapping phosphorylation sites on LATS1

To determine the phosphorylation sites on LATS1, two rounds of Mass Spectrometry analysis were carried out and 23 potential phosphorylated sites were found in total (**Table 6 and Figure 17A**).

Table 6. Mass spectrometry indicates potential Src-induced tyrosine phosphorylation sites on LATS1.

		1st	2nd
Peptide Sequence:	Residue #:	Ratio of mod/unmod	Ratio of mod/unmod
TFPASN**Y**TVSSR	Tyr 23	14/136=**0.103**	7/136=**0.051**
HGPPLGESVA**Y**HSESPNSQT	Tyr 200	12/66=**0.18**	1/12=**0.08**
RYSGNME**Y**VISR	Tyr 283	36/152=**0.24**	5/1=**5**
R**Y**SGNMEYVISR	Tyr 277	7/152=**0.05**	
R**Y**SGNME**Y**VISR	Tyr 277 and 283	6/116=**0.05**	
EAPN**Y**QGPPPPYPK	Tyr 552	1/80=**0.01**	1/18=**0.056**
EAPNYQGPPPP**Y**PK	Tyr 559	2/77=**0.03**	
HLLHQNPSVPP**Y**ESISKPSK	Tyr 573	44/168=**0.26**	21/138=**0.152**
EDESEKS**Y**ENV	Tyr 597	2/13=**0.15**	
IQS**Y**SPQAFK	Tyr 634	2/116=**0.02**	2/134=**0.015**
L**Y**YSFQDK	Tyr 769	1/1=**1**	
DKDNL**Y**FVM	Tyr 779	26/14=**1.9**	
D**Y**IPGGDMMSLLIR	Tyr 784	8/13=**0.62**	
F**Y**IAELTCAVESVHK	Tyr 808	1/82=**0.01**	
WTHDSK**Y**YQSG	Tyr861	1/1=**1**	
CLAHSLVGTPN**Y**IAPEVLLR	Tyr 916	1/128=**0.008**	2/12=**0.17**
QQSAS**Y**IPK	Tyr 1026	1/78=**0.01**	1/5=**0.2**
DTLNGW**Y**K	Tyr 1065	7/21=**0.33**	
NGKHPEHAF**Y**EFTFR	Tyr 1076	10/22=**0.45**	
DDNGGYP**Y**NYPKPIEY	Tyr 1092	5/13=**0.38**	
DDNGG**Y**PYNYPKPIEY	Tyr 1090	1/8=**0.13**	
NRDLV**Y**V	Tyr 1129		1/2=**0.5**

According to the ratio of mod/unmod and the conservation, Y916, Y1026 and Y1076 were chosen to be tested. First, single site mutations were introduced and examined. Tyrosine was mutated to phenylalanine at Y916, Y1026 and Y1076 (Y916F, Y1026F, Y1076F) so they cannot be phosphorylated. When the mutated

forms were co-transfected with Src-Y527F, each single mutation form of LATS1 showed decreased tyrosine phosphorylation level, which demonstrated the possibility that each site contributes to the phosphorylation by Src. Next, combinational mutation on all the three sites (3YF) was tested and the tyrosine phosphorylation was completely blocked (**Fig. 17B**). These findings show that all three tyrosine sites, Y916, Y1026 and Y1076, are phosphorylated by Src.

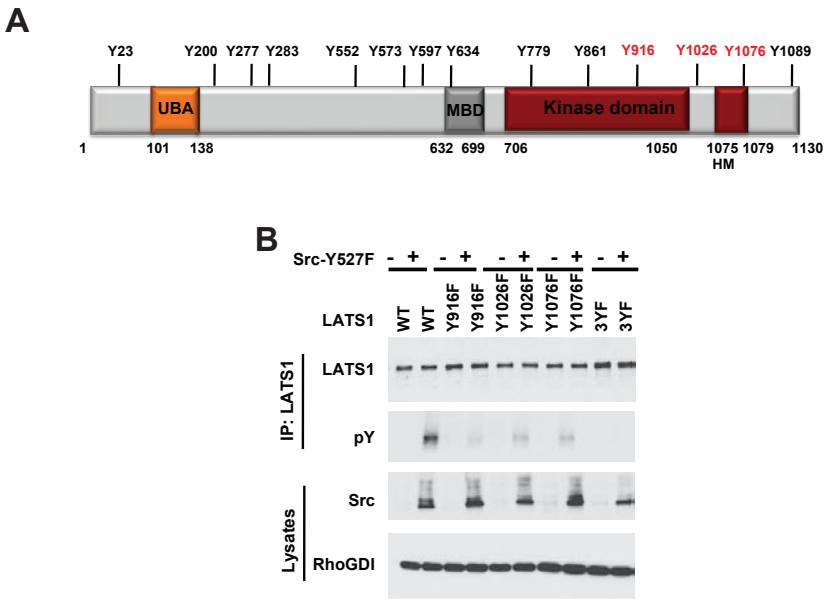

Figure 17. Mapping of LATS1 tyrosine phosphorylation sites by Src.

(A) A schematic illustration of domains and motifs of LATS1 and Tyr phosphorylation sites identified in Mass spectrometry mapping.

(B) 293T cells were co-transfected with Src-527F and LATS1 (wild type and different mutated forms), then LATS1 was immunoprecipitated followed by immunoblotting with indicated antibodies.

3.6 Mutation of Y916/Y1026/Y1076 largely prevents tyrosine phosphorylation of LATS1

To further understand the roles of these phosphorylation sites, the antibodies specifically targeting the phosphorylated LATS1 on each site were made and examined. Dot blotting showed all three antibodies worked well (**Figure 18A**). Consistently, the phosphorylation specific antibodies showed Src phosphorylated all three sites on wild type LATS1, but not mutant LATS1-3YF (**Figure 18B**). These results suggest that mutating three tyrosine sites together prevents LATS1 phosphorylation by Src.

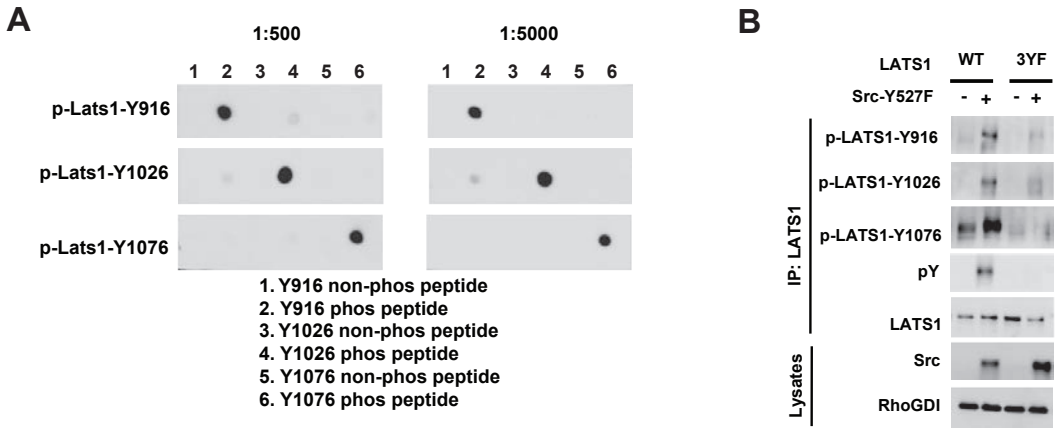

Figure 18. Generation and validation of the site-specific antibodies targeting phosphorylated LATS1 (Y916/Y1026/Y1076).

(A) Dot blotting of the phosphorylation specific antibodies targeting p-LATS1-Y916, p-LATS1-Y1026, and p-LATS1-Y1076.

(B) Src-527F and LATS1 or LATS1-3YF were co-expressed, and LATS1 was immunoprecipitated and immunoblotted with phosphorylation specific antibodies.

3.7 LATS1-Y916/1026/1076E robustly increases YAP translocation to the nucleus and promotes breast cancer cell invasive growth

After the validation of the Src-induced tyrosine phosphorylation at Y916/Y1026/Y1076 on LATS1, we evaluated the functions of these three sites. LATS1/2 knockout 293A cells were generated, and then wild type and different mutation forms of LATS1 were re-introduced. YAP tended to localize in the nucleus when LATS1/2 were knocked out, which was consistent with inhibitory function of LATS1/2 on YAP activation. Re-introduction of wild type LATS1 drove YAP out of the nucleus. However, re-introduction of LATS1-3YE, the form in which three tyrosine sites were mutated to glutamic acid to mimic the highly-phosphorylation state, could not induce the cytoplasmic translocation of YAP. In comparison, the re-introduction of single site mutation versions, LATS1-Y916E, -Y1026E, and -Y1076E, only partially changed the YAP shuttling between the cytoplasm and the nucleus (**Figure 19A**). To further confirm this conclusion, we preformed the same assays in MMTV-Neu cells and B77 cells and got the similar results (**Figure 19B**). These results suggest that highly phosphorylated LATS1 loses the inhibitory function on YAP and enhances YAP activation.

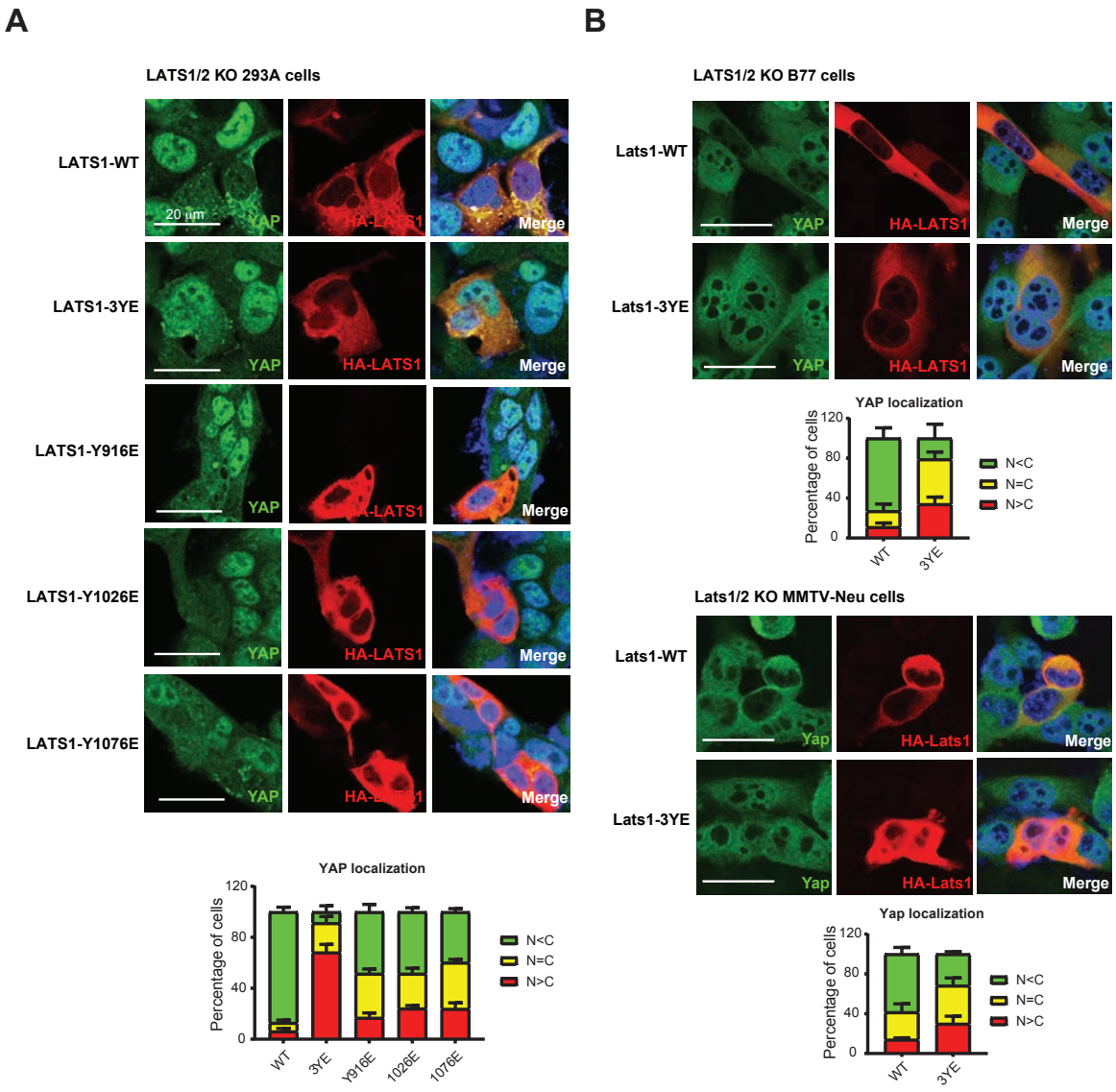

Figure 19. LATS1-3YE, but not LATS1-WT, robustly increases YAP translocation to the nucleus in LATS1/2 knockout cells.

(A-B) Immunofluorescence imaging and of YAP (GFP) and HA-LATS1 (RFP) in LATS1/2 knockout 293A (A), B77 and MMTV-Neu (B) cells re-introduced with wild type LATS1 or different forms of mutant LATS1. Error bars denote Mean + SD; Scale Bars, 20 μm.

To investigate the roles of the LATS1 phosphorylation on transcription level of YAP, a YAP promoter reporter named 8xGTII-RFP, which fused a destabilization domain to the RFP under the control of a YAP-responsive promoter, was introduced. Adding the stabilizer to cells leads to RFP accumulation when YAP is active. On one hand, re-introducing wild type LATS1 in LATS1/2 knockout cells dramatically decreased RFP level. On other hand, re-introduction of LATS1-3YE couldn't suppress the reporter level, revealed by the increasing merged Cy2 and Cy3 signals (**Figure 20**). The reporter assay demonstrates that LATS1 phosphorylation transcriptionally activates YAP.

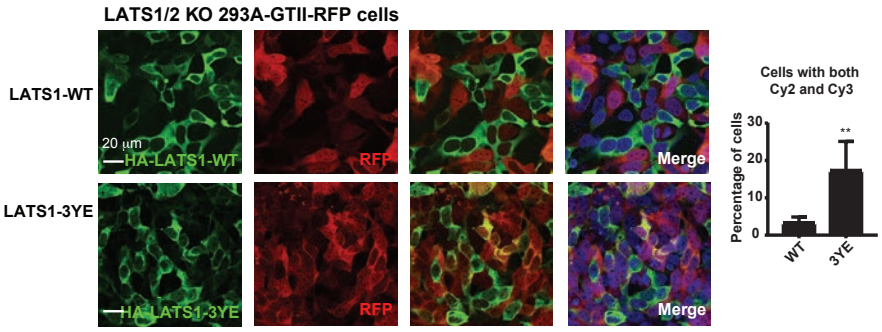

Figure 20. LATS1-3YE transcriptionally activates YAP in LATS1/2 knockout cells.

HA-LATS1-WT and HA-LATS1-3YE were expressed in LATS1/2 knockout 293A-GTII-RFP cells. HA-LATS1 (GFP) and YAP reporter (RFP) were examined by immunofluorescence and quantified. Error bars denote Mean + SD; P values (two-tailed t-test): **p<0.01; Scale Bars, 20 μm.

To further corroborate the roles of LATS1 phosphorylation in cell growth and invasion, invasive growth assays on Matrigel with or without collagen assay were performed in both Lats1/2 knock out MMTV-Neu cells and B77 cells. On soft and stiff Matrigel, only wild type Lats1 but not Lats1-3YE suppressed clone size and branching respectively, indicating Lats1 phosphorylation affected cell growth and invasion (**Figure 21A**). To study the effects of the Last1 phosphorylation on cell stemness features, which was a critical function of YAP/TAZ, tumor sphere assays were carried out in both Lats1/2 knockout MMTV-Neu cells and B77 cells. Tumor sphere formation was suppressed by wild type Lats1 but not mutant Lats1-3YE (**Figure 21B**). These results support the conclusion that LATS1 phosphorylation induced by Src has great impacts on YAP-mediated cell growth, invasion, and cell stemness traits, and highly phosphorylated LATS1-3YE can induce activation of YAP.

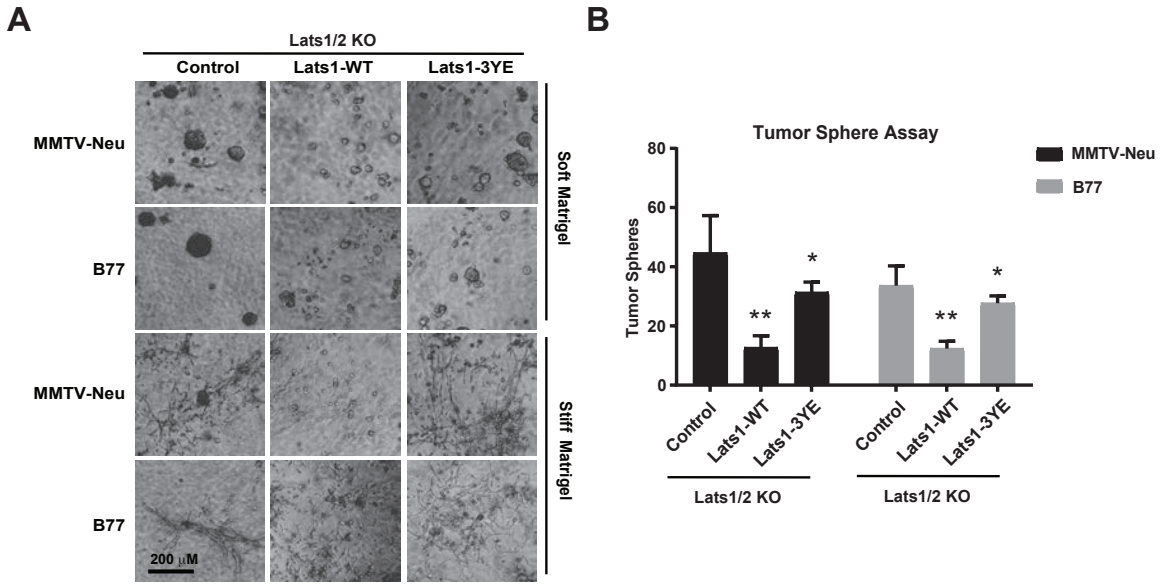

Figure 21. LATS1-3YE, but not LATS1-WT, promotes cell growth, invasion, and tumor sphere formation in LATS1/2 knockout cells.

(A) Cell growth and invasion assays on Soft Matrigel (Matrigel only) and Stiff Matrigel (Matrigel with collagen) in LATS1/2 knockout MMTV-Neu and B77 cells re-introduced with LATS1-WT and LATS1-3YE. Scale Bars, 200 μm.

(B) Quantification of tumor sphere assays in LATS1/2 knockout MMTV-Neu and B77 cells re-introduced with LATS1-WT and LATS1-3YE. Error bars denote Mean + SD; P values (two-tailed t-test): *p<0.05, **p<0.01.

3.8 Active Src induces tyrosine phosphorylation of MOB1

FAK has been shown to directly phosphorylate MOB1, a scaffold protein as part of the complex with LATS1 in the Hippo core kinase cascade, to activate YAP (20). To examine if this also applies to our system, MOB1 were co-transfected with active form Src or FAK in 293T cells, and tyrosine phosphorylation levels were tested. To our surprise, no obvious phosphorylation signal was detected when MOB1 was co-expressed with FAK, but a robust phosphorylation band appeared in the co-expression with Src, indicating Src also phosphorylated MOB1 (**Figure 22A**). To test if Src or FAK can phosphorylate other Hippo pathway components, MST1/2 and SAV were co-expressed with Src or FAK, and no phosphorylation was observed (**Figure 22B**). The published paper demonstrated MOB1-Y26 was phosphorylated by FAK (20) and p-MOB1-Y26 antibody was commercially available. Therefore, the phospho-dead MOB1-Y26F mutagenesis was introduced and tested first. Constitutively active Src, but not kinase dead Src, phosphorylated both wild type MOB1 and mutant MOB1-Y26F, suggesting Y26 was not the right site or not the only site for MOB1 phosphorylation by Src (**Figure 22C**).

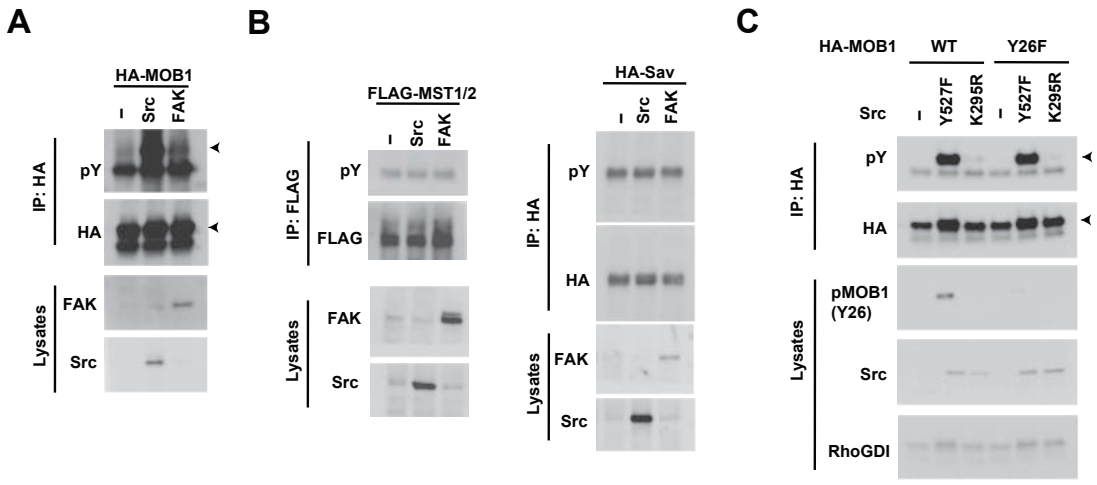

Figure 22. Active Src induces tyrosine phosphorylation of MOB1.

(A) 293T cells were co-transfected with HA-MOB1 and Src or FAK. Immunoprecipitation was performed followed by immunoblotting with indicated antibodies.

(B) FLAG-MST1/2, HA-SAV were co-transfected with Src or FAK in 293T cells. Immunoprecipitation was performed followed by immunoblotting with indicated antibodies.

(C) Wild type HA-MOB1 or mutant HA-MOB1-Y26F was co-expressed with Src in 293T cells, followed by immunoprecipitation and immunoblotting with indicated antibodies.

3.9 Identification of MOB1 phosphorylation sites by Src

Given MOB1 is a relatively small protein which only has 8 tyrosine sites, we performed single point mutagenesis for all the 8 sites individually from tyrosine to phenylalanine to make it phospho-dead and tested one by one. In the immunoblotting, none of the single mutations blocked MOB1 phosphorylation by Src, suggesting multiple tyrosine phosphorylation sites existed on MOB1 (**Figure 23A**). To map the exact sites, all 8 tyrosine sites were mutated to phenylalanine, which was MOB1-8YF,

and then each phenylalanine was mutated back to tyrosine one by one and tested again. MOB1-8YF largely blocked the phosphorylation signal, but when mutated back, each mutation showed contributions to the phosphorylation. These results indicate that Src phosphorylate all tyrosine sites on MOB1 (**Figure 23B**).

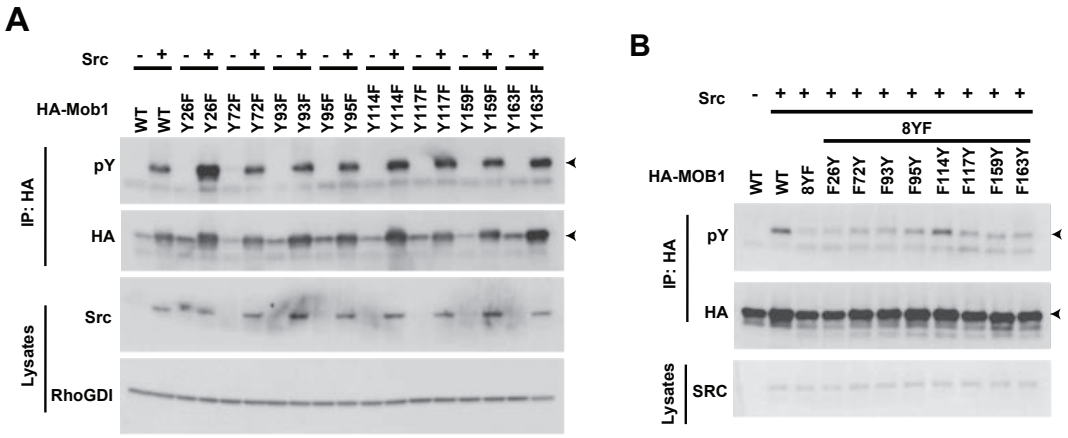

Figure 23. Identification of Src-induced tyrosine phosphorylation sites of MOB1.

(A) Different MOB1 mutation forms were co-transfected with Src in 293T cells. Immunoprecipitation was performed followed by immunoblotting with indicated antibodies.

(B) All tyrosine sites on MOB1 were mutated to phenylalanine and mutated back to tyrosine one by one. Immunoprecipitation was performed followed by immunoblotting with indicated antibodies.

3.10 MOB1-8YE increases YAP translocation to the nucleus, and promotes breast cancer cell invasive growth

To study the functions of MOB1 phosphorylation on YAP activation, wild type MOB1 and phospho-mimicking mutant MOB1-Y8E were re-introduced in MOB1A/B

knockout 293A cells. Re-introduction of wild type MOB1 could drive YAP out of the nucleus. However, re-introduction of MOB1-8YE could not induce the cytoplasmic translocation of YAP (**Figure 24**).

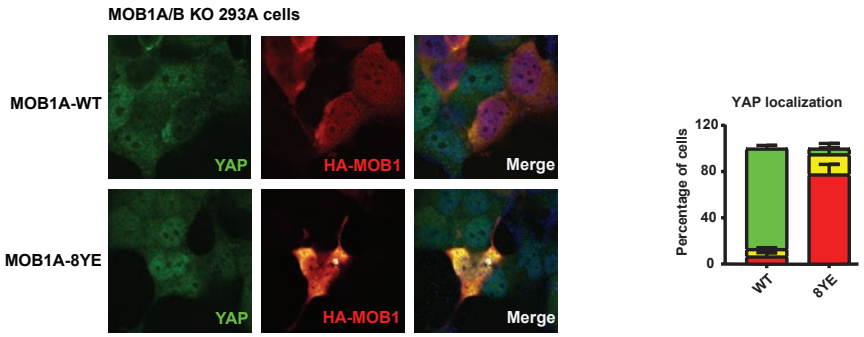

Figure 24. MOB1-8YE, but not MOB1-WT, robustly increases YAP translocation to the nucleus in MOB1A/B knockout cells.

Immunofluorescence imaging of YAP (GFP) and HA-MOB1 (RFP) and quantification of YAP localization in LATS1/2 knockout 293A cells re-introduced with wild type MOB1 or mutant MOB1-8YE. Error bars denote Mean + SD. Scale Bars, 20 μm.

Moreover, we utilized the previously described YAP promoter reporter system, followed by immunostaining. Wild type MOB1 dramatically decreased RFP, whereas MOB1-8YE had no effects on RFP level. These findings demonstrate that MOB1 phosphorylation by Src transcriptionally increases YAP activity (**Figure 25**).

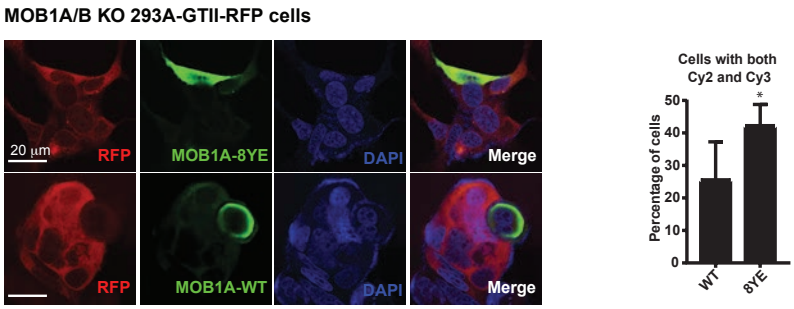

Figure 25. MOB1-8YE transcriptionally activates YAP in MOB1A/B knockout cells.

MOB1-WT and MOB1-8YE were re-introduced in MOB1A/B knockout 293A-GTII-RFP cells. HA-MOB1 (GFP) and YAP reporter (RFP) were examined by immunofluorescence and quantified. Scale Bars, 20 μm. Error bars denote Mean + SD; P values (two-tailed t-test): *p<0.05.

Then we evaluated the roles of MOB1 phosphorylation in cell growth and invasion in Mob1a/b knockout MMTV-Neu and B77 cells re-introduced with wild type or mutant Mob1. On soft and stiff Matrigel, only wild type Mob1 but not Mob1-8YE suppressed cell growth and invasion (**Figure 26**). These results suggest that MOB1 phosphorylation induced by Src has great impacts on YAP-mediated cell growth and invasion, and MOB1 in a high phosphorylation state can enhance YAP activation.

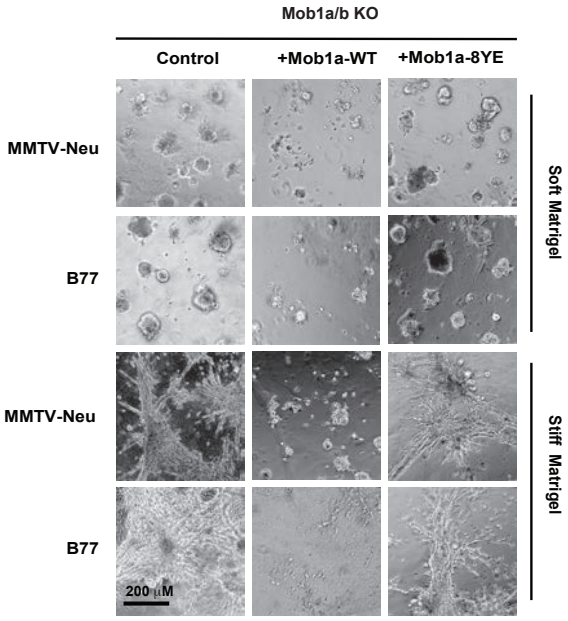

Figure 26. MOB1-8YE, but not MOB1-WT, promotes cell growth and invasion in MOB1A/B knockout cells.

Invasive cell growth assay on Soft Matrigel (Matrigel only) and Stiff Matrigel (Matrigel with collagen) in Mob1a/b knockout MMTV-Neu and B77 cells re-introduced with wild type Mob1 or Mob1-8YE. Scale Bars, 200 μm.

3.11 HER2 activates Src and induces LATS1/MOB1 phosphorylation

Although no direct phosphorylation of LATS1/MOB1 induced by FAK was found, whether FAK affects Src-induced phosphorylation was tested. FAK or siFAK were co-expressed with Src in 293T cells, tyrosine phosphorylation levels of LATS1 and MOB1 were detected. However, no obvious changes were found, suggesting FAK had no direct influences on Src to phosphorylate LATS1 and MOB1 (**Figure 27A**).

Next, we evaluated the effects of HER2 on Src-medicated LATS1/MOB1 phosphorylation. To examine whether HER2 activation affects Src activity and LATS1/MOB1 tyrosine phosphorylation levels, Neuregulin was added into SK-BR-3 cells and BT-474 cells at different time points. Upon HER2 activation, phosphorylation level of Src at Y416 and tyrosine phosphorylation levels of LATS1 and MOB1 increased (**Figure 27B**). Consistently, when treated with HER2 inhibitor Lapatinib, Src activity was suppressed, and phosphorylation levels of LATS1 and MOB1 decreased (**Figure 27C**). These results suggested that HER2 regulates Src activity to phosphorylate LATS1 and MOB1. Taken together, these findings reveal that in HER2 positive breast cancer, Src is activated by upstream HER2 signaling, thus phosphorylating and inhibiting the kinase activity of Hippo pathway components LATS1 and MOB1, which activates YAP.

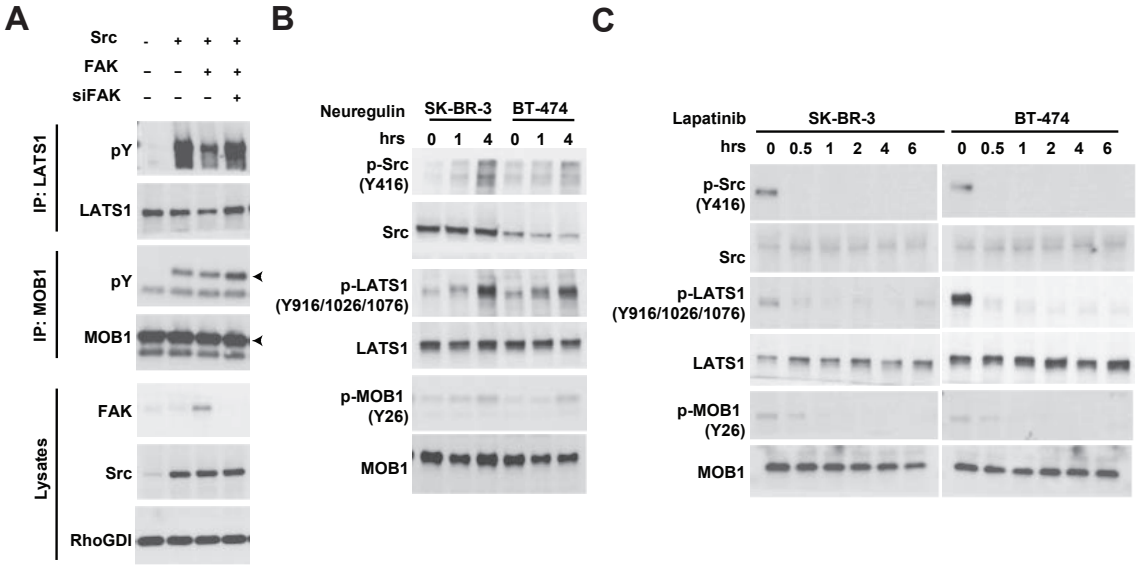

Figure 27. HER2 regulates Src-induced tyrosine phosphorylation of LATS1 and MOB1.

(A) Src, FAK and siFAK were transfected in 293T cells as indicated. Immunoprecipitation was performed followed by immunoblotting with indicated antibodies.

(B) Immunoblotting with indicated antibodies in SK-BR-3 cells and BT-474 cells treated with Neuregulin at different time points.

(C) Immunoblotting with indicated antibodies in SK-BR-3 cells and BT-474 cells treated with Lapatinib at different time points.

3.12 Depletion of Yap/Taz inhibits cancer growth and metastasis

To explore the biological effects of Yap/Taz depletion in breast cancer cells, functional assays both *in vitro* and *in vivo* were performed. Yap and/or Taz knockdown was carried out by Dox inducible shRNA and the efficiency was evaluated by immunoblotting (**Figure 28A**). Firstly, to test the cell growth and proliferation rate, MTT assays were conducted in both MDA-MB-231 cells and MMTV-Neu cells. Individual knockdown of Yap and Taz suppressed cell growth, whereas the proliferation rate was further reduced when Yap and Taz were knocked down together, indicating Yap and Taz had redundant functions in Her2 positive and triple negative breast cancer cells (**Figure 28B**). Next, Yap and Taz were knocked down in MMTV-Neu and MMTV-PyMT cells, and then placed on soft Matrigel (Matrigel only) and stiff Matrigel (Matrigel with collagen) for growth. Robust changes were observed in both soft and stiff conditions (**Figure 28C**). Consistently, in soft agar assays, knockdown of YAP/TAZ suppressed the colony formation more robustly than individual knockdown of YAP or TAZ in MDA-MB-231 cells and MMTV-Neu cells (**Figure 28D**). To examine the roles of Yap and Taz in cell stemness, tumor sphere assays were carried out in MMTV-Neu

and MDA-MB-231 cells. Consistently, knockdown of Yap/Taz in both cells dramatically decreased tumor sphere size (**Figure 28E**). These results suggest that Yap and Taz depletion inhibits cell growth, invasion, and stemness traits in breast cancer cells.

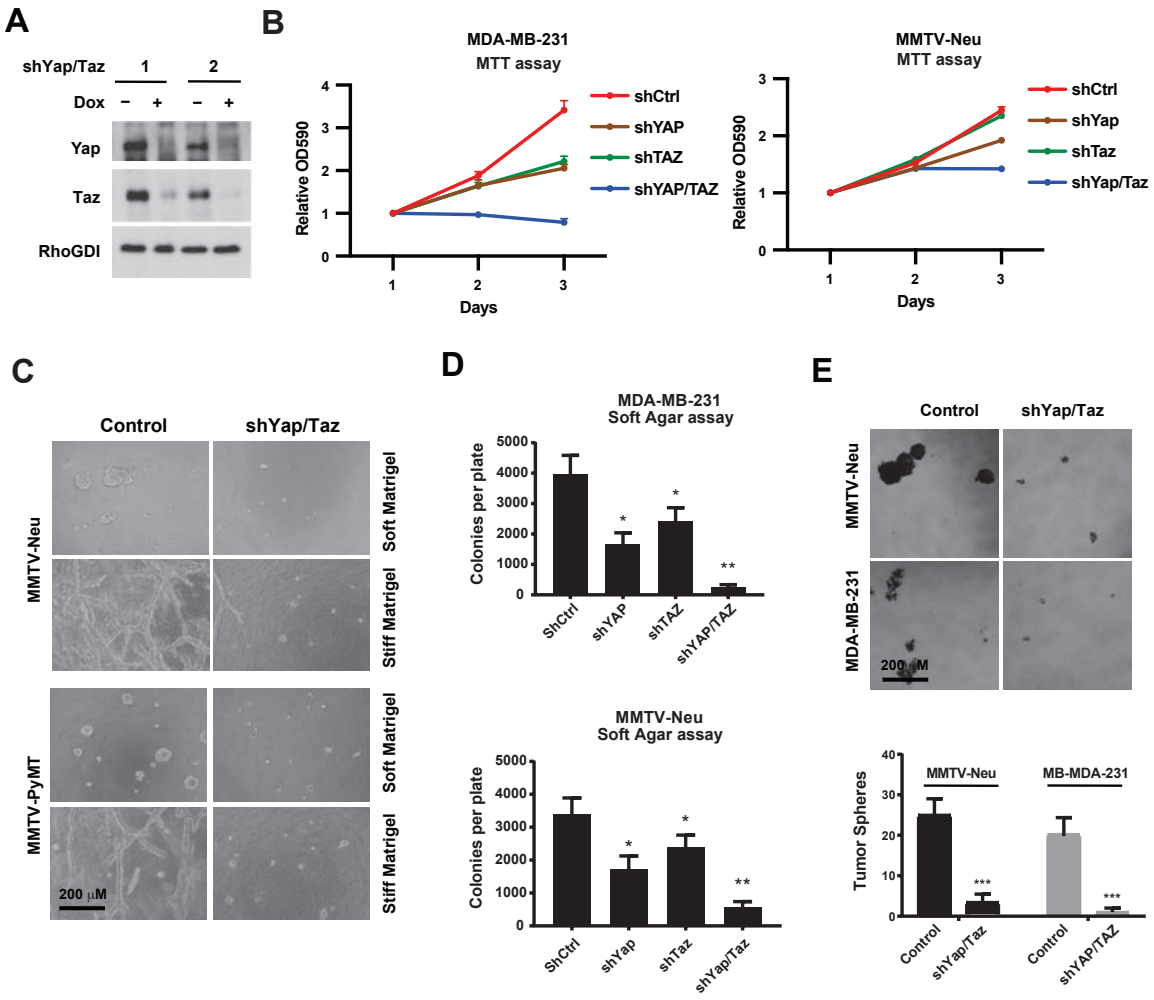

Figure 28. Depletion of Yap/Taz inhibits breast cancer cell growth and invasion *in vitro*.

(A) Immunoblotting of Yap and Taz after inducible knockdown of Yap/Taz in MMTV-Neu-TGL cells. Doxycycline (2 μg/ml, 4 days) was added for the induction.

(B) MTT assays in Yap/Taz knockdown MDA-MB-231 and MMTV-Neu cells.

(C) Invasive cell growth assays on Soft Matrigel (Matrigel only) and Stiff Matrigel (Matrigel with collagen) in Yap/Taz knockdown MMTV-Neu cells and MMTV-PyMT cells. Scale Bars, 200 μm.

(D) Soft agar assays in Yap/Taz knockdown MDA-MB-231 and MMTV-Neu cells. Error bars denote Mean ± SD; P values (two-tailed t-test): *p<0.05, **p<0.01.

(E) Tumor sphere assays and quantification in Yap/Taz knockdown MMTV-Neu and MDA-MB-231 cells. Error bars denote Mean + SD; P values (two-tailed t-test): ***p<0.0001. Scale bars, 200 μm.

Because of the redundant functions of Yap and Taz, both Yap and Taz were knocked down in the following *in vivo* experiments. To study the function of Yap and Taz in tumor growth and progression *in vivo*, inducible knockdown of Yap and Taz in MMTV-Neu-TGL cells was generated and injected into mammary fat pad or tail vein of female FVB/NJ mice. However, the mice did not develop mammary tumors or lung metastasis although it was a syngeneic model. We speculated that the transduced gene pWZL-Neu8142, which encodes oncogenic rat ErbB2, in MMTV-Neu cells, induced effective immune responses in FVB/NJ mice. Therefore, we repeated the experiments in female immune compromised nude mice instead. After two weeks of growth, when the tumor volume reached approximately 100 mm^3, Doxycycline was added to induce the knockdown of Yap and Taz. Tumor growth was monitored. After two weeks of Doxycycline treatment, mice were euthanized, and tumors were collected. In Doxycycline treated group, the tumor growth was significantly inhibited (**Figure 29A**). The findings indicated that Yap/Taz depletion suppresses primary

tumor in Her2 positive cancer cells. To examine Yap and Taz functions in breast cancer metastasis, Yap/Taz knockdown MMTV-Neu-TGL cells were injected through tail vein into female nude mice. After one week, Doxycycline was added to induce knockdown of Yap and Taz. Bioluminescence signals in lungs were significantly weaker in Yap/Taz knockdown group (**Figure 29B**). The results demonstrate that depletion of Yap/Taz suppresses metastatic outgrowth in lung of Her2 positive breast cancer.

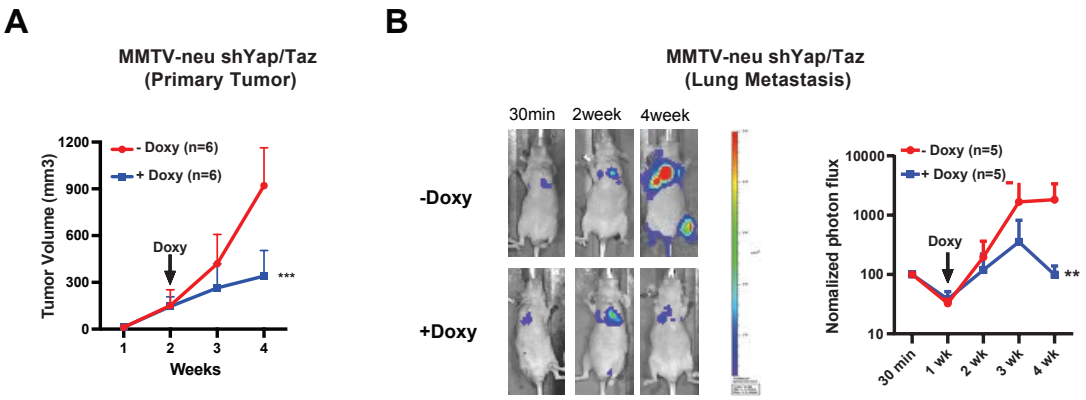

Figure 29. Inducible knockdown of Yap/Taz inhibits primary tumor and metastatic growth of Her2 positive breast cancer cells *in vivo*.

(A) Quantification of tumor volumes of female nude mice injected in mammary fat pad with inducible Yap/Taz knockdown MMTV-Neu-TGL cells. Doxycycline induction began at Week 2 after cell injection. Error bars denote Mean + SD; P values (two-tailed t-test): ***p<0.0001.

(B) Representative Images and normalized photon flux of nude mice injected through tail vein with inducible Yap/Taz knockdown MMTV-Neu-TGL cells. Doxycycline induction began at Week 1 after cell injection. Error bars denote Mean + SD; P values (two-tailed t-test): **p<0.01.

3.13 Depletion of Fak inhibits cancer growth and metastasis

Although no direct phosphorylation of LATS1 and MOB1 induced by FAK was found, pharmacological inhibition of FAK can inhibit YAP activation (**Figures 6-7**). Therefore, we evaluated the effects of genetic perturbation of FAK in breast cancer. We used inducible shPtk2 for the knockdown of Fak in MMTV-Neu cells. Knockdown efficiency was confirmed by immunoblotting (**Figure 30A**). Functional cell assays were performed to determine the effects of Fak depletion. On both soft and stiff matrices, the cell growth in Matrigel was suppressed by Fak knockdown (**Figure 30B**). The colony numbers on soft agar also decreased after Fak knockdown (**Figure 30C**). Consistently, knockdown of Fak led to the reduction in size and number of tumor spheres (**Figure 30D**). These results support the conclusion that Fak is important for cell growth, invasion, and stemness traits, in Her2 positive breast cancer.

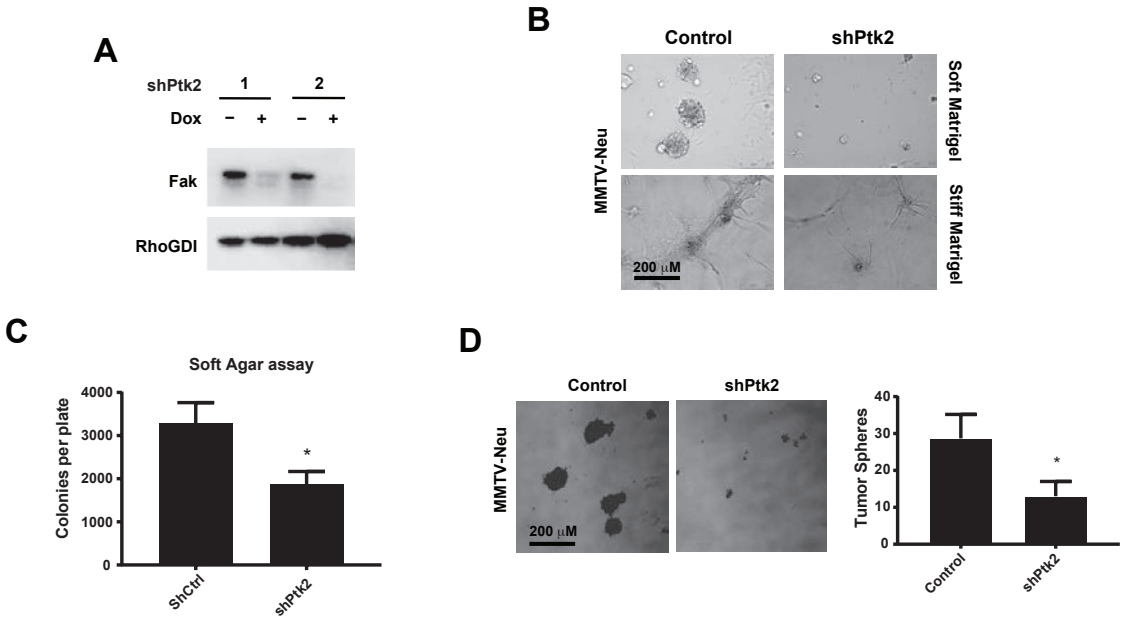

Figure 30. Fak depletion inhibits breast cancer cell growth and invasion *in vitro*.

(A) Immunoblotting of Fak after inducible knockdown of Ptk2 in MMTV-Neu-TGL cells. Doxycycline (2 μg/ml, 4 days) was added for the induction.

(B) Invasive cell growth assays on Soft Matrigel (Matrigel only) and Stiff Matrigel (Matrigel with collagen) in Ptk2 knockdown MMTV-Neu cells cells. Scale Bars, 200 μm.

(C) Soft agar assays in Ptk2 knockdown MMTV-Neu cells. Error bars denote Mean + SD; P values (two-tailed t-test): *p<0.05.

(D) Representative images and quantification of tumor sphere assays in Ptk2 knockdown MMTV-Neu cells. Error bars denote Mean + SD; P values (two-tailed t-test): *p<0.05. Scale bars, 200 μm.

To test the effects of Fak knockdown on primary tumor growth and metastasis *in vivo*, MMTV-Neu-TGL cells expressing inducible shPtk2 were injected in female nude mice. Fak knockdown slowed tumor growth in primary mammary tumors (**Figure 31A**) and lung metastases (**Figure 31B**).

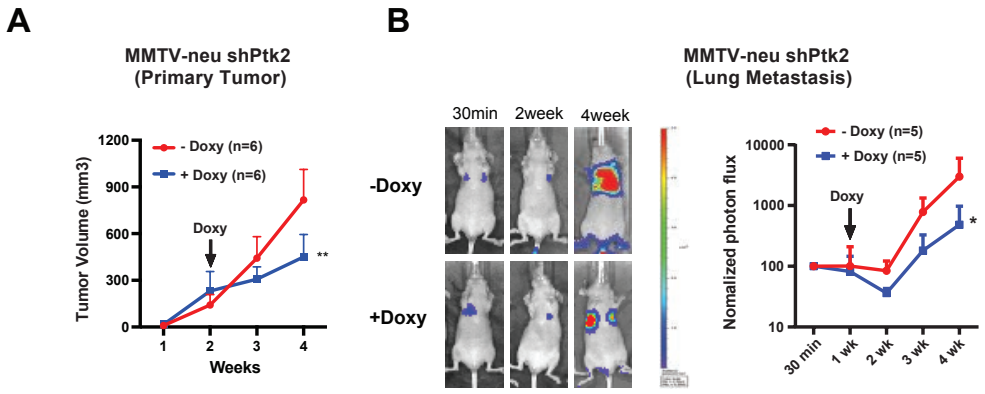

Figure 31. Fak depletion slows primary tumor and metastatic growth of Her2 positive breast cancer cells *in vivo*.

(A) Quantification of tumor volumes of female nude mice injected in mammary fat pad with inducible Ptk2 knockdown MMTV-Neu-TGL cells. Doxycycline induction began at Week 2 after cell injection. Error bars denote Mean + SD; P values (two-tailed t-test): **p<0.01.

(B) Representative Images and normalized photon flux of nude mice injected through tail vein with inducible Ptk2 knockdown MMTV-Neu-TGL cells. Doxycycline induction began at Week 1 after cell injection. Error bars denote Mean + SD; P values (two-tailed t-test): *p<0.05.

To further explore the connection between FAK and Hippo signaling from these *in vivo* studies, samples from both primary and metastatic tumors were collected for RNA extraction followed by RNA-seq analysis. The KEGG pathway analysis revealed that lots of known pathways associated with FAK signaling were enriched, such as tight junction, focal adhesion, and cell adhesion molecules. In addition, Hippo signaling pathways were also enriched in both primary and metastasis tumors, suggesting Fak functions upstream of Hippo signaling to regulate tumor growth and metastasis (**Figure 32A**). GSEA analysis indicated that both conserved Yap signature and Hippo pathway signature were enriched in control group compared to Fak knockdown group (**Figure 32B**). The RNA-seq data further confirmed that FAK was the upstream regulator of Hippo signaling in HER2 positive breast cancer cells.

A

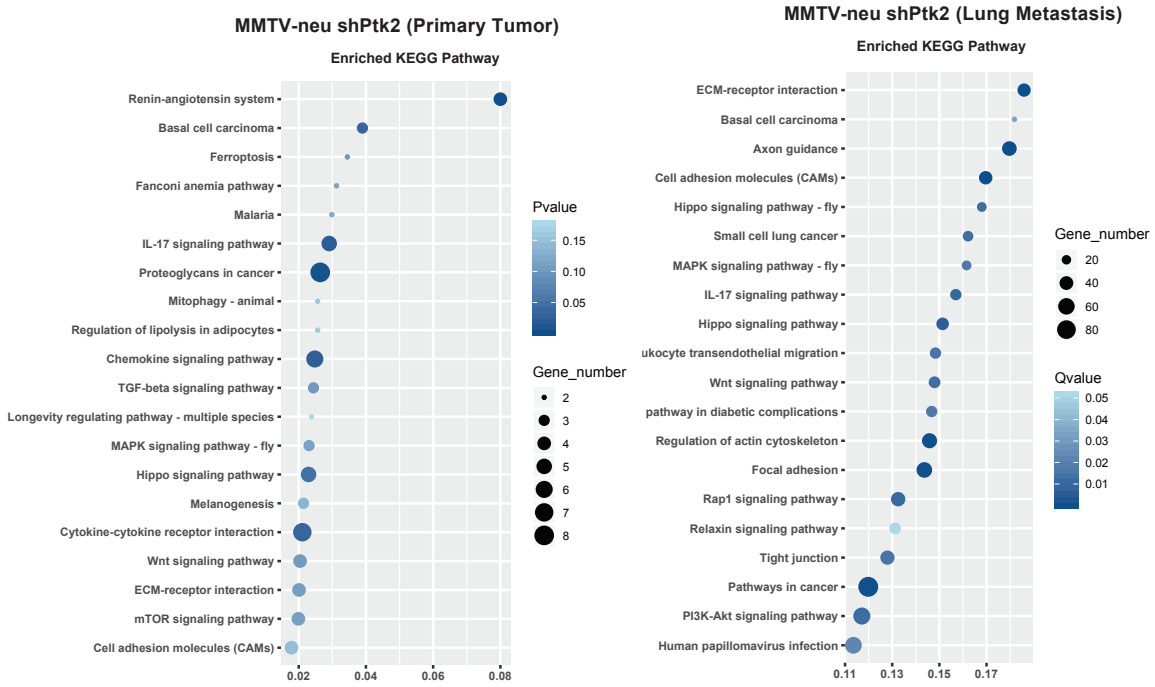

B

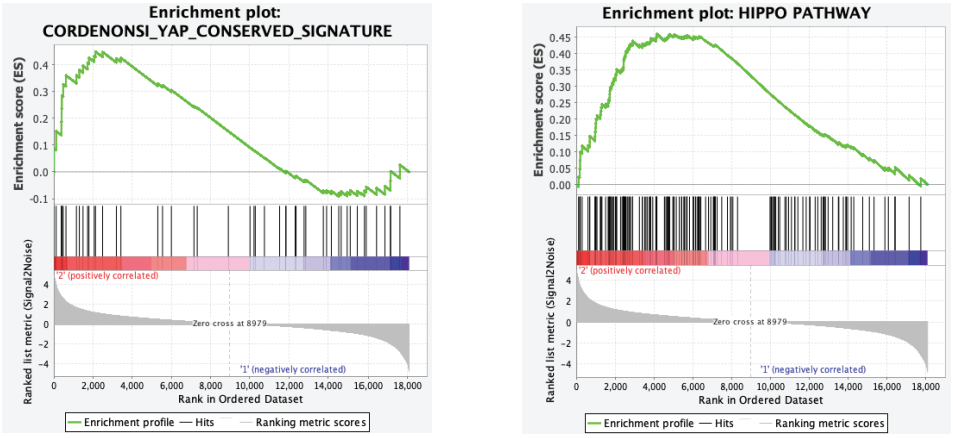

Figure 32. Yap signature and Hippo pathway signature are enriched in control group compared to Fak knockdown group.

(A) KEGG pathway enrichment analysis using RNA-seq data from dissociated tumor cells from female nude mice injected in fat pad or through tail vein with inducible Ptk2 knockdown MMTV-Neu-TGL cells.

(B) GSEA analysis of RNA-seq data from MMTV-Neu-shPtk2 lung metastatic tumors.

3.14 Dasatinib shows potential in enhancing the efficacy of Her2 inhibition in breast cancer growth and metastasis

To test preclinical efficacy of inhibition of FAK/SFK-YAP axis in HER2 positive breast cancer, we used a syngeneic mice model MMTV-Neu, which began to develop spontaneous breast tumors in 3 months after birth. When tumors reached 2 mm diameter, mice were treated with multi-kinase inhibitor Dasatinib and FAK inhibitor PF271 respectively (**Figure 33A**). Tumor sizes were monitored until the euthanasia after 3 weeks of treatment. Both Dasatinib and PF271 slowed down the tumor growth (**Figure 33B**). Immunohistochemistry staining for Ki67 and C-Caspase3 in the harvested tumors showed decreased cell proliferation and increased cell apoptosis after the treatment with Dasatinib and PF271 (**Figure 33C-D**). Hippo signaling markers Yap and p-Yap were also examined. Yap was mainly in the nucleus in control group while Yap tended to localize in the cytoplasm in Dasatinib and PF271 treated groups. Consistently, p-Yap increased after the treatment with Dasatinib and PF217, which indicated the suppressive activity of Yap (**Figure 33E**).

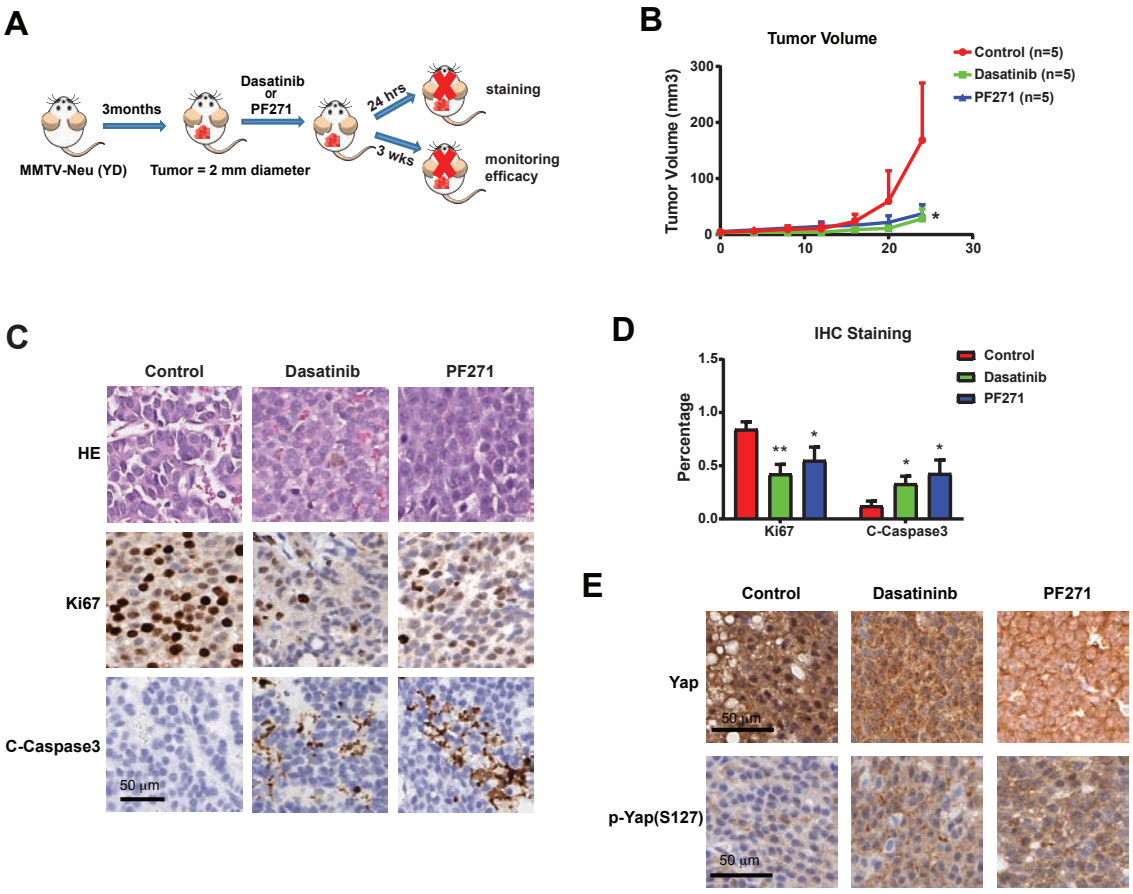

Figure 33. Dasatinib and PF271 suppress YAP activation and tumor growth in MMTV-neu spontaneous breast cancer models.

(A) A schematic illustration of workflow of inhibitor treatment in MMTV-Neu mice model.

(B) Quantification of tumor volume of MMTV-Neu mice treated with vehicle, Dastinib (20 mg/kg, oral gavage, qd) or PF271 (50 mg/kg, oral gavage, qd). Error bars denote Mean + SD; P values (two-tailed t-test): *p<0.05.

(C) Representative imaging of Hematoxylin and Eosin (H&E) staining and IHC staining of Ki67 and C-Caspase3 in the tumor samples harvested from MMTV-Neu mice after treatment. Scale Bars, 50 μm.

(D) Quantification of IHC staining of Ki67 and C-Caspase3 in the tumor samples harvested from MMTV-Neu mice after treatment. Error bars denote Mean + SD; P values (two-tailed t-test): *p<0.05, **p<0.01.

(E) Representative of IHC staining imaging of Yap and p-Yap (S127) in the tumor samples harvested from MMTV-Neu mice after treatment. Scale Bars, 50 μm.

Based on the model that YAP is activated by co-operational effects of matrix adhesion and HER2 in MMTV-Neu mice, we tested the clinical grade FAK inhibitor Defactinib or SFK inhibitor Dasatinib in combination with HER2 inhibitor Lapatinib. We anticipated synergistic effects of 2 drugs in each combination even if HER2 is the sole activator of FAK/SRC in these tumors, as hitting 2 steps in the same linear cascade has proven efficacious in the clinic (21). It was hard to get enough mice with consistent tumor growth rates in spontaneous breast cancer model, so we used female nude mice and injected them with MMTV-Neu cells. For primary tumors, MMTV-Neu cells were injected into mammary fat pad, and treated with vehicle, Lapatinib, Defactinib, Dasatinib, Lapatinib combined with Defactinib, or Lapatinib combined with Dasatinib. Drug treatments began once tumors reached approximately 100 mm^3. Tumor volumes were monitored during the treatment. Single treatment with Lapatinib or Dasatinib inhibited tumor growth, and Lapatinib and Dasatinib combination group showed lowest tumor growth rate (**Figure 34A**). In contrast, Defactinib alone or in combination with Lapatinib did not show favorable effects (**Figure 34B**). For metastatic tumors, MMTV-Neu cells were injected through tail vein, and treatments began after one week. Bioluminescent imaging and statistical analysis revealed that both Lapatinib and

Dasatinb alone suppressed growth in lung metastases, but combination of the two drugs further improved the effects (**Figure 34C**). Similar to primary tumors, Defactinib alone or in combination with Lapatinib did not inhibit metastatic growth (**Figure 34D**).

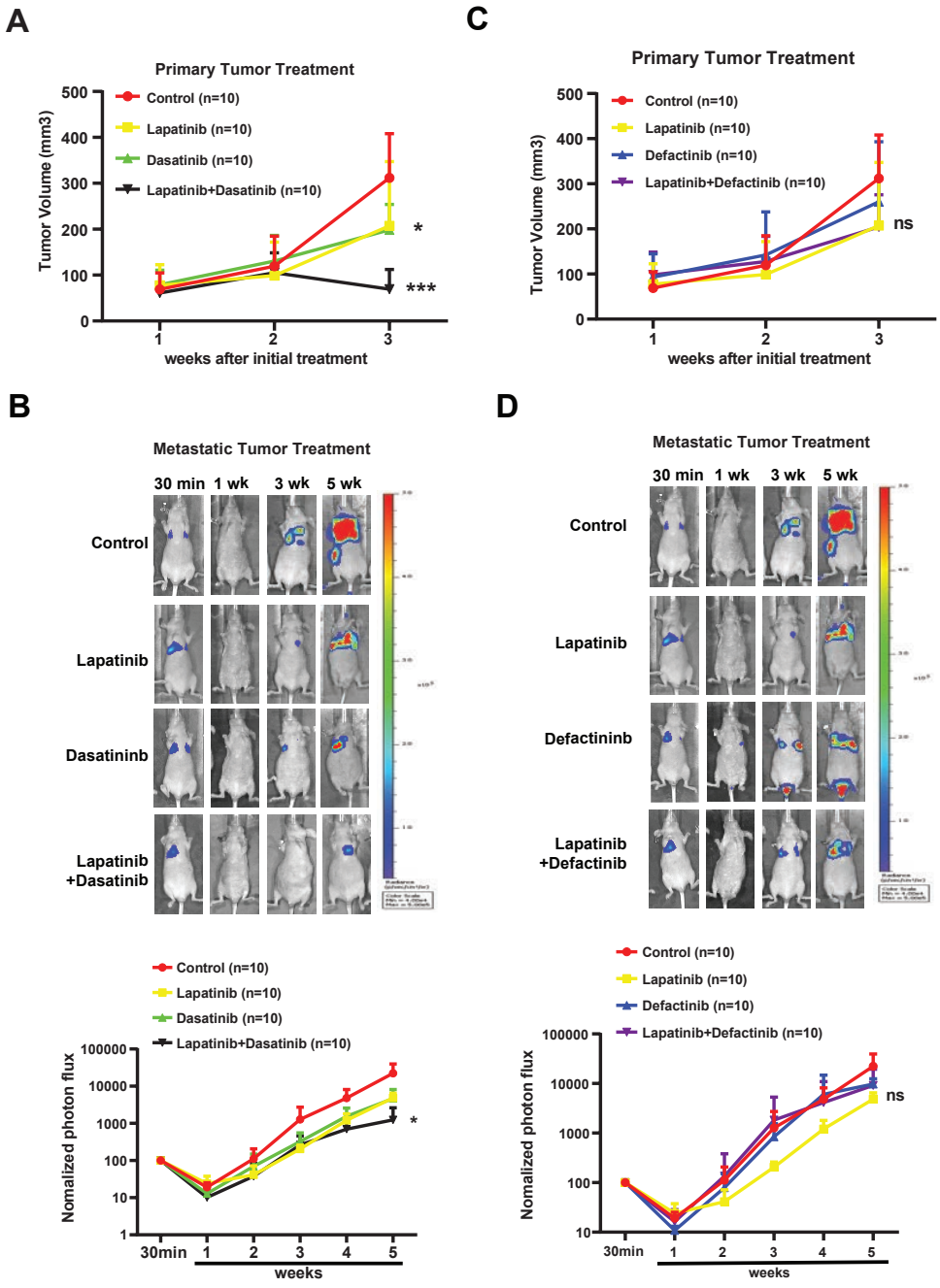

Figure 34. Dasatinib and Lapatinib combinational treatment inhibits HER2 positive breast tumor growth and metastasis.

(A) Quantification of tumor volumes of female nude mice injected in mammary fat pad with 300,000 MMTV-Neu cells after the treatment with vehicle, Lapatinib (50 mg/kg, oral gavage, qd), Dasatinib (50 mg/kg, oral gavage, qd), and Lapatinib with Dasatinib. Treatment began once tumors reached approximately 100 mm^3. Error bars denote Mean + SD; P values (two-tailed t-test): *p<0.05, ***p<0.0001.

(B) Representative Images and normalized photon flux of nude mice injected through tail vein with 300,000 MMTV-Neu cells after the treatment with vehicle, Lapatinib (50 mg/kg, oral gavage, qd), Dasatinib (50 mg/kg, oral gavage, qd), and Lapatinib with Dasatinib. Treatment began 1 Week after the injection. Error bars denote Mean + SD; P values (two-tailed t-test): *p<0.05.

(C) Quantification of tumor volumes of female nude mice injected in mammary fat pad with 300,000 MMTV-Neu cells after the treatment with vehicle, Lapatinib (50 mg/kg, oral gavage, qd), Defactinib (100 mg/kg, oral gavage, qd), and Lapatinib with Defactinib. Treatment began once tumors reached approximately 100 mm^3. Error bars denote Mean + SD; P values (two-tailed t-test): ns - no significance.

(D) Representative Images and normalized photon flux of nude mice injected through tail vein with 300,000 MMTV-Neu cells after the treatment with vehicle, Lapatinib (50 mg/kg, oral gavage, qd), Defactinib (50 mg/kg, oral gavage, qd), and Lapatinib with Defactinib. Treatment began 1 Week after the injection. Error bars denote Mean + SD; P values (two-tailed t-test): ns - no significance.

Next, the lung metastases samples were collected after the euthanasia of mice and subjected to IHC staining. Compared to the control group, Ki67 decrease and C-Caspase 3 increase were observed in all treatment groups, especially in Lapatinib and

Dasatinib combinational treatment group, which indicated Lapatinib combined with Dasatinib worked best in inhibiting lung metastatic growth. However, Ki67 and C-Caspase3 staining were not significantly altered by Defactinib individually or in combination with Lapatinib, which was consistent with the anticipation as the metastatic tumor growth was not inhibited (**Figure 35 A-B**). Moreover, Yap and p-Yap were examined. It was clearly that Yap localized in the nucleus in control group whereas Yap was mainly in the cytoplasm in Lapatinib and Dasatinib combinational treatment group. Yap activity decreased as p-Yap increased in the combinational treatment group (**Figure 35A**). Based on these results, we conclude that SFK inhibitor Dasatinib in combination with Lapatinib shows potential to treat HER2 positive breast cancer growth and metastasis.

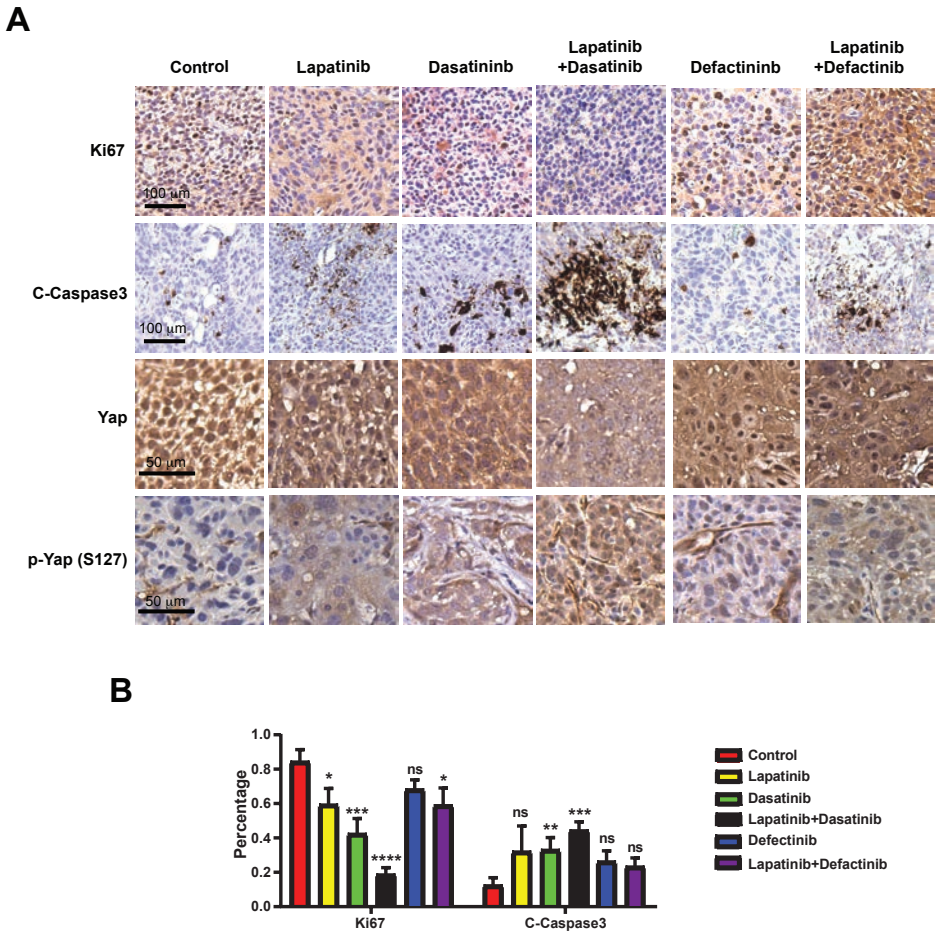

Figure 35. Dasatinib and Lapatinib combinational treatment shows most robust effects in inhibiting YAP activation in lung metastatic tumors.

(A) Representative of IHC staining imaging of Ki67, C-Caspase3, Yap, and p-Yap (S127) in the lung metastases samples harvested from MMTV-Neu cell-injected nude mice after different treatments. Scale Bars as indicated.

(B) Quantification of IHC staining of Ki67 and C-Caspase3 in the lung metastases samples harvested from MMTV-Neu cell-injected nude mice after different treatments.

Chapter 4. Discussion and Future Directions

4.1 Summary and Discussion

Tumor stiffening occurs with the tumor pathogenesis and progression. The matrix is stiffer in HER2 positive and triple negative breast cancer subtypes than the less aggressive luminal counterparts (*8*). The mechanical inputs from the ECM are sensed by mechanosensors at the cell membrane and relayed by mechanotransducers to promote YAP/TAZ activity at sites where mechanical forces are high (*76*). Consistently, we found that YAP is activated by rigid matrices in more aggressive HER2 positive SK-BR-3 and triple negative MDA-MB-231 cells. To understand the mechanotransducers of YAP activation, we used pharmacological inhibition and genetic perturbation of the integrin signaling components and identified a critical role for integrin signaling via FAK-SRC in activation of YAP/TAZ in HER2 positive and triple negative breast cancer cells. In HER2 positive cells, integrin signaling synergizes with HER2 to activate YAP. This provides new evidence for the joint regulation between integrin signaling and RTKs. But what triggers the FAK/SFK and YAP activation in triple negative cancer is poorly known. Studies have shown the effects of integrin-FAK signaling on tumor initiation, metastasis, and resistance to chemotherapy in triple negative breast cancer. EGFR and integrin b4 cooperate to active FAK and trigger the tumor initiation and metastasis in triple negative breast cancer (*72*). A recent study in triple negative MDA-MB-231 cells shows that EZH2-upregulated integrin b1 activates FAK, which phosphorylates TGFβ receptor type I (TGFβRI) at Y182 to increase its binding to TGFβ receptor type II (TGFβRII), thus activating TGFβ signaling and bone metastatic potential (*73*). ECM deposition and remodeling promote chemoresistance

by inducing FAK activation through integrin α1/α2/α5 (*46, 70*). These studies shed light on FAK activation by upstream integrin and RTKs. However, whether YAP is activated and whether YAP activation is required for these biological functions in triple negative breast cancer still await further investigation.

Although ECM stiffening and YAP/TAZ activation in breast cancer have been clearly implicated in previous research and further validated in our studies, the biochemical mechanisms that link ECM-responsive integrin-FAK/SFK signaling and YAP/TAZ activation are largely unknown. We conducted co-immunoprecipitation and identified the interaction between FAK/Src and YAP upstream regulator LAST1. Following studies show Src can induce phosphorylation of LATS. Mass spectrometry and mutagenesis analysis revealed that Src phosphorylates LATS at 3 conserved sites (Y916, Y1026, and Y1076), leading to loss of the kinase activity of LATS1. To determine whether Src-induced LATS1 is the driver mechanism, CRISPR-Cas9-mediated knockout of LATS1/2 was followed by reconstitution with wild type or an unphosphorylatable (Y916/1026/1076F or 3YF) or a phosphorylation-mimetic (Y916/1026/1076E or 3YE) mutant of LATS. Only 3YE mutant but not wild type or 3YF can induce the YAP activation and malignancy of HER2 positive and triple negative breast cancer cells. Another Hippo signaling component MOB1, can also be phosphorylated by Src. Contrary to the previous study, which demonstrates FAK phosphorylates MOB1, we did not see the FAK-mediated MOB1 phosphorylation (*117*). MOB1 is phosphorylated at 8 tyrosine sites and the phosphorylation-mimetic mutant MOB1-8YE can rescue the YAP activation and malignancy of MOB1A/B knockout HER2 positive and triple negative breast cancer cells. Both LATS and MOB1

phosphorylation by Src disable their kinase activity for YAP inhibition, thereby activating YAP. These results establish a novel link between FAK/SFK and YAP activation, in which LATS1and MOB1 are both directly phosphorylated by Src. In the Hippo signaling, LATS1 and MOB1 phosphorylation are mediated by MST. In addition to MST, LATS can be phosphorylated by MAP4Ks, PKA, CHK1/2, CDK1/CDC2, and Aurora A kinase (*83*). Opposed to that, MST-independent MOB1 phosphorylation is scarcely reported. EGFR promotes the phosphorylation of MOB1 and the inactivation of LATS1/2 independently of MST1/2. (*118*). Therefore, the identified Src-mediated direct phosphorylation on LATS and MOB1 expand the understanding of Hippo signaling.

We then used an inducible knockdown system to evaluate the biological functions YAP, TAZ, and FAK in HER2 positive and triple negative breast cancer cells. FAK knockdown decreases cell proliferation and invasive growth and inhibits mammary tumor growth and metastasis in mice. YAP and TAZ function largely in a redundant fashion to sustain tumor growth and metastasis. The YAP/TAZ knockdown shows higher inhibitory effects than FAK knockdown. These results make it rational to test the effects of FAK and/or YAP/TAZ inhibition in breast cancer.

First, we tested the individual drug SFK inhibitor Dasatinib and FAK inhibitor PF271 in spontaneous MMTV-Neu mammary tumor mouse model. Both drugs suppressed YAP activation and slowed down the tumor growth. Then, for larger scale experiments, we injected MMTV-Neu-TGL cells into mammary fat pat and tail vein for the drug evaluation in primary and metastatic tumors respectively. Integrin signaling contributes to the resistance of HER2 positive SK-BR-3 and BT-474 cells plated on

laminin-5 to HER2 inhibition. FAK inhibitor TAE226 csn sensitize the cells to HER2 antagonists, Trastuzumab and Lapatinib (*75*). Therefore, the simultaneous inhibition of integrin-FAK/SFK and HER2 may improve the efficacy. In both primary and metastatic tumors, the single drug administration with Dasatinib and Lapatinib showed efficacious tumor-inhibitory effects while Defactinib did not. The combination of Dasatinib and Lapatinib was most effective whereas Defactinib, when delivered together with Lapatinib, did not further improve the effects of Lapatinib. These preclinical studies demonstrate the synergistic anti-tumor effect between the blockade of integrin-FAK/Src-YAP axis and HER2. Although Defactinib inhibits YAP activation and cell growth in HER2 positive cell lines, but it was not effective in the tumor-bearing MMTV-Neu mice. The reason needs to be further studied. In MMTV-Neu mice, Fak deletion does not prevent the tumorigenesis and only inhibits the progression to a small extent (*119*). This may explain why MMTV-Neu cells do not respond to FAK inhibition in mice. It is necessary to test FAK inhibitors in other HER2 positive breast cancer models. Interestingly, Defactinib shows efficacy in inhibiting bone metastasis of triple negative MDA-MB-231 cells (*73*). In addition, several studies have shown basal-like triple negative breast cancer are most sensitive to Dasatinib compared to luminal subtypes (*120-122*). It will be important to evaluate the preclinical efficacy of FAK and SFK inhibitors alone or in combination with chemotherapy in triple negative breast cancer.

Taken together, this study demonstrates integrin-FAK/SFK mediates the mechanotransduction from stiff ECM and activates YAP, which is required for cell invasive growth and tumor metastasis; and unmasks the mechanisms through which

YAP is activated by integrin signaling - Src induces phosphorylation of LATS and MOB1, leading to their inactivation and ensuing YAP activation. Furthermore, Integrin signaling and HER2 jointly regulate YAP activation and combinational inhibition of these two pathways shows promising preclinical efficacy in HER2-positive breast cancer (**Figure 36**).

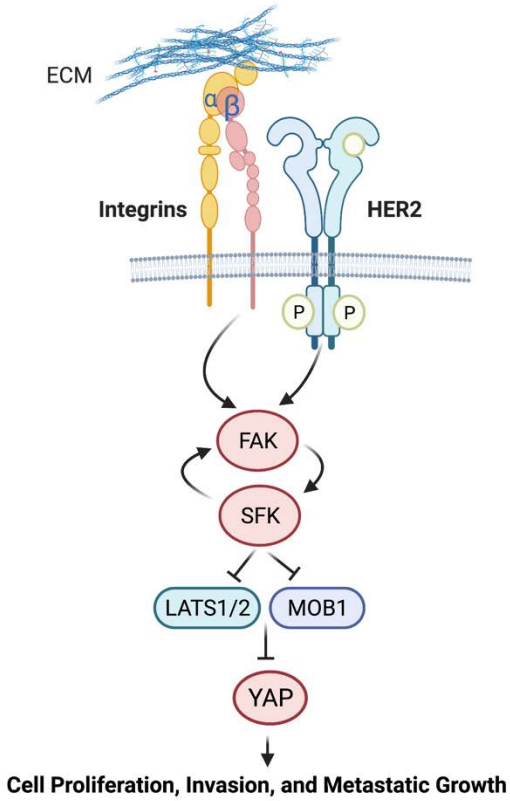

Figure 36. Graphic Summary.

In response to stiff matrix, integrin-FAK/SFK signaling and HER2 activate YAP. SFKs phosphorylate and inhibit the kinase activities of LATS and MOB1, thus deactivating the Hippo tumor suppressive pathway.

4.2 Future Directions

4.2.1 Identification of new regulators of YAP activation

First, exploring the upstream regulators of FAK and YAP activation in triple negative breast cancer is important. Since PTEN can dephosphorylate and inactivate FAK (*123*), we can first test the hypothesize that the inactivation of PTEN, which is frequent in triple negative breast cancers, contributes to activation of YAP.

In addition to the possible roles of PTEN, a non-biased high throughput screening can be very informative for the identification of new regulators of YAP activation. In collaboration with Drs. Ralph Garippa and Scott Lowe at Memorial Sloan Kettering Cancer Center, we have performed a genome-wide siRNA screen in triple negative MDA-MB-231 cells and HER2 positive AU565 cells expressing GFP-tagged YAP and identified siRNAs that block nuclear accumulation of GFP-YAP. We conducted the screens with the siGENOME siRNA library (Dharmacon; SMARTpools of 4 siRNAs per gene) (**Figure 37A**). The hits can be specific to HER2 positive or triple negative or shared by the two cells. We first analyzed the 69 overlapped hits that are shared by MDA-MB-231 and AU565 cells to regulate YAP activation, and found that many of them are cytoskeleton-related proteins (**Figure 37B-C**).

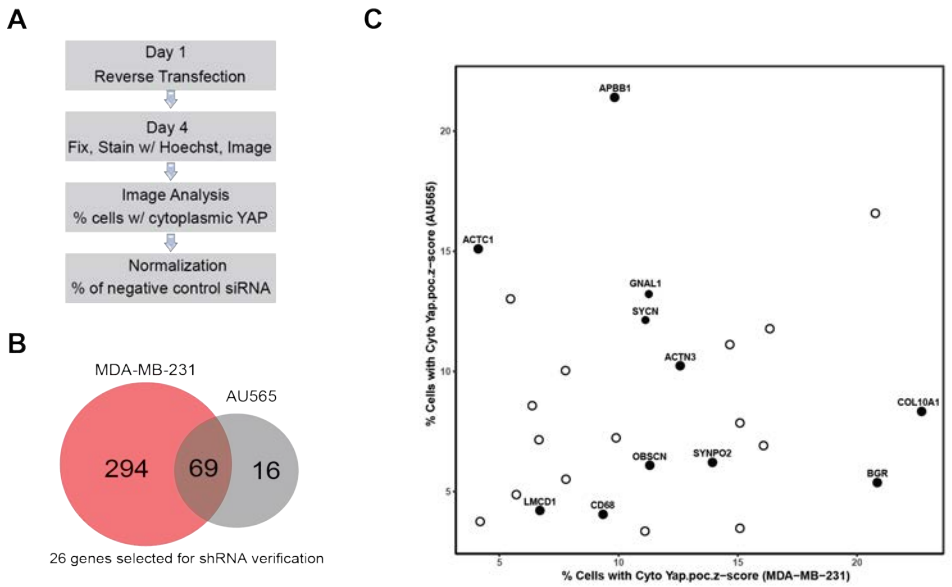

Figure 37. siGENOME siRNA Screen for YAP regulators in breast cancer cells.

(A) Workflow of the siRNA screen.

(B) Venn diagram of hits identified from triple negative MDA-MB-231 and HER2 positive AU565 cells.

(C) Representative cytoskeleton-related hits.

Several hits have been validated with CRISP-Cas9-mediated knockout. The knockout of these hits significantly induces the YAP translocation from the nucleus to the cytoplasm (**Figure 38**). Brief research on the hits indicates the effects of them on YAP activation is poorly understood. Synaptopodin-2 (SYNPO2) has been clearly linked to YAP activation. SYNPO2 is a putative tumor suppressor in different aggressive cancers. In triple negative breast cancer, SYNPO2 can stabilize LATS2 to inactivate YAP/TAZ and suppress tumor metastasis (*124*). In colorectal cancer,

SYNPO2 suppresses hypoxia-induced proliferation and migration of the cells by regulating YAP-Kruppel like factor 5 (KLF5) axis (*125*), but the detailed mechanisms are not known. Other than YAP activation, SYNPO2 regulates migration and invasion via PI3K/Akt/mTOR pathway in MCF-7, MDA-MB-231, BT-549, and MDA-MB-468 breast cancer cells (*126*). Some of the hits have not been implicated in YAP activation but linked to cancer biology. Amyloid b precursor protein binding family B member 1 (APBB1) regulates EMT-associated cell stem cell-like properties and g-radiation resistance via activation of IGF1Rb/AKT/GSK3b pathway in non-small cell lung cancer cells (*127*). Actin alpha cardiac muscle 1 (ACTC1) is a biomarker for invasion and prognosis in glioma (*128*). Giant obscurin (OBSCN) has been proved to be a potent tumor suppressor and the genetic mutations or epigenetic deregulation of OBSCN are implicated in progression of breast cancer and other cancer types (*129*). The studies of other lead hits are limited to normal development or dysfunction of bone and muscle (*130-132*). We can further validate these hits and investigate their regulation in YAP activation and tumor biological functions in breast cancer.

Moreover, for the identification of the druggable targets, a small molecule library can be used for the YAP activation screens.

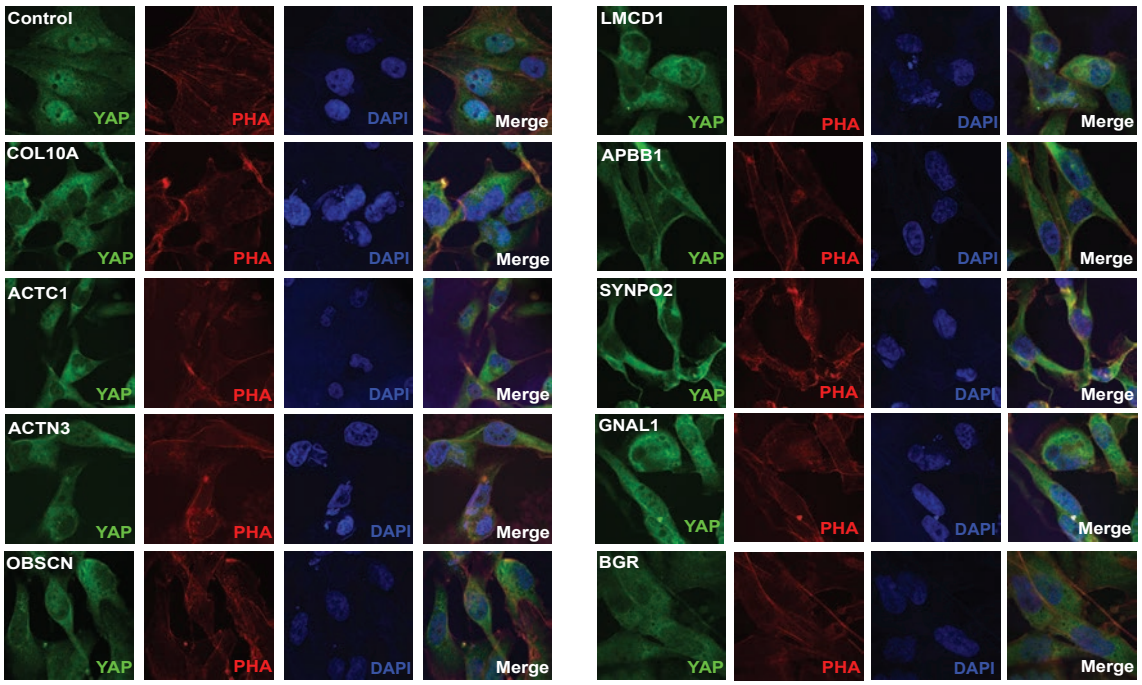

Figure 38. Validation of the screen hits.

Immunofluorescence staining of YAP after knockout of the indicated genes.

4.2.2 Dissection of the dynamics of tumor initiation and multi-step metastatic cascade regulated by YAP/TAZ

YAP/TAZ regulate cancer EMT, stemness, invasive growth in dense stiff matrices. However, the dynamic changes of YAP/TAZ activation and ECM stiffness from tumor initiation to metastasis have not been fully characterized. For the primary tumor growth, invasion, and intravasation, YAP/TAZ knockdown can be induced after the orthotopic injection of mouse breast cancer cells in a syngeneic model. By harvesting tumors and circulating tumor cells from different stages of tumor

development, we can investigate proliferation, apoptosis, and invasiveness of tumor cells, as well as the density and stiffness of the collagenous tumor matrix. To study the roles of YAP/TAZ in the extravasation and colonization phase of metastasis, tumor cells can be injected intracardially so that they can colonize bone, brain, and liver or intravenously to estimate colonization of the lung. The analysis of the dynamic changes will also help elucidate the effects of the microenvironment differences arising from various target organs on metastatic outgrowth. In the syngeneic models, immune components in the tumor microenvironment can also be analyzed. These studies will determine the biological functions of YAP/TAZ depletion and define the cellular mechanisms through which YAP/TAZ signaling affects tumor progression and metastasis.

4.2.3 Exploration of other therapeutic opportunities targeting ECM stiffening and mechanotransduction

The dense and stiff ECM is an attractive target for cancer treatment. The ECM-targeted therapy may benefit cancer patients by reducing the pro-tumor potential of ECM and lifting the mechanical restraints for other treatments to be more effectively delivered. The key enzymes mediating the ECM crosslinking have been successfully targeted in transgenic mouse models. LOX-targeted inhibitor and blocking antibody both prevent LOX-dependent collagen cross-linking and reduce MMTV-Neu-induced tissue fibrosis to lower breast cancer incidence and impede the progression (*18*). Targeting LOX also sensitizes the triple negative breast cancer xenografts to chemotherapy (*70*). However, the clinical trial results of LOX inhibitors have been

disappointing and attributed to poor drug bioavailability in tumors and inefficient enzymatic inhibition (*133, 134*). Another ECM crosslinking enzyme LH also shows the potential to be targeted. LH2 depletion in CAFs prevents matrix stiffening and suppresses collagen-mediated tumor cell invasion (*135*). Targeted depletion of the stromal component, hyaluronan (HA), has also been tested and proved to reduce the matrix density and improve the response of pancreatic adenocarcinoma cells to the standard chemotherapy Gemcitabine preclinically (*136, 137*). We can test these ECM targeted therapies in both HER2 positive and triple negative breast cancer models.

Mechanosensing and mechanotrasduction through integrin signaling can also be targeted. Despite encouraging preclinical results demonstrating that the inhibition of integrins $\alpha V\beta 3/\alpha V\beta 5$ and $\alpha 5\beta 1$ can provide promising therapeutic outcomes, clinical trials with these integrin-based therapeutics have not shown therapeutic benefits in cancer patients (*138*). The multifarious and redundant roles of integrins in cancer and the narrow therapeutic window for integrin-based therapeutics without compromising the integrin functions in normal cells contribute to the discouraging clinical outcomes (*65*). It is critical to identify the integrins that are non-essential in normal cells but play important roles in tumor malignancy in breast cancer cells or the cancer-associated stromal cells. Irina Primac et al. showed that integrin $\alpha 11$ coopts with PDGFRβ in CAFs to induce tumor invasiveness in MMTV-PyMT mice (*139*). This may provide a new therapeutic target for integrin-based therapies in breast cancer. Given the critical role of the FAK/SFK complex in promoting invasive growth, the inhibitors targeting FAK or SFKs have been extensively tested in different cancer types. In addition to our findings that SFK inhibitor Dasatinib synergizes with Lapatinib to inhibit invasive

growth and metastasis of HER2 positive breast cancer, FAK inhibitor Defactinib has shown promising efficacy in suppressing tumor incidence by preferentially targeting cancer stem cells (*140*) and inhibiting bone metastasis (*73*) in triple negative breast cancer xenografts. Higher sensitivity to Dasatinib is also found in triple negative breast cancer cells (*120-122*). These studies encourage us to test FAK/SFKs inhibition in triple negative breast cancer.

When the Hippo pathway is turned off by upstream mechanical or biochemical signals, YAP/TAZ enter the nucleus and form a complex with transcriptional enhanced associate domain (TEAD) to induce gene transcription. K-975 inhibits YAP/TAZ signaling by inhibiting the protein-protein interactions between YAP/TAZ and TEAD, and its potent efficacy has been shown in NF2-deficient mesothelioma cells (*141*). The effects of K-975 on matrix stiffness-induced YAP activation can be evaluated in HER2 positive and triple negative breast cancer cells. Also, we can compare the K975 sensitivity in LATS1/2 or MOB1A/B knockout breast cancer or B77 cells. Furthermore, we can test the efficacy of K-975 alone or in combination with Lapatinib in HER2 positive models and in combination with chemotherapy in triple negative models.

References

1. Sung, H., Ferlay, J., Siegel, R. L., Laversanne, M., Soerjomataram, I., Jemal, A., Bray, F., Global Cancer Statistics 2020: GLOBOCAN Estimates of Incidence and Mortality Worldwide for 36 Cancers in 185 Countries. *CA Cancer J Clin* **71**, 209-249 (2021).
2. Siegel, R. L., Miller, K. D., Fuchs, H. E., Jemal, A., Cancer statistics, 2022. *CA Cancer J Clin* **72**, 7-33 (2022).
3. Cancer Genome Atlas, Network, Comprehensive molecular portraits of human breast tumours. *Nature* **490**, 61-70 (2012).
4. Perou, C. M., Sorlie, T., Eisen, M. B., van de Rijn, M., Jeffrey, S. S., Rees, C. A., Pollack, J. R., Ross, D. T., Johnsen, H., Akslen, L. A., Fluge, O., Pergamenschikov, A., Williams, C., Zhu, S. X., Lonning, P. E., Borresen-Dale, A. L., Brown, P. O., Botstein, D., Molecular portraits of human breast tumours. *Nature* **406**, 747-752 (2000).
5. Kun, Y., How, L. C., Hoon, T. P., Bajic, V. B., Lam, T. S., Aggarwal, A., Sze, H. G., Bok, W. S., Yin, W. C., Tan, P., Classifying the estrogen receptor status of breast cancers by expression profiles reveals a poor prognosis subpopulation exhibiting high expression of the ERBB2 receptor. *Hum Mol Genet* **12**, 3245-3258 (2003).
6. Garrido-Castro, A. C., Lin, N. U., Polyak, K., Insights into Molecular Classifications of Triple-Negative Breast Cancer: Improving Patient Selection for Treatment. *Cancer Discov* **9**, 176-198 (2019).

7. Loibl, S., Gianni, L., HER2-positive breast cancer. *Lancet* **389**, 2415-2429 (2017).

8. Acerbi, I., Cassereau, L., Dean, I., Shi, Q., Au, A., Park, C., Chen, Y. Y., Liphardt, J., Hwang, E. S., Weaver, V. M., Human breast cancer invasion and aggression correlates with ECM stiffening and immune cell infiltration. *Integr Biol (Camb)* **7**, 1120-1134 (2015).

9. Lopez, J. I., Kang, I., You, W. K., McDonald, D. M., Weaver, V. M., In situ force mapping of mammary gland transformation. *Integr Biol (Camb)* **3**, 910-921 (2011).

10. Paszek, M. J., Zahir, N., Johnson, K. R., Lakins, J. N., Rozenberg, G. I., Gefen, A., Reinhart-King, C. A., Margulies, S. S., Dembo, M., Boettiger, D., Hammer, D. A., Weaver, V. M., Tensional homeostasis and the malignant phenotype. *Cancer Cell* **8**, 241-254 (2005).

11. Piersma, B., Hayward, M. K., Weaver, V. M., Fibrosis and cancer: A strained relationship. *Biochim Biophys Acta Rev Cancer* **1873**, 188356 (2020).

12. Sahai, E., Astsaturov, I., Cukierman, E., DeNardo, D. G., Egeblad, M., Evans, R. M., Fearon, D., Greten, F. R., Hingorani, S. R., Hunter, T., Hynes, R. O., Jain, R. K., Janowitz, T., Jorgensen, C., Kimmelman, A. C., Kolonin, M. G., Maki, R. G., Powers, R. S., Pure, E., Ramirez, D. C., Scherz-Shouval, R., Sherman, M. H., Stewart, S., Tlsty, T. D., Tuveson, D. A., Watt, F. M., Weaver, V., Weeraratna, A. T., Werb, Z., A framework for advancing our understanding of cancer-associated fibroblasts. *Nat Rev Cancer* **20**, 174-186 (2020).

13. Xing, X., Wang, Y., Zhang, X., Gao, X., Li, M., Wu, S., Zhao, Y., Chen, J., Gao, D., Chen, R., Ren, Z., Zhang, K., Cui, J., Matrix stiffness-mediated effects on macrophages polarization and their LOXL2 expression. *FEBS J* **288**, 3465-3477 (2021).

14. Garcia-Palmero, I., Torres, S., Bartolome, R. A., Pelaez-Garcia, A., Larriba, M. J., Lopez-Lucendo, M., Pena, C., Escudero-Paniagua, B., Munoz, A., Casal, J. I., Twist1-induced activation of human fibroblasts promotes matrix stiffness by upregulating palladin and collagen alpha1(VI). *Oncogene* **35**, 5224-5236 (2016).

15. Seo, B. R., Bhardwaj, P., Choi, S., Gonzalez, J., Andresen Eguiluz, R. C., Wang, K., Mohanan, S., Morris, P. G., Du, B., Zhou, X. K., Vahdat, L. T., Verma, A., Elemento, O., Hudis, C. A., Williams, R. M., Gourdon, D., Dannenberg, A. J., Fischbach, C., Obesity-dependent changes in interstitial ECM mechanics promote breast tumorigenesis. *Sci Transl Med* **7**, 301ra130 (2015).

16. Pankova, D., Jiang, Y., Chatzifrangkeskou, M., Vendrell, I., Buzzelli, J., Ryan, A., Brown, C., O'Neill, E., RASSF1A controls tissue stiffness and cancer stem-like cells in lung adenocarcinoma. *EMBO J* **38**, e100532 (2019).

17. Calvo, F., Ege, N., Grande-Garcia, A., Hooper, S., Jenkins, R. P., Chaudhry, S. I., Harrington, K., Williamson, P., Moeendarbary, E., Charras, G., Sahai, E., Mechanotransduction and YAP-dependent matrix remodelling is required for the generation and maintenance of cancer-associated fibroblasts. *Nat Cell Biol* **15**, 637-646 (2013).

18. Levental, K. R., Yu, H., Kass, L., Lakins, J. N., Egeblad, M., Erler, J. T., Fong, S. F., Csiszar, K., Giaccia, A., Weninger, W., Yamauchi, M., Gasser, D. L., Weaver, V. M., Matrix crosslinking forces tumor progression by enhancing integrin signaling. *Cell* **139**, 891-906 (2009).

19. Chen, Y., Terajima, M., Yang, Y., Sun, L., Ahn, Y. H., Pankova, D., Puperi, D. S., Watanabe, T., Kim, M. P., Blackmon, S. H., Rodriguez, J., Liu, H., Behrens, C., Wistuba, II, Minelli, R., Scott, K. L., Sanchez-Adams, J., Guilak, F., Pati, D., Thilaganathan, N., Burns, A. R., Creighton, C. J., Martinez, E. D., Zal, T., Grande-Allen, K. J., Yamauchi, M., Kurie, J. M., Lysyl hydroxylase 2 induces a collagen cross-link switch in tumor stroma. *J Clin Invest* **125**, 1147-1162 (2015).

20. Neesse, A., Algul, H., Tuveson, D. A., Gress, T. M., Stromal biology and therapy in pancreatic cancer: a changing paradigm. *Gut* **64**, 1476-1484 (2015).

21. Brauchle, E., Kasper, J., Daum, R., Schierbaum, N., Falch, C., Kirschniak, A., Schaffer, T. E., Schenke-Layland, K., Biomechanical and biomolecular characterization of extracellular matrix structures in human colon carcinomas. *Matrix Biol* **68-69**, 180-193 (2018).

22. Wozniak, M. A., Desai, R., Solski, P. A., Der, C. J., Keely, P. J., ROCK-generated contractility regulates breast epithelial cell differentiation in response to the physical properties of a three-dimensional collagen matrix. *J Cell Biol* **163**, 583-595 (2003).

23. Ondeck, M. G., Kumar, A., Placone, J. K., Plunkett, C. M., Matte, B. F., Wong, K. C., Fattet, L., Yang, J., Engler, A. J., Dynamically stiffened matrix promotes

malignant transformation of mammary epithelial cells via collective mechanical signaling. *Proc Natl Acad Sci U S A* **116**, 3502-3507 (2019).

24. Provenzano, P. P., Inman, D. R., Eliceiri, K. W., Knittel, J. G., Yan, L., Rueden, C. T., White, J. G., Keely, P. J., Collagen density promotes mammary tumor initiation and progression. *BMC Med* **6**, 11 (2008).

25. Samuel, M. S., Lopez, J. I., McGhee, E. J., Croft, D. R., Strachan, D., Timpson, P., Munro, J., Schroder, E., Zhou, J., Brunton, V. G., Barker, N., Clevers, H., Sansom, O. J., Anderson, K. I., Weaver, V. M., Olson, M. F., Actomyosin-mediated cellular tension drives increased tissue stiffness and beta-catenin activation to induce epidermal hyperplasia and tumor growth. *Cancer Cell* **19**, 776-791 (2011).

26. Chaudhuri, O., Koshy, S. T., Branco da Cunha, C., Shin, J. W., Verbeke, C. S., Allison, K. H., Mooney, D. J., Extracellular matrix stiffness and composition jointly regulate the induction of malignant phenotypes in mammary epithelium. *Nat Mater* **13**, 970-978 (2014).

27. Baker, A. M., Bird, D., Lang, G., Cox, T. R., Erler, J. T., Lysyl oxidase enzymatic function increases stiffness to drive colorectal cancer progression through FAK. *Oncogene* **32**, 1863-1868 (2013).

28. Navab, R., Strumpf, D., To, C., Pasko, E., Kim, K. S., Park, C. J., Hai, J., Liu, J., Jonkman, J., Barczyk, M., Bandarchi, B., Wang, Y. H., Venkat, K., Ibrahimov, E., Pham, N. A., Ng, C., Radulovich, N., Zhu, C. Q., Pintilie, M., Wang, D., Lu, A., Jurisica, I., Walker, G. C., Gullberg, D., Tsao, M. S., Integrin

alpha11beta1 regulates cancer stromal stiffness and promotes tumorigenicity and metastasis in non-small cell lung cancer. *Oncogene* **35**, 1899-1908 (2016).

29. Yuan, Y., Zhong, W., Ma, G., Zhang, B., Tian, H., Yes-associated protein regulates the growth of human non-small cell lung cancer in response to matrix stiffness. *Mol Med Rep* **11**, 4267-4272 (2015).
30. Lee, J., Condello, S., Yakubov, B., Emerson, R., Caperell-Grant, A., Hitomi, K., Xie, J., Matei, D., Tissue Transglutaminase Mediated Tumor-Stroma Interaction Promotes Pancreatic Cancer Progression. *Clin Cancer Res* **21**, 4482-4493 (2015).
31. Schrader, J., Gordon-Walker, T. T., Aucott, R. L., van Deemter, M., Quaas, A., Walsh, S., Benten, D., Forbes, S. J., Wells, R. G., Iredale, J. P., Matrix stiffness modulates proliferation, chemotherapeutic response, and dormancy in hepatocellular carcinoma cells. *Hepatology* **53**, 1192-1205 (2011).
32. Ishihara, S., Inman, D. R., Li, W. J., Ponik, S. M., Keely, P. J., Mechano-Signal Transduction in Mesenchymal Stem Cells Induces Prosaposin Secretion to Drive the Proliferation of Breast Cancer Cells. *Cancer Res* **77**, 6179-6189 (2017).
33. Bertero, T., Oldham, W. M., Grasset, E. M., Bourget, I., Boulter, E., Pisano, S., Hofman, P., Bellvert, F., Meneguzzi, G., Bulavin, D. V., Estrach, S., Feral, C. C., Chan, S. Y., Bozec, A., Gaggioli, C., Tumor-Stroma Mechanics Coordinate Amino Acid Availability to Sustain Tumor Growth and Malignancy. *Cell Metab* **29**, 124-140 e110 (2019).

34. Hupfer, A., Brichkina, A., Koeniger, A., Keber, C., Denkert, C., Pfefferle, P., Helmprobst, F., Pagenstecher, A., Visekruna, A., Lauth, M., Matrix stiffness drives stromal autophagy and promotes formation of a protumorigenic niche. *Proc Natl Acad Sci U S A* **118**, (2021).

35. Giancotti, F. G., Mechanisms governing metastatic dormancy and reactivation. *Cell* **155**, 750-764 (2013).

36. Fattet, L., Jung, H. Y., Matsumoto, M. W., Aubol, B. E., Kumar, A., Adams, J. A., Chen, A. C., Sah, R. L., Engler, A. J., Pasquale, E. B., Yang, J., Matrix Rigidity Controls Epithelial-Mesenchymal Plasticity and Tumor Metastasis via a Mechanoresponsive EPHA2/LYN Complex. *Dev Cell* **54**, 302-316 e307 (2020).

37. Wei, S. C., Fattet, L., Tsai, J. H., Guo, Y., Pai, V. H., Majeski, H. E., Chen, A. C., Sah, R. L., Taylor, S. S., Engler, A. J., Yang, J., Matrix stiffness drives epithelial-mesenchymal transition and tumour metastasis through a TWIST1-G3BP2 mechanotransduction pathway. *Nat Cell Biol* **17**, 678-688 (2015).

38. Torrino, S., Grasset, E. M., Audebert, S., Belhadj, I., Lacoux, C., Haynes, M., Pisano, S., Abelanet, S., Brau, F., Chan, S. Y., Mari, B., Oldham, W. M., Ewald, A. J., Bertero, T., Mechano-induced cell metabolism promotes microtubule glutamylation to force metastasis. *Cell Metab* **33**, 1342-1357 e1310 (2021).

39. Watson, A. W., Grant, A. D., Parker, S. S., Hill, S., Whalen, M. B., Chakrabarti, J., Harman, M. W., Roman, M. R., Forte, B. L., Gowan, C. C., Castro-Portuguez, R., Stolze, L. K., Franck, C., Cusanovich, D. A., Zavros, Y., Padi, M., Romanoski, C. E., Mouneimne, G., Breast tumor stiffness instructs bone

metastasis via maintenance of mechanical conditioning. *Cell Rep* **35**, 109293 (2021).

40. Dong, Y., Zheng, Q., Wang, Z., Lin, X., You, Y., Wu, S., Wang, Y., Hu, C., Xie, X., Chen, J., Gao, D., Zhao, Y., Wu, W., Liu, Y., Ren, Z., Chen, R., Cui, J., Higher matrix stiffness as an independent initiator triggers epithelial-mesenchymal transition and facilitates HCC metastasis. *J Hematol Oncol* **12**, 112 (2019).
41. Wong, C. C., Tse, A. P., Huang, Y. P., Zhu, Y. T., Chiu, D. K., Lai, R. K., Au, S. L., Kai, A. K., Lee, J. M., Wei, L. L., Tsang, F. H., Lo, R. C., Shi, J., Zheng, Y. P., Wong, C. M., Ng, I. O., Lysyl oxidase-like 2 is critical to tumor microenvironment and metastatic niche formation in hepatocellular carcinoma. *Hepatology* **60**, 1645-1658 (2014).
42. McKenzie, A. J., Hicks, S. R., Svec, K. V., Naughton, H., Edmunds, Z. L., Howe, A. K., The mechanical microenvironment regulates ovarian cancer cell morphology, migration, and spheroid disaggregation. *Sci Rep* **8**, 7228 (2018).
43. Dai, J., Qin, L., Chen, Y., Wang, H., Lin, G., Li, X., Liao, H., Fang, H., Matrix stiffness regulates epithelial-mesenchymal transition via cytoskeletal remodeling and MRTF-A translocation in osteosarcoma cells. *J Mech Behav Biomed Mater* **90**, 226-238 (2019).
44. Hayashi, M., Yamamoto, Y., Ibusuki, M., Fujiwara, S., Yamamoto, S., Tomita, S., Nakano, M., Murakami, K., Iyama, K., Iwase, H., Evaluation of tumor stiffness by elastography is predictive for pathologic complete response to

neoadjuvant chemotherapy in patients with breast cancer. *Ann Surg Oncol* **19**, 3042-3049 (2012).

45. Lin, C. H., Pelissier, F. A., Zhang, H., Lakins, J., Weaver, V. M., Park, C., LaBarge, M. A., Microenvironment rigidity modulates responses to the HER2 receptor tyrosine kinase inhibitor lapatinib via YAP and TAZ transcription factors. *Mol Biol Cell* **26**, 3946-3953 (2015).

46. Fatherree, J. P., Guarin, J. R., McGinn, R. A., Naber, S. P., Oudin, M. J., Chemotherapy-Induced Collagen IV Drives Cancer Cell Motility through Activation of Src and Focal Adhesion Kinase. *Cancer Res* **82**, 2031-2044 (2022).

47. Gao, J., Rong, Y., Huang, Y., Shi, P., Wang, X., Meng, X., Dong, J., Wu, C., Cirrhotic stiffness affects the migration of hepatocellular carcinoma cells and induces sorafenib resistance through YAP. *J Cell Physiol* **234**, 2639-2648 (2019).

48. Shen, Y., Wang, X., Lu, J., Salfenmoser, M., Wirsik, N. M., Schleussner, N., Imle, A., Freire Valls, A., Radhakrishnan, P., Liang, J., Wang, G., Muley, T., Schneider, M., Ruiz de Almodovar, C., Diz-Munoz, A., Schmidt, T., Reduction of Liver Metastasis Stiffness Improves Response to Bevacizumab in Metastatic Colorectal Cancer. *Cancer Cell* **37**, 800-817 e807 (2020).

49. Drain, A. P., Zahir, N., Northey, J. J., Zhang, H., Huang, P. J., Maller, O., Lakins, J. N., Yu, X., Leight, J. L., Alston-Mills, B. P., Hwang, E. S., Chen, Y. Y., Park, C. C., Weaver, V. M., Matrix compliance permits NF-kappaB activation to drive therapy resistance in breast cancer. *J Exp Med* **218**, (2021).

50. Dong, Y., Xie, X., Wang, Z., Hu, C., Zheng, Q., Wang, Y., Chen, R., Xue, T., Chen, J., Gao, D., Wu, W., Ren, Z., Cui, J., Increasing matrix stiffness upregulates vascular endothelial growth factor expression in hepatocellular carcinoma cells mediated by integrin beta1. *Biochem Biophys Res Commun* **444**, 427-432 (2014).

51. Zhao, D., Xue, C., Li, Q., Liu, M., Ma, W., Zhou, T., Lin, Y., Substrate stiffness regulated migration and angiogenesis potential of A549 cells and HUVECs. *J Cell Physiol* **233**, 3407-3417 (2018).

52. Stylianopoulos, T., Martin, J. D., Chauhan, V. P., Jain, S. R., Diop-Frimpong, B., Bardeesy, N., Smith, B. L., Ferrone, C. R., Hornicek, F. J., Boucher, Y., Munn, L. L., Jain, R. K., Causes, consequences, and remedies for growth-induced solid stress in murine and human tumors. *Proc Natl Acad Sci U S A* **109**, 15101-15108 (2012).

53. Zhang, J., Zhang, S., Gao, S., Ma, Y., Tan, X., Kang, Y., Ren, W., HIF-1alpha, TWIST-1 and ITGB-1, associated with Tumor Stiffness, as Novel Predictive Markers for the Pathological Response to Neoadjuvant Chemotherapy in Breast Cancer. *Cancer Manag Res* **12**, 2209-2222 (2020).

54. Madsen, C. D., Pedersen, J. T., Venning, F. A., Singh, L. B., Moeendarbary, E., Charras, G., Cox, T. R., Sahai, E., Erler, J. T., Hypoxia and loss of PHD2 inactivate stromal fibroblasts to decrease tumour stiffness and metastasis. *EMBO Rep* **16**, 1394-1408 (2015).

55. Abaricia, J. O., Shah, A. H., Olivares-Navarrete, R., Substrate stiffness induces neutrophil extracellular trap (NET) formation through focal adhesion kinase activation. *Biomaterials* **271**, 120715 (2021).

56. Taufalele, P. V., Wang, W., Simmons, A. J., Southard-Smith, A. N., Chen, B., Greenlee, J. D., King, M. R., Lau, K. S., Hassane, D. C., Bordeleau, F., Reinhart-King, C. A., Matrix stiffness enhances cancer-macrophage interactions and M2-like macrophage accumulation in the breast tumor microenvironment. *Acta Biomater*, (2022).

57. Azadi, S., Aboulkheyr Es, H., Razavi Bazaz, S., Thiery, J. P., Asadnia, M., Ebrahimi Warkiani, M., Upregulation of PD-L1 expression in breast cancer cells through the formation of 3D multicellular cancer aggregates under different chemical and mechanical conditions. *Biochim Biophys Acta Mol Cell Res* **1866**, 118526 (2019).

58. Miyazawa, A., Ito, S., Asano, S., Tanaka, I., Sato, M., Kondo, M., Hasegawa, Y., Regulation of PD-L1 expression by matrix stiffness in lung cancer cells. *Biochem Biophys Res Commun* **495**, 2344-2349 (2018).

59. Erez, N., Truitt, M., Olson, P., Arron, S. T., Hanahan, D., Cancer-Associated Fibroblasts Are Activated in Incipient Neoplasia to Orchestrate Tumor-Promoting Inflammation in an NF-kappaB-Dependent Manner. *Cancer Cell* **17**, 135-147 (2010).

60. Li, T., Yang, Y., Hua, X., Wang, G., Liu, W., Jia, C., Tai, Y., Zhang, Q., Chen, G., Hepatocellular carcinoma-associated fibroblasts trigger NK cell dysfunction via PGE2 and IDO. *Cancer Lett* **318**, 154-161 (2012).

61. Mariathasan, S., Turley, S. J., Nickles, D., Castiglioni, A., Yuen, K., Wang, Y., Kadel, E. E., III, Koeppen, H., Astarita, J. L., Cubas, R., Jhunjhunwala, S., Banchereau, R., Yang, Y., Guan, Y., Chalouni, C., Ziai, J., Senbabaoglu, Y., Santoro, S., Sheinson, D., Hung, J., Giltnane, J. M., Pierce, A. A., Mesh, K., Lianoglou, S., Riegler, J., Carano, R. A. D., Eriksson, P., Hoglund, M., Somarriba, L., Halligan, D. L., van der Heijden, M. S., Loriot, Y., Rosenberg, J. E., Fong, L., Mellman, I., Chen, D. S., Green, M., Derleth, C., Fine, G. D., Hegde, P. S., Bourgon, R., Powles, T., TGFbeta attenuates tumour response to PD-L1 blockade by contributing to exclusion of T cells. *Nature* **554**, 544-548 (2018).

62. Cohen, N., Shani, O., Raz, Y., Sharon, Y., Hoffman, D., Abramovitz, L., Erez, N., Fibroblasts drive an immunosuppressive and growth-promoting microenvironment in breast cancer via secretion of Chitinase 3-like 1. *Oncogene* **36**, 4457-4468 (2017).

63. Costa, A., Kieffer, Y., Scholer-Dahirel, A., Pelon, F., Bourachot, B., Cardon, M., Sirven, P., Magagna, I., Fuhrmann, L., Bernard, C., Bonneau, C., Kondratova, M., Kuperstein, I., Zinovyev, A., Givel, A. M., Parrini, M. C., Soumelis, V., Vincent-Salomon, A., Mechta-Grigoriou, F., Fibroblast Heterogeneity and Immunosuppressive Environment in Human Breast Cancer. *Cancer Cell* **33**, 463-479 e410 (2018).

64. Martino, F., Perestrelo, A. R., Vinarsky, V., Pagliari, S., Forte, G., Cellular Mechanotransduction: From Tension to Function. *Front Physiol* **9**, 824 (2018).

65. Cooper, J., Giancotti, F. G., Integrin Signaling in Cancer: Mechanotransduction, Stemness, Epithelial Plasticity, and Therapeutic Resistance. *Cancer Cell* **35**, 347-367 (2019).

66. Paszek, M. J., DuFort, C. C., Rossier, O., Bainer, R., Mouw, J. K., Godula, K., Hudak, J. E., Lakins, J. N., Wijekoon, A. C., Cassereau, L., Rubashkin, M. G., Magbanua, M. J., Thorn, K. S., Davidson, M. W., Rugo, H. S., Park, J. W., Hammer, D. A., Giannone, G., Bertozzi, C. R., Weaver, V. M., The cancer glycocalyx mechanically primes integrin-mediated growth and survival. *Nature* **511**, 319-325 (2014).

67. Giancotti, F. G., Tarone, G., Positional control of cell fate through joint integrin/receptor protein kinase signaling. *Annu Rev Cell Dev Biol* **19**, 173-206 (2003).

68. Pylayeva, Y., Gillen, K. M., Gerald, W., Beggs, H. E., Reichardt, L. F., Giancotti, F. G., Ras- and PI3K-dependent breast tumorigenesis in mice and humans requires focal adhesion kinase signaling. *J Clin Invest* **119**, 252-266 (2009).

69. Bianchi-Smiraglia, A., Paesante, S., Bakin, A. V., Integrin beta5 contributes to the tumorigenic potential of breast cancer cells through the Src-FAK and MEK-ERK signaling pathways. *Oncogene* **32**, 3049-3058 (2013).

70. Saatci, O., Kaymak, A., Raza, U., Ersan, P. G., Akbulut, O., Banister, C. E., Sikirzhytski, V., Tokat, U. M., Aykut, G., Ansari, S. A., Dogan, H. T., Dogan, M., Jandaghi, P., Isik, A., Gundogdu, F., Kosemehmetoglu, K., Dizdar, O., Aksoy, S., Akyol, A., Uner, A., Buckhaults, P. J., Riazalhosseini, Y., Sahin, O.,

Targeting lysyl oxidase (LOX) overcomes chemotherapy resistance in triple negative breast cancer. *Nat Commun* **11**, 2416 (2020).

71. Guo, W., Pylayeva, Y., Pepe, A., Yoshioka, T., Muller, W. J., Inghirami, G., Giancotti, F. G., Beta 4 integrin amplifies ErbB2 signaling to promote mammary tumorigenesis. *Cell* **126**, 489-502 (2006).

72. Tai, Y. L., Chu, P. Y., Lai, I. R., Wang, M. Y., Tseng, H. Y., Guan, J. L., Liou, J. Y., Shen, T. L., An EGFR/Src-dependent beta4 integrin/FAK complex contributes to malignancy of breast cancer. *Sci Rep* **5**, 16408 (2015).

73. Zhang, L., Qu, J., Qi, Y., Duan, Y., Huang, Y. W., Zhou, Z., Li, P., Yao, J., Huang, B., Zhang, S., Yu, D., EZH2 engages TGFbeta signaling to promote breast cancer bone metastasis via integrin beta1-FAK activation. *Nat Commun* **13**, 2543 (2022).

74. Shen, M., Jiang, Y. Z., Wei, Y., Ell, B., Sheng, X., Esposito, M., Kang, J., Hang, X., Zheng, H., Rowicki, M., Zhang, L., Shih, W. J., Celia-Terrassa, T., Liu, Y., Cristea, I., Shao, Z. M., Kang, Y., Tinagl1 Suppresses Triple-Negative Breast Cancer Progression and Metastasis by Simultaneously Inhibiting Integrin/FAK and EGFR Signaling. *Cancer Cell* **35**, 64-80 e67 (2019).

75. Yang, X. H., Flores, L. M., Li, Q., Zhou, P., Xu, F., Krop, I. E., Hemler, M. E., Disruption of laminin-integrin-CD151-focal adhesion kinase axis sensitizes breast cancer cells to ErbB2 antagonists. *Cancer Res* **70**, 2256-2263 (2010).

76. Halder, G., Dupont, S., Piccolo, S., Transduction of mechanical and cytoskeletal cues by YAP and TAZ. *Nat Rev Mol Cell Biol* **13**, 591-600 (2012).

77. Meng, Z., Qiu, Y., Lin, K. C., Kumar, A., Placone, J. K., Fang, C., Wang, K. C., Lu, S., Pan, M., Hong, A. W., Moroishi, T., Luo, M., Plouffe, S. W., Diao, Y., Ye, Z., Park, H. W., Wang, X., Yu, F. X., Chien, S., Wang, C. Y., Ren, B., Engler, A. J., Guan, K. L., RAP2 mediates mechanoresponses of the Hippo pathway. *Nature* **560**, 655-660 (2018).

78. Dupont, S., Morsut, L., Aragona, M., Enzo, E., Giulitti, S., Cordenonsi, M., Zanconato, F., Le Digabel, J., Forcato, M., Bicciato, S., Elvassore, N., Piccolo, S., Role of YAP/TAZ in mechanotransduction. *Nature* **474**, 179-183 (2011).

79. Harvey, K. F., Pfleger, C. M., Hariharan, I. K., The Drosophila Mst ortholog, hippo, restricts growth and cell proliferation and promotes apoptosis. *Cell* **114**, 457-467 (2003).

80. Huang, J., Wu, S., Barrera, J., Matthews, K., Pan, D., The Hippo signaling pathway coordinately regulates cell proliferation and apoptosis by inactivating Yorkie, the Drosophila Homolog of YAP. *Cell* **122**, 421-434 (2005).

81. Wu, S., Huang, J., Dong, J., Pan, D., hippo encodes a Ste-20 family protein kinase that restricts cell proliferation and promotes apoptosis in conjunction with salvador and warts. *Cell* **114**, 445-456 (2003).

82. Chan, E. H., Nousiainen, M., Chalamalasetty, R. B., Schafer, A., Nigg, E. A., Sillje, H. H., The Ste20-like kinase Mst2 activates the human large tumor suppressor kinase Lats1. *Oncogene* **24**, 2076-2086 (2005).

83. Furth, N., Aylon, Y., The LATS1 and LATS2 tumor suppressors: beyond the Hippo pathway. *Cell Death Differ* **24**, 1488-1501 (2017).

84. Hergovich, A., Schmitz, D., Hemmings, B. A., The human tumour suppressor LATS1 is activated by human MOB1 at the membrane. *Biochem Biophys Res Commun* **345**, 50-58 (2006).

85. Yu, F. X., Zhao, B., Guan, K. L., Hippo Pathway in Organ Size Control, Tissue Homeostasis, and Cancer. *Cell* **163**, 811-828 (2015).

86. Zeng, Q., Hong, W., The emerging role of the hippo pathway in cell contact inhibition, organ size control, and cancer development in mammals. *Cancer Cell* **13**, 188-192 (2008).

87. Zhao, B., Li, L., Lei, Q., Guan, K. L., The Hippo-YAP pathway in organ size control and tumorigenesis: an updated version. *Genes Dev* **24**, 862-874 (2010).

88. Zheng, Y., Pan, D., The Hippo Signaling Pathway in Development and Disease. *Dev Cell* **50**, 264-282 (2019).

89. Zhao, B., Wei, X., Li, W., Udan, R. S., Yang, Q., Kim, J., Xie, J., Ikenoue, T., Yu, J., Li, L., Zheng, P., Ye, K., Chinnaiyan, A., Halder, G., Lai, Z. C., Guan, K. L., Inactivation of YAP oncoprotein by the Hippo pathway is involved in cell contact inhibition and tissue growth control. *Genes Dev* **21**, 2747-2761 (2007).

90. Chen, Q., Zhang, N., Gray, R. S., Li, H., Ewald, A. J., Zahnow, C. A., Pan, D., A temporal requirement for Hippo signaling in mammary gland differentiation, growth, and tumorigenesis. *Genes Dev* **28**, 432-437 (2014).

91. Ma, S., Meng, Z., Chen, R., Guan, K. L., The Hippo Pathway: Biology and Pathophysiology. *Annu Rev Biochem* **88**, 577-604 (2019).

92. Ghasemi, H., Mousavibahar, S. H., Hashemnia, M., Karimi, J., Khodadadi, I., Mirzaei, F., Tavilani, H., Tissue stiffness contributes to YAP activation in

bladder cancer patients undergoing transurethral resection. *Ann N Y Acad Sci* **1473**, 48-61 (2020).

93. Aragona, M., Panciera, T., Manfrin, A., Giulitti, S., Michielin, F., Elvassore, N., Dupont, S., Piccolo, S., A mechanical checkpoint controls multicellular growth through YAP/TAZ regulation by actin-processing factors. *Cell* **154**, 1047-1059 (2013).

94. Torrino, S., Roustan, F. R., Kaminski, L., Bertero, T., Pisano, S., Ambrosetti, D., Dufies, M., Uhler, J. P., Lemichez, E., Mettouchi, A., Gesson, M., Laurent, K., Gaggioli, C., Michiels, J. F., Lamaze, C., Bost, F., Clavel, S., UBTD1 is a mechano-regulator controlling cancer aggressiveness. *EMBO Rep* **20**, (2019).

95. Rice, A. J., Cortes, E., Lachowski, D., Cheung, B. C. H., Karim, S. A., Morton, J. P., Del Rio Hernandez, A., Matrix stiffness induces epithelial-mesenchymal transition and promotes chemoresistance in pancreatic cancer cells. *Oncogenesis* **6**, e352 (2017).

96. Gao, H., Chakraborty, G., Zhang, Z., Akalay, I., Gadiya, M., Gao, Y., Sinha, S., Hu, J., Jiang, C., Akram, M., Brogi, E., Leitinger, B., Giancotti, F. G., Multi-organ Site Metastatic Reactivation Mediated by Non-canonical Discoidin Domain Receptor 1 Signaling. *Cell* **166**, 47-62 (2016).

97. Liu, Q. P., Luo, Q., Deng, B., Ju, Y., Song, G. B., Stiffer Matrix Accelerates Migration of Hepatocellular Carcinoma Cells through Enhanced Aerobic Glycolysis Via the MAPK-YAP Signaling. *Cancers (Basel)* **12**, (2020).

98. Molina, E. R., Chim, L. K., Salazar, M. C., Mehta, S. M., Menegaz, B. A., Lamhamedi-Cherradi, S. E., Satish, T., Mohiuddin, S., McCall, D., Zaske, A.

M., Cuglievan, B., Lazar, A. J., Scott, D. W., Grande-Allen, J. K., Ludwig, J. A., Mikos, A. G., Mechanically tunable coaxial electrospun models of YAP/TAZ mechanoresponse and IGF-1R activation in osteosarcoma. *Acta Biomater* **100**, 38-51 (2019).

99. Miskolczi, Z., Smith, M. P., Rowling, E. J., Ferguson, J., Barriuso, J., Wellbrock, C., Collagen abundance controls melanoma phenotypes through lineage-specific microenvironment sensing. *Oncogene* **37**, 3166-3182 (2018).

100. Nukuda, A., Sasaki, C., Ishihara, S., Mizutani, T., Nakamura, K., Ayabe, T., Kawabata, K., Haga, H., Stiff substrates increase YAP-signaling-mediated matrix metalloproteinase-7 expression. *Oncogenesis* **4**, e165 (2015).

101. Langmead, B., Salzberg, S. L., Fast gapped-read alignment with Bowtie 2. *Nat Methods* **9**, 357-359 (2012).

102. Elosegui-Artola, A., Andreu, I., Beedle, A. E. M., Lezamiz, A., Uroz, M., Kosmalska, A. J., Oria, R., Kechagia, J. Z., Rico-Lastres, P., Le Roux, A. L., Shanahan, C. M., Trepat, X., Navajas, D., Garcia-Manyes, S., Roca-Cusachs, P., Force Triggers YAP Nuclear Entry by Regulating Transport across Nuclear Pores. *Cell* **171**, 1397-1410 e1314 (2017).

103. Yang, N., Chen, T., Wang, L., Liu, R., Niu, Y., Sun, L., Yao, B., Wang, Y., Yang, W., Liu, Q., Tu, K., Liu, Z., CXCR4 mediates matrix stiffness-induced downregulation of UBTD1 driving hepatocellular carcinoma progression via YAP signaling pathway. *Theranostics* **10**, 5790-5801 (2020).

104. Feng, F., Feng, X., Zhang, D., Li, Q., Yao, L., Matrix Stiffness Induces Pericyte-Fibroblast Transition Through YAP Activation. *Front Pharmacol* **12**, 698275 (2021).

105. Ferrari, N., Ranftl, R., Chicherova, I., Slaven, N. D., Moeendarbary, E., Farrugia, A. J., Lam, M., Semiannikova, M., Westergaard, M. C. W., Tchou, J., Magnani, L., Calvo, F., Dickkopf-3 links HSF1 and YAP/TAZ signalling to control aggressive behaviours in cancer-associated fibroblasts. *Nat Commun* **10**, 130 (2019).

106. Zhang, K., Grither, W. R., Van Hove, S., Biswas, H., Ponik, S. M., Eliceiri, K. W., Keely, P. J., Longmore, G. D., Mechanical signals regulate and activate SNAIL1 protein to control the fibrogenic response of cancer-associated fibroblasts. *J Cell Sci* **129**, 1989-2002 (2016).

107. Gao, H., Chakraborty, G., Lee-Lim, A. P., Mo, Q., Decker, M., Vonica, A., Shen, R., Brogi, E., Brivanlou, A. H., Giancotti, F. G., The BMP inhibitor Coco reactivates breast cancer cells at lung metastatic sites. *Cell* **150**, 764-779 (2012).

108. Pelossof, R., Fairchild, L., Huang, C. H., Widmer, C., Sreedharan, V. T., Sinha, N., Lai, D. Y., Guan, Y., Premsrirut, P. K., Tschaharganeh, D. F., Hoffmann, T., Thapar, V., Xiang, Q., Garippa, R. J., Ratsch, G., Zuber, J., Lowe, S. W., Leslie, C. S., Fellmann, C., Prediction of potent shRNAs with a sequential classification algorithm. *Nat Biotechnol* **35**, 350-353 (2017).

109. Fellmann, C., Hoffmann, T., Sridhar, V., Hopfgartner, B., Muhar, M., Roth, M., Lai, D. Y., Barbosa, I. A., Kwon, J. S., Guan, Y., Sinha, N., Zuber, J., An

optimized microRNA backbone for effective single-copy RNAi. *Cell Rep* **5**, 1704-1713 (2013).

110. Sanjana, N. E., Shalem, O., Zhang, F., Improved vectors and genome-wide libraries for CRISPR screening. *Nat Methods* **11**, 783-784 (2014).

111. Shalem, O., Sanjana, N. E., Hartenian, E., Shi, X., Scott, D. A., Mikkelson, T., Heckl, D., Ebert, B. L., Root, D. E., Doench, J. G., Zhang, F., Genome-scale CRISPR-Cas9 knockout screening in human cells. *Science* **343**, 84-87 (2014).

112. Labun, K., Krause, M., Torres Cleuren, Y., Valen, E., CRISPR Genome Editing Made Easy Through the CHOPCHOP Website. *Curr Protoc* **1**, e46 (2021).

113. Tse, J. R., Engler, A. J., Preparation of hydrogel substrates with tunable mechanical properties. *Curr Protoc Cell Biol* **Chapter 10**, Unit 10 16 (2010).

114. Sebastiaan Winkler, G., Lacomis, L., Philip, J., Erdjument-Bromage, H., Svejstrup, J. Q., Tempst, P., Isolation and mass spectrometry of transcription factor complexes. *Methods* **26**, 260-269 (2002).

115. Love, M. I., Huber, W., Anders, S., Moderated estimation of fold change and dispersion for RNA-seq data with DESeq2. *Genome Biol* **15**, 550 (2014).

116. Subramanian, A., Tamayo, P., Mootha, V. K., Mukherjee, S., Ebert, B. L., Gillette, M. A., Paulovich, A., Pomeroy, S. L., Golub, T. R., Lander, E. S., Mesirov, J. P., Gene set enrichment analysis: a knowledge-based approach for interpreting genome-wide expression profiles. *Proc Natl Acad Sci U S A* **102**, 15545-15550 (2005).

117. Feng, X., Arang, N., Rigiracciolo, D. C., Lee, J. S., Yeerna, H., Wang, Z., Lubrano, S., Kishore, A., Pachter, J. A., Konig, G. M., Maggiolini, M., Kostenis,

E., Schlaepfer, D. D., Tamayo, P., Chen, Q., Ruppin, E., Gutkind, J. S., A Platform of Synthetic Lethal Gene Interaction Networks Reveals that the GNAQ Uveal Melanoma Oncogene Controls the Hippo Pathway through FAK. *Cancer Cell* **35**, 457-472 e455 (2019).

118. Ando, T., Arang, N., Wang, Z., Costea, D. E., Feng, X., Goto, Y., Izumi, H., Gilardi, M., Ando, K., Gutkind, J. S., EGFR Regulates the Hippo pathway by promoting the tyrosine phosphorylation of MOB1. *Commun Biol* **4**, 1237 (2021).
119. Lahlou, H., Sanguin-Gendreau, V., Frame, M. C., Muller, W. J., Focal adhesion kinase contributes to proliferative potential of ErbB2 mammary tumour cells but is dispensable for ErbB2 mammary tumour induction in vivo. *Breast Cancer Res* **14**, R36 (2012).
120. Finn, R. S., Dering, J., Ginther, C., Wilson, C. A., Glaspy, P., Tchekmedyian, N., Slamon, D. J., Dasatinib, an orally active small molecule inhibitor of both the src and abl kinases, selectively inhibits growth of basal-type/"triple-negative" breast cancer cell lines growing in vitro. *Breast Cancer Res Treat* **105**, 319-326 (2007).
121. Huang, F., Reeves, K., Han, X., Fairchild, C., Platero, S., Wong, T. W., Lee, F., Shaw, P., Clark, E., Identification of candidate molecular markers predicting sensitivity in solid tumors to dasatinib: rationale for patient selection. *Cancer Res* **67**, 2226-2238 (2007).
122. Tryfonopoulos, D., Walsh, S., Collins, D. M., Flanagan, L., Quinn, C., Corkery, B., McDermott, E. W., Evoy, D., Pierce, A., O'Donovan, N., Crown, J., Duffy,

M. J., Src: a potential target for the treatment of triple-negative breast cancer. *Ann Oncol* **22**, 2234-2240 (2011).

123. Tamura, M., Gu, J., Danen, E. H., Takino, T., Miyamoto, S., Yamada, K. M., PTEN interactions with focal adhesion kinase and suppression of the extracellular matrix-dependent phosphatidylinositol 3-kinase/Akt cell survival pathway. *J Biol Chem* **274**, 20693-20703 (1999).

124. Liu, J., Ye, L., Li, Q., Wu, X., Wang, B., Ouyang, Y., Yuan, Z., Li, J., Lin, C., Synaptopodin-2 suppresses metastasis of triple-negative breast cancer via inhibition of YAP/TAZ activity. *J Pathol* **244**, 71-83 (2018).

125. OuYang, C., Xie, Y., Fu, Q., Xu, G., SYNPO2 suppresses hypoxia-induced proliferation and migration of colorectal cancer cells by regulating YAP-KLF5 axis. *Tissue Cell* **73**, 101598 (2021).

126. Xia, E., Zhou, X., Bhandari, A., Zhang, X., Wang, O., Synaptopodin-2 plays an important role in the metastasis of breast cancer via PI3K/Akt/mTOR pathway. *Cancer Manag Res* **10**, 1575-1583 (2018).

127. Lee, J. H., Kim, J. Y., Kim, S. Y., Choi, S. I., Kim, K. C., Cho, E. W., Kim, I. G., APBB1 reinforces cancer stem cell and epithelial-to-mesenchymal transition by regulating the IGF1R signaling pathway in non-small-cell lung cancer cells. *Biochem Biophys Res Commun* **482**, 35-42 (2017).

128. Ohtaki, S., Wanibuchi, M., Kataoka-Sasaki, Y., Sasaki, M., Oka, S., Noshiro, S., Akiyama, Y., Mikami, T., Mikuni, N., Kocsis, J. D., Honmou, O., ACTC1 as an invasion and prognosis marker in glioma. *J Neurosurg* **126**, 467-475 (2017).

129. Guardia, T., Eason, M., Kontrogianni-Konstantopoulos, A., Obscurin: A multitasking giant in the fight against cancer. *Biochim Biophys Acta Rev Cancer* **1876**, 188567 (2021).

130. Myllyharju, J., Extracellular matrix and developing growth plate. *Curr Osteoporos Rep* **12**, 439-445 (2014).

131. Pickering, C., Kiely, J., ACTN3, Morbidity, and Healthy Aging. *Front Genet* **9**, 15 (2018).

132. Zhu, B., Xue, F., Zhang, C., Li, G., LMCD1 promotes osteogenic differentiation of human bone marrow stem cells by regulating BMP signaling. *Cell Death Dis* **10**, 647 (2019).

133. Benson, A. B., 3rd, Wainberg, Z. A., Hecht, J. R., Vyushkov, D., Dong, H., Bendell, J., Kudrik, F., A Phase II Randomized, Double-Blind, Placebo-Controlled Study of Simtuzumab or Placebo in Combination with Gemcitabine for the First-Line Treatment of Pancreatic Adenocarcinoma. *Oncologist* **22**, 241-e215 (2017).

134. Hecht, J. R., Benson, A. B., 3rd, Vyushkov, D., Yang, Y., Bendell, J., Verma, U., A Phase II, Randomized, Double-Blind, Placebo-Controlled Study of Simtuzumab in Combination with FOLFIRI for the Second-Line Treatment of Metastatic KRAS Mutant Colorectal Adenocarcinoma. *Oncologist* **22**, 243-e223 (2017).

135. Pankova, D., Chen, Y., Terajima, M., Schliekelman, M. J., Baird, B. N., Fahrenholtz, M., Sun, L., Gill, B. J., Vadakkan, T. J., Kim, M. P., Ahn, Y. H., Roybal, J. D., Liu, X., Parra Cuentas, E. R., Rodriguez, J., Wistuba, II,

Creighton, C. J., Gibbons, D. L., Hicks, J. M., Dickinson, M. E., West, J. L., Grande-Allen, K. J., Hanash, S. M., Yamauchi, M., Kurie, J. M., Cancer-Associated Fibroblasts Induce a Collagen Cross-link Switch in Tumor Stroma. *Mol Cancer Res* **14**, 287-295 (2016).

136. Maloney, E., DuFort, C. C., Provenzano, P. P., Farr, N., Carlson, M. A., Vohra, R., Park, J., Hingorani, S. R., Lee, D., Non-Invasive Monitoring of Stromal Biophysics with Targeted Depletion of Hyaluronan in Pancreatic Ductal Adenocarcinoma. *Cancers (Basel)* **11**, (2019).

137. Provenzano, P. P., Cuevas, C., Chang, A. E., Goel, V. K., Von Hoff, D. D., Hingorani, S. R., Enzymatic targeting of the stroma ablates physical barriers to treatment of pancreatic ductal adenocarcinoma. *Cancer Cell* **21**, 418-429 (2012).

138. Alday-Parejo, B., Stupp, R., Ruegg, C., Are Integrins Still Practicable Targets for Anti-Cancer Therapy? *Cancers (Basel)* **11**, (2019).

139. Primac, I., Maquoi, E., Blacher, S., Heljasvaara, R., Van Deun, J., Smeland, H. Y., Canale, A., Louis, T., Stuhr, L., Sounni, N. E., Cataldo, D., Pihlajaniemi, T., Pequeux, C., De Wever, O., Gullberg, D., Noel, A., Stromal integrin alpha11 regulates PDGFR-beta signaling and promotes breast cancer progression. *J Clin Invest* **129**, 4609-4628 (2019).

140. Kolev, V. N., Tam, W. F., Wright, Q. G., McDermott, S. P., Vidal, C. M., Shapiro, I. M., Xu, Q., Wicha, M. S., Pachter, J. A., Weaver, D. T., Inhibition of FAK kinase activity preferentially targets cancer stem cells. *Oncotarget* **8**, 51733-51747 (2017).

141. Kaneda, A., Seike, T., Danjo, T., Nakajima, T., Otsubo, N., Yamaguchi, D., Tsuji, Y., Hamaguchi, K., Yasunaga, M., Nishiya, Y., Suzuki, M., Saito, J. I., Yatsunami, R., Nakamura, S., Sekido, Y., Mori, K., The novel potent TEAD inhibitor, K-975, inhibits YAP1/TAZ-TEAD protein-protein interactions and exerts an anti-tumor effect on malignant pleural mesothelioma. *Am J Cancer Res* **10**, 4399-4415 (2020).

VITA

Xiaobo Wang was born in Northwestern China. He is the son of Yu Wang and Mingfang Du. After completing his work at Lintao High School, Xiaobo entered Chongqing Medical University and obtained the degree of Bachelor of Medicine with a major in Basic Medical Sciences in 2012. He received the degree of Master of Science with a major in Biochemistry and Molecular Biology from Shanghai Jiao Tong University in 2016. In August of 2016 Xiaobo moved to Houston, Texas and entered The University of Texas MD Anderson Cancer Center UTHealth Graduate School of Biomedical Sciences. As a Graduate Research Assistant, Xiaobo worked at MD Anderson Cancer Center from 2016 to 2021 and Columbia University from 2021 to 2022.